UILU-ENG 90-3602

Report No. 154

FATIGUE CRACK CLOSURE— STUDY OF CREEP AND CONSTRAINT EFFECTS

by

Wei Sun
Department of Mechanical and Industrial Engineering

A Report of the

MATERIALS ENGINEERING—MECHANICAL BEHAVIOR

College of Engineering, University of Illinois at Urbana-Champaign

June 1990

ACKNOWLEDGEMENT

The work on high temperature fatigue crack closure was supported by General Electrical company, AEBG. The cooperation of Dr. H. Popp and Mr. B. Lawless of GE is appreciated. The research on crack closure under plane stress and plane strain condition was supported by the Fracture Control Program, College of Engineering, University of Illinois at Urbana-Champaign. Computer access was gained by grants from National Center for Supercomputing Applications, University of Illinois at Urbana-Champaign.

My advisor, Professor Huseyin Sehitoglu, is gratefully acknowledged for his patience, friendship, guidance and encouragement throughout the entire of my research work. Former graduate student, Dr. Craig McClung is sincerely thanked for his help and suggestion. Thanks are also extended to Suzanne Faikus for preparing most of figures.

Finally, special thanks to my father for his encouragement, and especially to my husband for his support, help and love.

TABLE OF CONTENTS

LIST OF TABLES

LIST OF FIGURES

NOMENCLATURE

a	Crack Length
A	Material Constant for Power Law Hardening
B	Specimen Thickness
c	Half of Notch Width
C	Material constant in Paris Law Crack Growth Relationship
d	Contact Distance Behind Crack Tip
da/dN	Crack Growth Rate
$d\bar{\varepsilon}^P$	Equivalent Plastic Strain Increment
$d\varepsilon_{ij}^P$	Plastic Strain Rate Tensor
$d\mu$	Positive Scalar in Ziegler's Rule
$d\lambda$	Positive Scalar during Active Plastic Straining
dS_{ij}^c	Deviatoric Back Stress Tensor
E	Modulus of Elasticity
H	Plastic Modulus
ΔK	Stress Intensity Range
ΔK_{eff}	Effective Stress Intensity Range
K_{max}	Maximum Stress Intensity
l	Crack Size
m	Creep Exponent
n	Strain Hardening Exponent
N	Material Constant for Power Law Hardening
P_{max}	Maximum Applied Load Level
P_{open}	Applied Load Level at Crack Opening
P_o	Reference Load

q	Substep number
r	Distance Behind the Crack Tip
r_p	Reversed Plastic Zone Size
	(Active Plastic Zone at Minimum Load)
R	Stress Ratio
ΔS_{eff}	Effective Stress Range
s_{ij}, s^c_{ij}	Deviatoric Stress,Deviatoric Back Stress Tensor
S_{max}	Maximum Applied Stress
S_{open}, S_{clos}	Applied Stress Level at Crack Opening or Closure
t_h	Hold Time Period
u_x	Displacement in x-Direction with Respect to Crack Tip
U	Effective Stress Ratio
U_o	Time Independent Effective Stress Ratio
W	Specimen Width
x,y,z	Coordinate Axis
z	Exponent in Paris Law Crack Growth Relationship
$\alpha_x,\alpha_y,\alpha_z$	Normal Back Stress Components
β	Specimen Geometry Constant in Limit Load Equation
δ	Crack Opening Displacements
$\dot{\varepsilon}^c_{ij}$	Creep Strain Components
$\dot{\varepsilon}^e_{ij}$	Elastic Strain Components
$\dot{\varepsilon}^p_{ij}$	Plastic Strain Components
$\dot{\varepsilon}^c_o$	Constant (= 10^{-5} 1/s)
$\dot{\bar{\varepsilon}}^c$	Equivalent Creep Strain
$\bar{\varepsilon}^p_o$	Equivalent Yield Strain

$\varepsilon_x^p, \varepsilon_y^p, \varepsilon_z^p$	Normal Strain Components
$\varepsilon_x, \varepsilon_y, \varepsilon_z$	Normal Plastic (Inelastic) Strain Components
γ	Specimen Geometry Constant
σ_c	Creep Strength
σ_o	Yield Strength
$\bar{\sigma}$	Von Mises Equivalent Stress

1. INTRODUCTION

1.1 Background

In 1968, Elber observed that fatigue-crack surfaces come to contact even during tension-tension cyclic loading, and crack surfaces open at an applied tensile load near 50% of the maximum load [1-3]. A plasticity induced, crack closure mechanism was forwarded to explain this phenomenon.

During crack growth, plastic zone develops around the crack tip as the yield strength of the material is exceeded. As the crack grows this material is unloaded, and the plastically "stretched" material causes the crack surfaces come to contact before zero load is reached. Upon further unloading compressive residual stresses develop behind the crack tip. Crack opening stress, S_{open}, (or crack opening load, P_{open}) is defined as the value of applied stress (or applied load) at which the residual stresses are overcome and when the crack is fully open. Fatigue crack growth occurs during the period when the crack is fully open. Therefore, an effective stress intensity factor range, $\Delta K_{eff} = K_{max} - K_{open}$, is used in fatigue crack growth characterization. This replaces the total stress intensity range parameter, ΔK.

In recent years much attention has been focused on the fatigue crack closure phenomenon. This mechanism and the influence of the plastic wake on the local crack tip strain fields provided insight into understanding of fatigue-crack growth of metallic materials. Early studies used the concept of crack closure to explain R-ratio effects and overload effects. The concept of plasticity induced crack closure has been recently used to explain state of stress effects, notch size effects, applied stress (load)

level effects and accelerated growth of short cracks [4-8]. The experimental determination of crack closure loads still remains a difficult problem. Analytical or numerical determination of crack closure has advantages as this would allow many variables that effect closure to be determined.

Finite element analysis is a helpful tool in characterizing crack opening and crack closure under complicated loading conditions, complex material behavior and complex geometries. Two-dimensional finite-element analysis of crack growth and closure under plane-stress and plane-strain conditions have been conducted [9-12]. Specialized FEM codes are developed with provisions for crack opening and crack contact. (These features are not available in commercial codes such as ABAQUS or ANSYS). In a previous study, a two dimensional finite element model has been developed by Lalor, Sehitoglu [13] and McClung [14], in which crack extension is allowed through the mesh. The crack is advanced one element each cycle, opening and closing of crack surfaces are monitored. These studies provided additional information on stress-strain fields, plastic zone changes and different material behaviors effects on crack closure.

1.2 Current Work and Purpose of This Research

The present research represents an extension of the finite element model described above, and deals with the application of crack closure in two areas of fatigue crack growth. The first part is analysis of crack growth under time dependent loading conditions. This analysis studies crack closure under hold periods at maximum load and different frequencies during high temperature fatigue crack growth. Specifically, the effects of applied maximum stress level, creep constitutive relations and holding

period at maximum stress are studied. The effect of time dependent deformation due to creep on the crack tip stress-strain fields and crack tip displacements, and the implications of crack closure results in describing high temperature fatigue crack growth rate data are reported.

In the second part of the present research, the constraint effect (plane stress vs. plane strain) on crack closure is studied. Crack growth simulations on compact tension specimen (CT) under plane stress and plane strain conditions are conducted and the inelastic stress-strain fields near crack tip are studied. The mechanisms of material transfer to crack surface are discussed. Results provide insight into closure behavior under plane stress and plane strain condition.

2. TIME-DEPENDENT FATIGUE CRACK CLOSURE AT HIGH TEMPERATURES

2.1 Background

Fatigue creep crack growth studies received much attention for number of years. This problem is an important design concern for elevated temperature components and is also important in predicting the residual life of these components which are in service. Crack growth rates and fatigue lives at high temperatures are significantly influenced by loading frequency and hold time effects within the cycle [15-23]. The experiments performed by James [15] and Saxena [16, 17] show that the decrease in frequency and increase in hold times within the cycle may result in accelerated crack growth rates up to two order of magnitude. The effect of crack opening and closure under these conditions have not been considered. However, the dependence of effective stress range on material properties, constraint condition (out-of-plane and in-plane), R-ratio and stress level has been documented under time independent loading conditions. Both experimental studies and analytical work [24] confirm the significance of crack closure mechanism.

The present research is concentrated on the stress-strain fields near the crack tip under time dependent loading condition. It will be shown that plasticity induced crack closure occurs under time dependent high temperature conditions, and should be accounted in crack growth analysis. The influence of tensile hold periods and different creep laws on crack opening and crack closure behavior is reported. The results can be used to predict crack growth data and predict lives at different hold periods and frequencies.

The concept of crack closure for the case of cycling with hold period is illustrated in Figure 1a. The crack profile at maximum stress prior to the tensile hold (a) and after the tensile hold (b) is indicated in this figure. Crack opening displacements increase during the hold period. Upon unloading, crack closure (contact of crack surfaces) occurs at S_{clos} (c); and at minimum stress (d), the contact zone extends partially behind the crack tip. The contact zone sustains compressive stresses that may exceed the yield strength. Upon application of tensile stress, the compressive residual stresses behind the crack are relieved and the crack opens at S_{open} (e).

In the presence of tensile hold periods, the crack tip opening displacements and crack tip strains increase with time. Then, the residual displacements become a small fraction of the crack opening displacements. Similarly the applied stresses may overcome the compressive stresses at a lower applied load. This would result in a decrease in S_{open} and S_{clos}. Therefore, the effective stress range, $\Delta S_{eff} = S_{max} - S_{open}$, over which the crack is open is increased. An increase in effective stress range translates to a higher crack driving force and higher crack growth rates.

2.2 Finite Element and Constitutive Modeling

2.2.1 Finite Element model

The crack opening and closure stress levels are determined using a finite element analysis that allows crack growth through the mesh. The finite element analysis permits the study of complex material and loading variables on crack opening and closure. Simplified analysis based on Dugdale type models are also possible, but idealized stress-strain behavior and several assumptions on contact zone, residual stress distribution are

needed. Also Dugdale type of models are limited to applied stress levels below yield stress. Despite the significance of crack closure and its first-order effect on crack growth rates, its characterization under time-dependent fatigue loading has not been considered. This would involve a substantial computational effort.

A specialized finite element program has been developed to analyze the crack closure behavior under time-dependent loading. Truss elements along the crack line with adjustable stiffness levels were used to simulate opening and closing of the crack. Four noded isoparametric elements were used, which represents an advance over constant strain triangular elements. The material model is based on the concepts of incremental, rate independent plasticity combined with time dependent creep. The Von Mises criteria was used to identify the yield surface and nonlinear kinematic hardening was used to simulate the varying plastic modulus with deformation and to account for the Bauschinger effect. Typical execution times for a single simulation were of the order of 300 hours on HP9000 computer and 30 minutes on CRAY-XMP 48 supercomputer. All runs reported in this study were performed on the CRAY-XMP 48.

The finite element mesh is shown in Figure 1b, which has 1189 elements and 1267 nodes. The coordinates (x, y) and the origin are indicated. Since many cycles (20 or more) are considered in the simulations, the use of higher order elements require computer power beyond that used for present research. The element size is as small as 14 μm near the notch surface. Truss (spring) elements were attached along the crack line but not shown in Figure 1b. Crack growth from a circular notch is considered. The presence of the notch results in transient opening levels which stabilize

rapidly in most cases. This geometry is essentially representative of center crack plate under Mode I loading.

The sensitivity of the mesh on the crack opening and closure information has been evaluated. At low stresses, $S_{max}/\sigma_o < 0.4$, where S_{max} is the maximum stress of the cycle and σ_o is uniaxial yield strength, the requirements for fineness of the mesh are very restrictive. The size of the elements should be fine enough to capture both the forward and the reversed plastic zone of the crack. Low stresses have not been considered in this study since they lie outside the regime of interest where experimental data is available. Furthermore, at low stresses the crack opening stress levels are not strong functions of applied maximum stress.

The types of cycle studied in the present research are given in Figures 2a and 2b. The different cases with continuous cycling are indicated in Figure 2a, and cycling with tensile hold periods is depicted in Figure 2b. The crack opening and closure stress levels within the cycle and the location of crack advance are indicated in these diagrams. The locations of a, b, c, d, e, f, correspond to these are depicted in Figure 1a. The crack advance occurred immediately at the first increment of unloading after the hold period. One node is released every cycle. In early work, the location of node release within the cycle did not have a significant effect on the crack opening levels [25]. Crack opening was defined as the stress level at which all the compressive residual stresses behind the crack were overcome by the applied stress. The crack closure stress, S_{clos}, was defined as the stress level at which the first contact of crack surfaces occur during the unloading portion of the cycle. Since the crack is advanced in the first increment of unloading, the first node behind the crack tip closes immediately. It is

realized that this is not the first contact. Same definition of crack opening and closure stress levels and node release scheme were used for the case with hold periods, as well as continuous cycling case considered in this study.

In this study each loading, unloading and holding segments were divided into 20 equal increments. However, larger number of increments were used when the creep strain rates were high. An explicit time-stepping procedure with variable time increment [26] is used in this study. When y-component incremental creep strain, $\Delta\varepsilon^{c}_{yy}$ is larger than 6×10^{-6} at the crack tip, subincrements are needed. The number of subincrements is determined by:

$$q = \Delta\varepsilon^{c}_{yy}/(10\% \times \varepsilon^{c}_{yy}) \qquad (1)$$

where ε^{c}_{yy} is y-component of total creep strain earned in the current cycle. If the calculated subincremental number, q, is smaller than 1, no subincrement is needed. The crack opening and closure stress levels for several creep laws were established. The creep laws selected represent conditions where significant creep strains below yield strength or significant creep strains above yield strength occur respectively. For the cycling with holding period cases, elastic-plastic deformation occurred during rapid loading and unloading portion of the cycle and creep strain rates were dominant during the hold period. The creep strains increased with number of cycles and the creep zone reached the free edges of the specimen in certain cases.

Given the basic da/dN versus stress intensity range curve obtained under rapid cycling conditions, it is possible to predict the crack growth rates with different hold periods or different load frequencies if the corresponding crack opening stress levels were determined. In this study the maximum stress levels ranging from 0.5 to 0.9 of yield stress were considered. The hold times at maximum stress were chosen as 30 seconds, 90 seconds and 300 seconds for the case of cycling with loading period. The frequencies were chosen as 0.0032 Hz and 0.025 Hz for the continuous cycling cases. The results are compared to time-independent case. The analysis is capable of handling any stress (strain) time variation. Since the majority of experimental studies of time-dependent fatigue crack growth were undertaken under the R = 0 condition, similar conditions were considered in this study.

2.2.2 Plasticity Model

The details of the plasticity modeling may be found elsewhere [13, 25]. Briefly, kinematic hardening with Von Mises yield surface was used in this study. The material stress-strain response was considered stable and cyclic hardening or softening was considered.

An incremental, rate independent, classical plasticity model is used in this study. Kinematic hardening is employed to best simulate the anisotropy (Bauschinger effect) associated with reversed yielding. With this rule, the yield surface maintains it's original dimensions but translates in stress space during plastic staining [27].

The initial yield condition according to Von Mises is given by:

$$f(S_{ij}, S_{ij}^c) = [\tfrac{2}{3}(S_{ij} - S_{ij}^c)(S_{ij} - S_{ij}^c)]^{1/2} = \sigma_o \qquad (2)$$

where σ_o is the initial yield stress in tension (a constant). S_{ij} is the stress deviator given by:

$$S_{ij} = \sigma_{ij} - \tfrac{1}{3}\sigma_{kk}\,\delta_{ij} \qquad (3)$$

where σ_{ij} is the stress component vector and δ_{ij} is the Kronecker delta. S_{ij}^c represents the position of the center of the yield surface in deviatoric stress space due to work hardening. The center of the yield surface translates incrementally according to Ziegler's rule [28]:

$$\dot{S}_{ij}^c = d\mu\,(S_{ij} - S_{ij}^c) \qquad (4)$$

where $d\mu$ is a positive scalar to be determined. From the consistency condition, $d\mu$ is established as $H \cdot d\bar{\varepsilon}^p / \sigma_o$, where $H = d\bar{\sigma}/d\bar{\varepsilon}^p$ is the slope of stress-plastic strain curve in uniaxial tension.Bilinear stress-strain curve is often modeled where H = constant in kinematic hardening models. Drucker and Palgen [29] allowed H to vary a AJ_2^N (where A and N are constants and $J_2 = \tfrac{1}{2}S_{ij}S_{ij}$) to simulate stress hardening. This representation is incorporated into the finite element code.

The plastic strain increments are, based on Druckers postulate, in the direction of the outward normal to the yield surface. This flow rule is expressed as:

$$\dot{\varepsilon}_{ij}^p = d\lambda\,\partial f(S_{ij}, S_{ij}^c)/\partial S_{ij} \qquad (5)$$

where $d\lambda$ is a positive scalar during active plastic straining and zero for purely elastic responses [13]. The stress-strain curve (for time independent loading) studied has the following form:

$$\bar{\sigma}/\sigma_0 = (\bar{\varepsilon}^p/\bar{\varepsilon}^p_0)^n \qquad (6)$$

where σ_0, $\bar{\varepsilon}^p_0$ and n are yield stress, equivalent yield strain and strain hardening exponent respectively.

The constants A and N may be easily related to the usual parameters in a simple Ramberg-Osgood power-law formation (Equation (6)) by the expressions

$$N = (\frac{1}{n} - 1)/2 \qquad (7)$$

$$A = 3^N \varepsilon^p_0/(n\sigma_0^{1/n}) \qquad (8)$$

Another advantage of this type of stress-strain relation is its easy adaptation to much more complex constitutive behaviors. Previous studies except reference [25] have not considered strain hardening in the plasticity formulation. Frequently, the elastic perfectly plastic stress-strain response and the bilinear material response [13] have been adopted in many of the analytical models and in finite element work.

These constants are indicated in Figure 3 and describe the stress-strain response of Rene 95 at 1200 ^{o}F [30]. The stress strain curve described

by Equation (6) is shown in Figure 3 along with the experimental data. The correlation is very satisfactory.

2.2.3 Creep Model

Existing constitutive equations relevant to the analysis of inelastic behavior is classified under two categories: one is so called superposition model or classical model, in which the total strain rate is composed of time-dependent creep rate and time-independent elastic-plastic component. The other is the so called "unified constitutive models", in which unified inelastic strain can describe the time-dependent inelastic behavior of materials [31]. The latter equations are not widely used in FEM codes due to longer computer times. The classical model was used in the present study because of its simplicity and its ready adaptation to the plasticity model. In the present work the total stain rate is taken as sum of elastic, plastic and creep strain rate components ($\dot{\varepsilon}_{ij} = \dot{\varepsilon}^{e}_{ij} + \dot{\varepsilon}^{p}_{ij} + \dot{\varepsilon}^{c}_{ij}$) .

Steady state creep is used in the present research. The creep law is of the following form:

$$\dot{\bar{\varepsilon}}^{c}/\dot{\varepsilon}^{c}_{o} = (\bar{\sigma}/\sigma_{c})^{m} \ (1/s) \qquad (9)$$

where $\dot{\varepsilon}^{c}_{o} = 1\text{x}10^{-5}$ 1/s, m is the creep exponent, and σ_{c} is creep strength, and $\dot{\bar{\varepsilon}}^{c}, \bar{\sigma}$ denote equivalent creep strain rate and equivalent stress respectively. The creep strain components are given as:

$$\dot{\varepsilon}^{c}_{ij} = \frac{3}{2}\dot{\varepsilon}^{c}_{o}(\bar{\sigma}/\sigma_{c})^{m-1} S_{ij}/\sigma_{c} \qquad (10)$$

The stress-strain curve described by combination of equation (6) and (9) are shown in Figure 4a for different σ_c levels selected in this study. The stress-strain curves are given for a strain rate of $4x10^{-5}$ 1/s for all cases. It is noted that the stresses decrease appreciably when σ_c/σ_0 ratio approached 0.8.

The plasticity model employed in the finite element code was compared to result from ABAQUS and the agreement in strains was within 3% [5]. The results of creep strain change with time under constant load from this study and from ABAQUS are compared in Fig. 4b. The agreement for equivalent creep strains is within 0.5%.

When $\sigma_c > \sigma_0$, creep strain rates become significant at stresses above the yield strength. When $\sigma_c < \sigma_0$ the the creep rates can be also significant in the elastic regime. In the present research, σ_c/σ_0 ratios in the range of 0.8 to 1.3 were considered. The corresponding crack opening stress levels were established.

The normalization of the stresses with σ_c and σ_0 have several advantages. It is possible to use the results of this study to explain frequency and hold time effects on other materials when the S_{max}/σ_0, σ_c/σ_0 ratios are known. These non-dimensional quantities have a first order effect on crack opening levels. The influence of strain hardening exponent, n, and creep exponent, m, have also been studied. However, the effect of the exponents on the results is small compared with S_{max}/σ_0, σ_c/σ_0 effects.

2.3. BASIC RESULTS

Crack opening and closure levels under uniaxial zero to tensile loading with different hold times or different loading frequencies are

examined. Plane stress analysis is considered. Since high stresses and plastic and creep zones near the crack tip comparable to crack size are considered, plane stress analysis is much more representative of the constraint on the crack tip. The effects of duration of hold period, loading frequency and the creep law on crack closure levels will be presented. The plastic stress-strain relationship (Equation (2)) is maintained constant throughout this work.

The following output information was obtained: a) The crack opening and closure levels as a function of crack length. After a short transient period the crack opening and closure levels become stabilized. The stabilized levels are reported in this study. b) The crack tip displacement profiles, plastic zone and creep zone at maximum load prior to hold period, at maximum load after the hold period and at minimum load. c) The stress distributions ahead of crack tip and behind the crack. d) The variation of b) and c) with cycles. e) The stress strain history of a material point as the crack tip approaches, reaches, and passes it.

2.3.1 The Effect of S_{max}/σ_o

Crack opening stress, S_{open}, normalized by the maximum stress in the cycle is presented as a function of S_{max}/σ_o for the case of time independent loading in Figure 5. The results are presented for R = 0 case and reveal a decrease of S_{open}/S_{max} level with increasing maximum stress level in the cycle. The crack opening stress level, S_{open}/S_{max}, decreased from 0.7 to 0.55 upon an increase of S_{max}/σ_o ratio from 0.6 to 0.9. The important observation in Figure 5 is that the crack is closed during majority of the cycle. These results are consistent with the analytical work [6, 11, 13, 24, 25] and experimental work [3, 24]. For example, for the case [25], σ_o = 40

ksi, n = 0.19, E = 30,000 ksi (1070 steel properties), S_{open}/S_{max} was in the range 0.64 - 0.51 when the S_{max}/σ_o was in the range 0.6 - 0.9. The variation of crack closure levels with maximum applied stress is also indicated in Figure 5. The crack closure levels are consistently lower than crack opening levels, and the difference increases with increasing maximum stress level.

The effective stress range ratio, U, is defined as

$$U = \Delta S_{eff}/\Delta S = (1 - S_{open}/S_{max})/(1-R) \qquad (11)$$

and represents the effective portion of the stress range driving the crack. The term R in Equation (11) is the R-ratio and is equal to S_{min}/S_{max}. The effective stress ratios for the time independent case and for other cases, where σ_c/σ_o, m and t_h were varied, are summarized in Table 1 and will be discussed later. In Table 1, first row gives the S_{max}/σ_o levels in the range 0.5 to 0.9. Note that U_o is the time-independent effective stress ratio and is given as second row. The U values are given as italic. To read Table 1 consider the following example. The U value corresponding to σ_c/σ_o = 1.3, t_h = 300s, m = 5, S_{max}/σ_o = 0.6 is 0.37.

The crack growth rate as a function of effective stress intensity range (ΔK_{eff} = UΔK) is given as

$$da/dN = C\,(U\,\Delta K)^z \qquad (12)$$

where U ΔK is the effective stress intensity range, C and z are material constants. If elastic-plastic fracture mechanics parameters were used instead

of linear elastic fracture mechanics then the stress range would be replaced by the effective stress range similar to Equation (11).

2.3.2 The Effect of σ_c

The influence of different σ_c (Equation 9) on the changes in crack opening stress level is examined for a constant m (m = 5). The σ_c level was chosen in the range from 0.8 σ_o to 1.3 σ_o. The hold period was maintained constant at 300 seconds. The results are presented in Figure 6. It is evident that as the creep strain rates become more significant (σ_c decreases) the opening levels decrease and the effective stress range increases consistently. In engineering materials the σ_c level decreases as the temperature is increased. Therefore, these results are consistent with higher crack growth rates observed experimentally in materials as the temperature increases. The results are summarized in Table 1.

These results can be understood upon consideration of crack opening profiles at S_{max}/σ_o = 0.7 and 0.8. The crack opening displacements (δ) as a function of the distance behind the crack tip (r) are indicated in Figure 7a and 7b for the $\sigma_c = 1.3\sigma_o$ case. The crack length (a) includes half the notch width (c) and the crack size measured from the notch surface (l). Therefore, a = l + c. The results are shown at the beginning and conclusion of the hold period, and at minimum load. It is noted that the crack is partially closed at minimum load and an increase in COD occurs during the 300s hold period. The crack opening displacements for the 0.8 case are substantially larger than the 0.7 case. The crack opening displacements at maximum and minimum load under time independent loading conditions are given in Figures 7c and 7d as a comparison. The crack opening displacements for 0.7

and 0.8 cases are much lower compared to the cases with hold periods (Figures 7a, 7b).

2.3.3 Effect of Hold Period at Maximum Load

The hold period at maximum tensile load was chosen as 30 seconds, 90 seconds and 300 seconds, the loading time and unloading times are 5 seconds, respectively. The σ_c and m were held at 1.3 σ_0 and 5 respectively. The results are shown in Figure 8. Note that at intermediate stresses ($S_{max}/\sigma_0 < 0.6$) the 30 seconds and 90 seconds hold time has minimal effect on the results, however, the hold time effect becomes significant at high stresses ($S_{max}/\sigma_0 > 0.6$).

A better understanding of the results can be gained by examining the crack opening displacements for the $S_{max}/\sigma_0 = 0.8$ case. The crack opening displacements versus position behind the crack tip is indicated in Figure 9a for different hold time cases. The crack opening profiles corresponding to the conclusion of the hold period are given for all cases. Similar results were obtained for $S_{max}/\sigma_0 = 0.7$ case (Figure 9b). Note that the sensitivity of the crack opening displacements on hold time is lower for 0.7 case compared to 0.8 case.

2.3.4 The Effect of Creep Exponent, m

The effect of creep exponent on the results is shown in Figure 10. In this case σ_c was maintained at 1.3 σ_0. A higher creep exponent (m = 10) results in an increase in opening levels. The slope of S_{open}/S_{max} versus S_{max}/σ_0 curves in Figure 10 decreased with the increasing of creep exponent. This occurs because remote creep strains are smaller for m = 10

compared to m = 5 when $\sigma_c/\sigma_o > 1$. When $\sigma_c/\sigma_o < 1$, the higher m would result in higher creep strain rates. Comparison of Figure 8 and 10 indicate that a significant change in the creep exponent did not cause a wide variation of opening stress levels. All the baseline results given in Sections 2.3.1 through 2.3.4 are summarized in Table 1.

2.3.5 The Effect of Loading Frequency

The loading frequency for continues cycling cases was chosen as 0.003 Hz (loading time + unloading time = 310 seconds) and 0.025 Hz (loading time + unloading time = 20 seconds), therefore the time periods for one cycle are the same as hold time cases. The σ_c and m were held at 1.3 σ_o and 5 respectively. The effect of frequency on crack opening levels is shown in Figure 11. When the applied load increases, the crack opening stress for the case of 0.003Hz decreases faster than that of the 0.025 Hz case. The slopes of S_{open}/S_{max} versus S_{max}/σ_o curves are lower compared with the hold time effect curves on Figure 8. This is because majority of creep strain developed at maximum applied load for hold time case, and the high creep rates result in lower crack opening levels.

2.3.6 The Effect of Waveform Shape

To examine the effect of the shape of loading waveform, fast loading -slow unloading cases (T_{load} = 5, T_{unload} = 305 seconds) and slow loading - fast unloading cases (T_{load} = 305, T_{unload} = 5 seconds) were studied. The loading frequency was held constant at 0.003 Hz. The results are shown on Figure 12.

The slopes of S_{open}/S_{max} versus S_{max}/σ_o curves for all three continues cycling cases are very similar, which are lower than the slope for hold time cases. The slow loading-fast unloading cases result in the lowest opening stress levels, while the fast loading-slow unloading cases result in the highest opening levels. The stress-strain history of a material point at the crack line for slow loading-fast unloading and fast loading-slow unloading cases are shown in Figures 13a and 13b, respectively. This material point is located 13 elements from the initial crack tip and is reached by the crack tip in 13 cycles. During the loading portion, 19 steps are needed from minimum load (Step #720) to yield strength level (Step #739) and 11 steps from the yield stress level to maximum load (Step #750). During unloading, the stress decreases very rapidly from maximum to Step #753 which has similar stress level to Step #739. Since the slow loading-fast unloading cases result in higher creep strains in the tensile direction, the crack opening load is lower for these cases. The cases which loading and unloading times are equal result in tensile creep strains which are higher than that of fast loading-slow unloading cases and smaller than that of slow loading-fast unloading cases. The results discussed in Sections 2.3.5 and 2.3.6 are summarized in Table 2.

2.3.7 Development of Plastic versus Creep Zones

The plastic zone sizes at maximum load (forward plastic zone) and minimum load (reversed plastic zone) for the zero hold time case are indicated in Figures 14a and 14b. The horizontal and vertical scales are similar in these cases. Note that the reversed plastic zone is smaller, and extends behind the crack tip. When hold times are incorporated within the

cycle, a creep zone develops as shown in Figures 15 for the same maximum stress levels and crack length considered in Figures 14.

In several studies creep zone was defined as the boundary where the creep and elastic strains are equivalent. Alternately, a creep zone could be defined as the region over which the creep strain changes by a specific strain level. In the present work, two creep zones are defined as the regions where the the equivalent creep strains reach 0.005 and 0.01, respectively. The 0.005 and 0.01 creep strain contours are indicated in Figures 15a and 15b. Note that the creep zone can grow much more rapidly than the plastic zone depending on the creep law and the applied stresses. In certain cases the creep zones reached the outer edge of the specimen after many cycles as shown in Figure 16 for S_{max}/σ_o = 0.8 case. The plastic zones, however, were much more localized (Figures 14a, 14b)

2.3.8 Stress-strain History Along the Crack Line

The difference between the continuous cycling without creep and cycling with hold time cases could be recognized by examining the results shown in Figures 17a, 17b, 17c, and 17d. The stresses and strains at a single material point (x = 0.67 mm = constant) are illustrated as the crack approaches this point, reaches it and then passes this point. The crack tip reaches the material point in five cycles. As the crack tip approaches the material point, the stress and strain ranges at the material point increases, and stresses at crack tip approach completely reversed (R = -1) conditions. Once the crack tip passes the material point, the material point sustains compressive stresses upon contact of crack surfaces.

Both S_{max}/σ_o = 0.6 and 0.7 cases with hold time (Figures 17a, 17b) and without hold time (Figures 17c, 17d) were considered to illustrate stress and strain variation during cycling. In these cases the material point is reached in eight cycles.

In S_{max}/σ_o = 0.6 case, the maximum stress at the material point decreases during the hold period as the crack tip is approaching this point (Figure 17a). At the same time, there is an attendant increase in strain during the hold period. Once the crack tip reaches the material point the strain increases rapidly while the stress remains relatively constant. The crack opening displacements increase during the hold period. At higher stress levels (S_{max}/σ_o = 0.7) the creep strain in the vicinity of the crack tip increases at a higher rate than the 0.6 case. There is a slight increase of stress at crack tip during the hold period. As the mean strains increase, changes in geometry near the crack tip cause an elevation of stress. In the 0.7 case the constraint on the crack tip region is smaller and the material away from the crack as well as in the vicinity of the crack undergoes higher creep strain rates.

Note that the mean tensile strain at the material point increases with cycles until the crack tip reaches this point. This verifies that simulation of history of cyclic crack growth is necessary to establish the crack tip parameters and crack opening stress levels.

To further illustrate the creep strain changes, the history at material point x = 0.712 mm is given in Figures 17e, 17f. In this case, the stress-strain point at the beginning of the hold period is indicated with a dark period (".."). It is found that stress decreases as the crack tip is approaching the

material point, and stress remains constant or increases as the crack tip reaches the material point.

2.3.9 Stress Distribution at Maximum and Minimum Applied Stress

The normalized stress distribution, σ_{yy}/σ_o, at maximum load (before and after hold period) and at minimum load are studied along the crack (Figures 18a and 18b). In the case of S_{max}/σ_o = 0.6 (Figure 18a), the stress relaxation ahead of the crack tip is evident during the tensile hold period. At minimum applied load compressive stresses behind the crack exceed the yield strength. The contact zone behind the crack does not extend all along the crack length. Therefore, the compressive stresses decrease as the notch surface is approached.

The stress distributions for S_{max}/σ_o = 0.8 case is indicated in Figure 18b. There is a slight increase of stress at crack tip during hold period, while at a distance ahead of the crack tip, stress relaxation occurred. The increase in stress at crack tip is due to changes in finite geometry of the crack tip regions which was also evident in Figure 17c. High compressive stresses at minimum load developed for 0.8 case. However, the contact zone behind the crack over which compressive stresses act is rather narrow in 0.8 case compared with 0.6 case.

2.4. Discussion

In high temperature creep-fatigue studies "life to certain crack size" or "crack growth rates" are established [15-20]. These experiments are often conducted at low frequencies and/or with hold periods. In many cases the governing stress-strain relation and the creep law (primary or steady state)

are not included. It is evident from the present research that this information is necessary to interpret elevated temperature crack growth results and to develop a life prediction methodology.

Experimental crack growth data on Rene 95 generated by General Electric Company are shown in Figure 20. The results of tests with hold periods of 300 seconds and without hold time are given in this figure. The experiments were performed on K-Bar geometry which is a plate with an EDM notch in the center as a crack starter. In these experiments, the applied stress level was in range 0.5 to 1.0 of yield strength. The crack growth rate with 300 seconds hold time are approximately a factor of 10 higher than the case of continuous cycling without creep. The predicted data using closure modified stress intensity range is also shown on this figure. For Rene 95, σ_c/σ_o = 1.3 were used and stress-strain properties were given in Figure 3. The difference between the experimental crack growth data and the predicted data is very small.

Saxena [16,17] published crack growth data on A470 steel obtained at different hold time periods (5 seconds and 50 seconds) and different frequencies (range from 0.02 Hz to 5 Hz). The creep law and yield strength data were given but the applied load level information was not available. For the A470 steel at 538 ^{o}C σ_c/σ_o ratio was 1.2. The corresponding crack opening levels are readily available from our study and prediction of Saxena's data using S_{max}/σ_o=0.8 data was favorable.

Wu's work [32] on 304 stainless steel was conducted at S_{max}/σ_o ratio of 0.9. Creep constants for this material at 649 ^{o}C were m = 11.5 and σ_c/σ_o = 1, σ_o = 34 ksi. Experiments at different frequencies (0.05 Hz, 10 Hz) and under tensile hold periods of 1 min and 10 min were conducted.

Microstructural examination of material indicated that crack growth was transgranular in all cases except 10 min hold case where both intergranular/transgranular crack growth was observed. The 0.05 Hz and 10 Hz tests result is the order of x20 of that 1 min hold time case. A further x3 increase in damage rates developed for 10 min hold case compared to 1 min hold case.

The simulations indicate that higher crack growth rates are expected with increasing of maximum stress level, S_{max}, and increasing hold periods, t_h. These effects as well as the material properties are incorporated in the effective stress ratio, U. The dependence of U on material and test variables can be obtained by fitting curves to the results obtained from the finite element analysis. It is noted that at long hold periods U approaches 1 and the hold period effect saturates. This saturation time is strongly dependent on S_{max}/σ_o ratio and material properties. Based on the finite element results, the variation of U with applied stress levels and creep properties is represented in the following form:

$$U-U_o=(1-S_{max}/2\sigma_o)\{1-\exp[\gamma(S_{max}/\sigma_o)^m t_h \dot{\varepsilon}_o^c/(\sigma_c/\sigma_o)^m]\} \qquad (13)$$

where γ is dependent on specimen geometry constant and equals to $-6x10^3$ for CCT specimen used in this study. The meaning of other terms were given early (see Nomenclature). The plot of U levels based Equation 13 versus σ_c/σ_o is given in Figure 20. It noted that the dimensionless parameter within the exponential represents a measure of remote creep strain change per hold period, t_h. In the limit as σ_c/σ_o -> 0, the U

approaches 1. Most of the F.E.M results are predicted very closely by Equation 13 which is shown as dashed line.

Plane stress analysis was performed in this study and plane stress is relevant to crack growth outside small scale yielding. Plane strain analysis would be relevant at low stresses where the plastic and creep zones are small compared to crack size and specimen thickness. In most cases of high temperature fatigue crack growth, high crack growth rates are studied and the plane stress conditions is more realistic in simulating this behavior.

Steady state creep properties have been used in the analysis. The use of transient creep properties only influence short hold time results and the transient opening levels during the first few cycles of crack advance. However, the stabilized opening levels would be more likely dictated by the steady state creep analysis.

It is noted that the mechanisms of oxidation at crack tips has not been considered in this research. Depending on the alloy and temperature these mechanisms may be enhanced during the crack tips, the closure mechanism studied will be the most dominant factor on crack growth rates.

2.6. Conclusions

1. Crack closure is significant under time dependent fatigue loading and influences the fatigue crack growth rate.

2. Crack closure (hence crack growth rate) is a strong function of hold period. The crack opening levels decreased (hence U increased) with period. The results depend also strongly on σ_c/σ_o ratio. Lower σ_c/σ_o results in increase in effective stress ratio, U.

3. Based on the crack closure analysis, the material and loading conditions, which give the highest values of $U-U_o$, hence the highest effect on crack growth rates were identified.

4. The present results provided a working model of creep law dependent crack closure levels and fatigue-creep crack growth rates.

3.FATIGUE CRACK CLOSURE IN PLANE STRESS AND PLANE STRAIN

3.1 Background

It is now widely recognized that fatigue crack closure plays a major role in determining the fatigue crack growth rate of materials. Numerous researchers have experimentally and numerically verified and used crack closure concept to predict fatigue crack growth. The closure results have been obtained over a wider range of specimen geometries and test conditions. However, values of crack closure presented in the literature have been inconsistent, they are strongly dependent on specimen geometry variations, including the shape of specimen, crack length, in-plane size, and specimen thickness.

A three dimensional specimen geometry is usually simplified to either plane stress condition when the thickness of specimen is well thin, or plane strain condition when the thickness is very large. In plane stress case, the stresses in z-direction (thickness direction) are zero while strains in z-direction are not zero. It is not difficult to discover that the contraction in z-direction provides the material transfer to crack surface to cause the crack closure. Material transfer mechanism is more complicated for plane strain case because there in no contraction in z-direction. Fleck and Neuman [33] showed that plasticity induced crack closure can occur under plane strain condition with their finite element work. However, plane strain closure levels decreased with increasing crack length in their analyses which is not consistent with experimental work. Lalor, Sehitoglu [13] and McClung [14] reported results of crack opening levels under plane stress and

plane strain conditions. There is a significant difference in closure levels between these conditions.

This research provides further understanding of insight into crack closure behavior under plane stress and plane strain conditions and lends support that crack closure can indeed occur under plane strain conditions. Results of crack opening load levels from a compact tension specimen is reported. Inelastic stress-strain fields near crack tip, stress-strain response along the crack line during cycling, and plastic zone as well as the crack displacements are reported. Mechanisms of material transfer to crack surface have been discussed, inelastic strain accumulation in x (transverse, along crack growth) direction and material transfer in x- direction have been as closure mechanism in plane strain.

3.2 Finite Element Formulation

A standard one-inch compact tension (CT) specimen is used in this study. The finite element mesh, which includes 803 elements and 876 nodes, is shown in Figure 21a. The x-y directions are indicated in the diagram, the z-direction is the thickness direction. Only half of the specimen is considered due to symmetry. Two initial crack lengths, a = 0.3W and a = 0.6W, are considered, where W is the width of the specimen. A magnified view of near crack tip is shown in Figure 21b. The element length near crack tip, Δa, is 0.00075W. This size is fine enough to capture forward and reversed plastic zone at the crack tip for the cases considered. Mode I load is applied to the specimen in this study.

The material stress-strain behavior was assumed to be bilinear with an initial yield stress, σ_o, of 430 MPa, and Young's modulus, E, of 205.4 GPa.

Two plastic modulus levels, H = 0.07E and H = 0.01E were considered. According to the elastic-perfectly plastic analysis, a lower bound limit load, P_o, for compact tension specimen is calculated as [34]:

$$P_o = 1.071\,\beta\, b\, B\, \sigma_o \tag{14a}$$

for plane stress and

$$P_o = 1.455\,\beta\, b\, B\, \sigma_o \tag{14b}$$

for plane strain. Where b = W-a, B is thickness of the specimen, and β is a function of a/W

$$\beta = [(2a/b)^2 + 4a/b + 2]^{1/2} - 2a/b - 1 \tag{14c}$$

The reduced integration modification by Nagtegaal, Parks and Rice [35] has been incorporated in the formulation to avoid mesh locking problems in plane strain case. The modified strain increment in plane strain finite element code is defined as following:

$$\dot{\varepsilon}_{ij} = \frac{1}{2}(\dot{u}_{i,j} + \dot{u}_{j,i}) + \frac{1}{3}\delta_{ij}\left(\int_{V_\alpha} \dot{u}_{k,k}\, dV_\alpha - \dot{u}_{k,k}\right) \tag{15}$$

where $\dot{u}$ is displacement increment, V_α is the volume of the α^{th} element.

3.3 Basic Results

3.3.1 The Effect of Applied Load

The normalized crack opening load, $P_{open}/P_{max,}$ versus normalized applied load, $P_{max}/P_{o,}$ for different H/E ratios under plane stress conditions are shown in Figure 22. Crack opening levels for H/E=0.01 cases are higher at low applied load and lower at high applied load. Figure 23 represents the comparison of crack opening levels for plane strain with plane stress for H/E=0.01 cases. The crack opening levels for plane strain are lower because of the higher constraint. The crack opening levels for both plane strain and plane stress decrease rapidly to zero with the increasing of applied loads. The summary of crack opening load levels is shown in Table 3.

The crack tip stresses are very high for the cases with H/E=0.07 under plane strain. When applied load level reaches $0.4P_o$, the stress levels near crack tip far exceed the fracture stress of engineering materials.

Results of crack opening levels for a/W=0.3 are very similar with a/W=0.6 at low applied loads. When applied load is higher than $0.4P_o$, the extensive yielding occurs at the hole region where remote loading is applied. This yielding has effect on the crack opening result. The applied load is much lower because the reference load is much lower for a/W=0.6 case and the yielding does not occur at the hole region. Therefore, F.E.M results for a/W=0.6 case is reported.

In this study, crack opening levels for P_{max}/P_o ratios in the range of 0.1 to 1.0 are studied. P_{max}/P_o = 0.2 and 0.5 cases will be discussed in depth in next sections. The corresponding maximum stress intensity levels were 13 ksi$\sqrt{in}$ (P_{max}/P_o = 0.2) and 32 ksi$\sqrt{in}$ (P_{max}/P_o = 0.5) for plane stress case, 17 ksi$\sqrt{in}$ (0.2) and 43 ksi$\sqrt{in}$ (0.5) for plane strain case.

3.3.2 Stress-Strain History Along Crack Line

The stresses and strains for x and y directions at a material point along the crack line were monitored throughout the entire load history, as the crack tip approaches, reaches and passes the location of the material point. The lower left integration point in Element #282 is referred to as material point. Element #282 is the third element away from the original location of the crack tip. At the first cycle, the crack tip is at Node #295 (Figure 26), which is three elements away from the material point. The load history is shown in Figures 24a and 24b for P_{max}/P_o = 0.2 and 0.5. Every cycle requires 40 increments for most of the cases studied in this research. But for P_{max}/P_o = 0.5 plane strain case, 80 increments are needed to improve the resolution in determining the crack opening load level.

The stress-strain behavior in y and x directions at lower left integration point of Element #282 as the crack advances are indicted in Figures 25a and 25b. The applied load is P_{max}/P_o = 0.2 and the case is under plane strain condition. The vertical axis is normalized by stress over yield strength. The crack is advanced at Step #21, 61, 101, 141 etc. The inelastic strain for the material point is less than 0.001. Upon subsequent cycling, gradual accumulation of inelastic strains in positive y and negative x directions develop simultaneously as the crack approaches the material point. At Step #100, Node #314 is the crack tip and the material point is reached, the stress levels in x and y directions reach their maximum values. At Step #140 the crack tip has passed the material point and stresses at the material point are lowered. The series of crack opening and closure events are summarized in Table 4. Note that the crack tip opens at Step #126, therefore, the P_{open}/P_{max} ratio is 0.3 after four cycles. However, the crack

opening load is not stabilized after four cycles, and the crack opening loads increase to their steady state levels (P_{opcn}/P_{max} -> 0.31) with increasing number of cycles.

For P_{max}/P_o = 0.5 plane strain case, the stress-strain response for x and y directions is illustrated in Figures 27a and 27b, and crack opening and closure information is given in Table 5. Higher Crack tip inelastic strain and more significant mean stress decrease with cycles were observed compared with P_{max}/P_o = 0.2 case. The loading history effect on the strains at crack tip is much stronger for this case as the material point is approached. Strain accumulation approaching 0.02 has been observed in both x and y directions. The tensile stresses at the material point decrease as crack tip approaches is. The stresses increase once the crack tip passes the material point. This occurs for P_{max}/P_o ratios above 0.4 under plane strain condition.

Figures 28a and 28b show the stress-strain behavior at Element #282 under plane stress condition at y and x directions for P_{max}/P_o = 0.2, while Figures 29a and 29b for P_{max}/P_o = 0.5. The strain accumulation in x direction is not observed. The stresses near the crack tip are lower compared to plane strain. In these cases the tensile stress decreases once the crack tip passes the material point. The crack opening load levels in these cases are significantly higher than the plane strain case.

3.3.3. Stress Strain Fields Near the Crack Tip

Figures 30a and 30b show the normalized stresses distribution, σ_{yy}/σ_o and σ_{xx}/σ_o ahead of the crack at maximum load for plane stress and plane strain conditions, respectively. The applied load is P_{max}/P_o = 0.2. For a

typical case of CT specimen, σ_{yy}/σ_0 decreases from maximum value at the crack tip to negative at the edge of the specimen; σ_{xx}/σ_0 decreases from maximum to zero. Figures 30c and 30d indicate the stress fields near the crack tip. Both σ_{xx} and σ_{yy} near crack tip for plane strain are much higher than that for plane stress.

It is well known that the severe stress concentration at the crack tip leads to triaxial stress states with significant hydrostatic components. The associated constrains on deformation will vary with specimen thickness, proximity to the specimen surface, and distance from the crack tip. However, a two-dimensional analysis can achieve this effect by modeling the entire plate as under the influence of plane strain. Table 6 and 7 indicate the summary of stresses, strains, and back stresses at maximum and minimum load when the crack tip approaches the material point, reaches it and passes it for P_{max}/P_o = 0.2 and 0.5 cases. The H/E ratio is 0.01. The incompressibility condition is satisfied for the plastic strain components such that the summation of plastic strain components is zero. α_x, α_y and α_z refer to back stress components. Due to the low hardening modulus the back stresses are small fraction of the stress components compare to the cases where H/E = 0.07. Note that the material point also undergoes shear stress and shear strain but they are not included in the Tables.

3.3.4 Plastic Zone at Maximum and Minimum Load

Figures 31a and 31b represent the forward (at maximum load) and reversed (at minimum load) plastic zone at a common crack length (a/W = 0.615) for plane stress, and Figures 32a and 32b for plane strain under $P_{max}/P_o = 0.5$.

Plastic zone is butterfly-shaped for plane strain case and lobe-shaped for plane stress. However, the plastic zone is very small compared to the width of the specimen. For $P_{max}/P_o = 0.5$ plane strain case, the ratio of plastic zone over specimen width, r_p/W, is 0.07 for forward plastic zone and 0.02 for reversed plastic zone. The plastic zone is small compared to the crack size, too. Therefore the cases studied in this research can be considered as under small scale yielding condition.

For $a/W = 0.3$ case, the plasticity occurs at the hole region (where load is applied) when the applied load reaches $P_{max}/P_o = 0.4$. The plastic zone at the hole region is larger than that at the crack tip. This plastic zone in the hole region has some effect on the P_{open}/P_{max} results. For $a/W = 0.6$ case, there is no plastic zone near the hole, but plastic deformation occurs at the edge of the specimen due to the compressive stress when applied load is higher than $P_{max}/P_o = 0.8$. It should be note that the mesh near the edge of the specimen is not fine enough, therefore, the plastic zone shape is only approximate.

3.3.5 Crack Opening Displacement

The COD at maximum and minimum load for $P_{max}/P_o = 0.5$ plane strain case after three cycles is indicated in Figure 33a. In the x-axis the distance behind crack tip, r, which extends from 0 to 0.18 inches, is indicated. In this case the crack tip opens in the second increment of the loading and the steady state crack opening load level is $P_{open}/P_{max} = 0.1$. The crack contact zone is limited to one element behind the crack tip. The region near the crack tip is shown in Figure 33b, and r extends from 0 to 0.045 inches. The COD at maximum and minimum load for $P_{max}/P_o = 0.5$

plane stress case is indicated in Figures 34a and 34b. The region of contact crack surfaces extends three elements behind the crack tip. Note that the fatigue contact region is very small, therefore the initial crack size (stationary crack size) does not have a bearing on the results.

The displacement in x direction, which is defined with respect to the current position of the crack tip, is shown in Figure 35 for both plane stress and plane strain condition at maximum load. The applied load, P_{max}/P_o, is 0.5. The displacement is positive ahead of the crack tip, and is negative behind the crack tip. This means that with respect to the edge of the specimen, the crack is extended (in transverse direction) by the application of load.

The displacement near crack tip for the case of plane strain is shown in Figure 36a for a fatigue crack. The displacement in x direction is negative along the initial (stationary) crack, and is positive along the fatigue crack. Since stresses are very high near the crack tip, the magnitude of the negative plastic strain in x-direction is higher than the positive elastic strain in x direction (See Table 7). All 18 nodes behind the crack tip have positive displacement in x direction after 20 loading cycles due to this negative plastic strain. The displacement in x-direction near crack tip for plane stress Pmax/Po=0.5 case after 20 cycles is shown in Figure 36b. This displacement along the fatigue crack is negative, and its magnitude is smaller than the plane strain case.

The schematic profile of crack surfaces during a loading cycle is illustrated in Figure 37. Note that the left side pictures indicated the crack profile under plane strain condition, the right side ones indicate the crack profile under plane stress condition. At maximum load, the crack

displacement for plane strain is higher for plane stress (a). During unloading, crack surfaces come to contact at crack tip first for plane stress case, and discontinuous crack closure occurs in plane strain or crack closure occurs behind the crack tip (b). At minimum load, only a part of fatigue crack surfaces come to contact for plane strain, however, the contact distance extends all along fatigue crack length for plane stress (c). When applied load reaches the opening load level (d), the crack opens. The displacements in x-direction is significant for plane strain, (consistent with the blunting effect observed in plane strain), where displacements in x-direction for plane stress are small. The crack is advanced one element size at maximum load (e).

The results have been checked against ABAQUS Finite Element Code for the stationary crack cases, the displacements in x and y direction between our code and ABAQUS agree within 2%. The displacements are compared in Table 8.

3.4 Discussion

As the crack advances, the material is transferred to crack surfaces. An angled view of the crack plane is indicated in Figure 38. The x-y-z direction are indicated as well as the r direction defined as a-x. The location of crack front is where r=0. The arrows indicate the motion of material upon crack advance. In plane stress case contraction in z-direction develops and the material at crack front (dashed region) is transferred into crack flanks. In plane strain case, the contraction in z-direction is zero, or total strain in z-direction is zero. This material does not contribute to crack closure. However, an alternate mechanism involving contraction of

material in x-direction at crack front provides material that would enter crack surfaces and cause crack closure. The crack closure due to x-contraction is operative primarily in plane strain but it does exist to a lesser extent in plane stress. This contraction is consistent with negative strain accumulation in x-direction shown in Figures 26b and 27b.

The plane stress and plane strain conditions described represent condition operating at the surface and in interior of a cracked body respectively. Therefore, material transfer to crack flanks at the specimen surface and in the interior would be different. Bulk closure measurements represent a combination of plane stress and plane strain cases, with plane strain conditions dominating when the plastic zone size with respect to specimen thickness is small. The region, over which the contraction in x-direction develops in plane strain, extends over the reversed plastic zone.

Stable crack opening levels for compact tension specimen are lower than center cracked tension specimen for the same ΔK level. This may be readily attributed to the lack of residual displacements over the majority of the crack in CT case. For CCT specimen, the plastic zone is much larger than CT case, it is large compared to the size of the specimen. Therefore, the cases studied for CCT were considered as outside small scale yielding region.

The results demonstrate that remote measurement techniques of crack closure such as clip gages, and back face strain gages would have limitations in determination of crack opening and crack closure loads. The contact zone is a very small fraction of the total crack size particularly for plane strain cases. Only direct measurement of crack tip displacements would capture the true crack opening and closure load levels.

Blom and Holm [36] reported their work on finite element analysis of CT specimen. They reported the crack opening load was P_{open}/P_{max} = 0.3 for plane strain and and P_{open}/P_{max} = 0.45 for plane stress case. Their P_{max}/P_0 ratio was 0.2 for plane stress and 0.43 for plane strain case. These results are in qualitative agreement with results reported in this study. Stress-strain behavior near crack tip is not available in their study therefore a direct comparison of results can not be made at this time.

3.5. Conclusions

1. In plane strain, mechanism of material transfer to crack surfaces through transverse (x-direction) contraction of material at crack tip is proposed. Inelastic strain accumulation in x-direction confirms the presence of this mechanism.
2. In plane stress, crack closure occurs due to a mechanism of material transfer to crack surfaces through thickness (z-direction) contraction.
3. Crack opening load levels of the compact tension specimen for plane strain and plane stress cases have been determined for R=0 loading. The normalized crack opening levels decrease with increasing maximum load level in both plane stress and plane strain cases and plane strain closure levels are lower.
4. Understanding of stress-strain history near crack tip is relevant to understanding crack growth mechanisms, and to determination of crack closure behavior. The results demonstrate these stress and strain fields are multiaxial .

Table 1 Summary of Baseline Effective Stress Ratios U and U_o for Different S_{max}/σ_o, σ_c/σ_o, (–>1 denotes approaching unity)

		S_{max}/σ_o				
		0.50	0.60	0.70	0.80	0.90
U_o +		*0.30*	*0.30*	*0.35*	*0.40*	*0.45*
	σ_c/σ_o=0.85	*0.55*	*0.70*	*–>1*	*–>1*	*–>1*
	1.00	*0.40*	*0.60*	*–>1*	*–>1*	*–>1*
t_h=300	1.15	*0.30*	*0.50*	*0.75*	*–>1*	*–>1*
m=5.	1.30	*0.30*	*0.37*	*0.55*	*0.75*	*–>1*
	1.60	*0.30*	*0.30*	*0.40*	*0.55*	*0.66*
m=5	t_h=30s	*0.30*	*0.35*	*0.38*	*0.43*	*0.52*
σ_c/σ_o=1.3	90s	*0.30*	*0.36*	*0.40*	*0.50*	*0.65*
m=10	t_h=30s	*0.30*	*0.30*	*0.36*	*0.41*	*0.45*
σ_c/σ_o=1.3	90s	*0.30*	*0.30*	*0.37*	*0.44*	*0.50*
	300s	*0.30*	*0.30*	*0.38*	*0.48*	*0.65*

+ U_o = Time Independent Effective Stress Ratio

Table 2 Summary of Effective Stress Ratios for Different Loading Frequencies and Unloading Time Cases

	S_{max}/σ_o			
	0.60	0.70	0.80	0.90
t_{load}=20, t_{unload}=20	*0.37*	*0.40*	*0.44*	*0.50*
t_{load}=155,t_{unload}=155	*0.38*	*0.45*	*0.53*	*0.66*
t_{load}=5, t_{unload}=305	*0.37*	*0.43*	*0.52*	*0.63*
t_{load}=305, t_{unload}=5	*0.40*	*0.47*	*0.55*	*0.67*

Table 3 Summary of Crack Opening Load Levels for CT Specimen under Different Conditions

	P_{max}/P_o					
	0.20	0.40	0.50	0.60	0.80	1.00
plσ, H/E=0.07	*0.52*	*0.43*	/	*0.30*	*0.28*	*0.23*
plσ, H/E=0.01	*0.58*	*0.55*	*0.50*	*0.42*	*0.27*	*0.14*
plε, H/E=0.01	*0.31*	*0.24*	*0.10*	*0.05*	*−>0*	*−>0*

Table4 Series of Crack Opening and Closure Events for $P_{max}/P_o = 0.2$ Plane Strain Case

Step #	Status
86	Node #302 open, Node #314 becomes the crack tip
101	Node #314 released, but closes immediately
117	Node #302 closed, Node #302 becomes the crack tip
124	Node #302 open, Node #314 becomes the crack tip
126	Node #314 open, crack tip passes Element #282
157	Node #302 closed, Node #314 still open, discontinues crack closure
158	Node #314 closed ,crack tip is at Node #302

Table 5 Series of Crack Opening and Closure Events for $P_{max}/P_o = 0.5$ Plane Strain Case

Step #	Status
162	Node #302 open, Node #314 becomes the crack tip
201	Node #314 released, but closes immediately
241	Node #314 open, crack tip passes Element #282

Table 6 Summary of Stresses, Strains, Back Stresses at Maximum and Minimum Load as the Crack Approaches, Reaches and Passes the Material Point ($P_{max}/P_o = 0.2$)

	Max. Load	Min. Load	Max. Load	Min. Load	Max. Load	Min. Load
step#	60	80	100	120	140	160
σ_x	109[+]	-26	111	-57	91	-24
ε_x	0.0013	-0.0009	0.0002	-0.0022	-0.0020	-0.0031
ε_x^p	0	0	-0.0006	-0.0006	-0.0029	-0.0029
α_x	0.06	0.06	0.8	0.8	4.3	4.6
σ_y	150	7	174	-32	116	-45
ε_y	0.0032	0.0006	0.0051	0.0010	0.0061	0.0020
ε_y^p	0.0001	0.0001	0.0015	0.0015	0.0041	0.0031
α_y	0.08	0.08	1.2	1.2	6.5	6.3
σ_z	80	-3	112	1	99	-11
ε_z	0	0	0	0	0	0
ε_z^p	-0.0001	-0.0001	-0.0009	-0.0009	-0.0012	-0.0003
α_z	0.04	0.04	0.7	0.7	5	5.5

+ Stresses and back stresses are given in ksi

Table 7 Summary of Stresses, Strains, Back Stresses at Maximum and Minimum Load as the Crack Approaches, Reaches and Passes the Material Point ($P_{max}/P_o = 0.5$)

	Max. Load	Min. Load	Max. Load	Min. Load	Max. Load	Min. Load
step#	120	160	200	240	280	300
σ_x	124	-100	74	-124	239	2
ε_x	-0.0026	-0.0054	-0.0155	-0.0149	-0.0108	-0.0093
ε_x^p	-0.0032	-0.0041	-0.0153	-0.0141	-0.0139	-0.0095
α_x	3.1	2.5	6.1	3.2	59	60
σ_y	197	136	152	-189	250	-7
ε_y	0.0089	0.0014	0.0200	0.0088	0.0193	0.0078
ε_y^p	0.0051	0.0043	0.0168	0.0125	0.0157	0.0080
α_y	4.7	4.1	12.4	8.4	67	63
σ_z	153	-65	113	-143	242	-1
ε_z	0	0	0	0	0	0
ε_z^p	-0.0019	-0.0002	-0.0015	0.0017	-0.0032	0.0007
α_z	3.3	3.3	8.9	6.4	61	61

Table 8. Comparison of Displacements Along a Stationary Crack Line of This Study and ABAQUS (Displacements are in inches)

($pl\varepsilon$, P_{max}/P_o=0.2)

	ABAQUS		This Study	
Node+	u_x	u_y	u_x	u_y
233	-2.62e-4	4.02e-4	-2.6e-4	4.01e-4
238	-2.59e-4	3.35e-4	-2.6e-4	3.34e-4
244	-2.56e-4	2.85e-4	-2.6e-4	2.85e-4
251	-2.52e-4	2.27e-4	-2.5e-4	2.26e-4
258	-2.45e-4	1.47e-4	-2.5e-4	1.46e-4
265	-2.40e-4	9.35e-5	-2.4e-4	9.14e-5
287	-2.30e-4	4.93e-5	-2.3e-4	4.36e-5

($pl\varepsilon$, P_{max}/P_o=0.5)

	ABAQUS		This Study	
Node+	u_x	u_y	u_x	u_y
233	-6.59e-4	1.04e-3	-6.6e-4	1.05e-3
238	-6.51e-4	8.70e-4	-6.5e-4	8.78e-4
244	-6.41e-4	7.47e-4	-6.4e-4	7.55e-4
251	-6.27e-4	6.04e-4	-6.3e-4	6.11e-4
258	-5.98e-4	4.17e-4	-6.0e-4	4.23e-4
265	-5.75e-4	3.17e-4	-5.8e-4	3.22e-4
287	-5.40e-4	2.03e-4	-5.4e-4	2.15e-4

($pl\sigma$, P_{max}/P_o=0.2)

	ABAQUS		This Study	
Node+	u_x	u_y	u_x	u_y
233	-2.17e-4	3.27e-4	-2.2e-4	3.25e-4
238	-2.15e-4	2.73e-4	-2.1e-4	2.71e-4
244	-2.13e-4	2.33e-4	-2.1e-4	2.32e-4
251	-2.10e-4	1.86e-4	-2.1e-4	1.85e-4
258	-2.04e-4	1.23e-4	-2.0e-4	1.22e-4
265	-2.02e-4	8.11e-5	-2.0e-4	8.02e-5
287	-1.99e-4	4.47e-5	-2.0e-4	4.32e-5

+ All nodes are behind crack tip

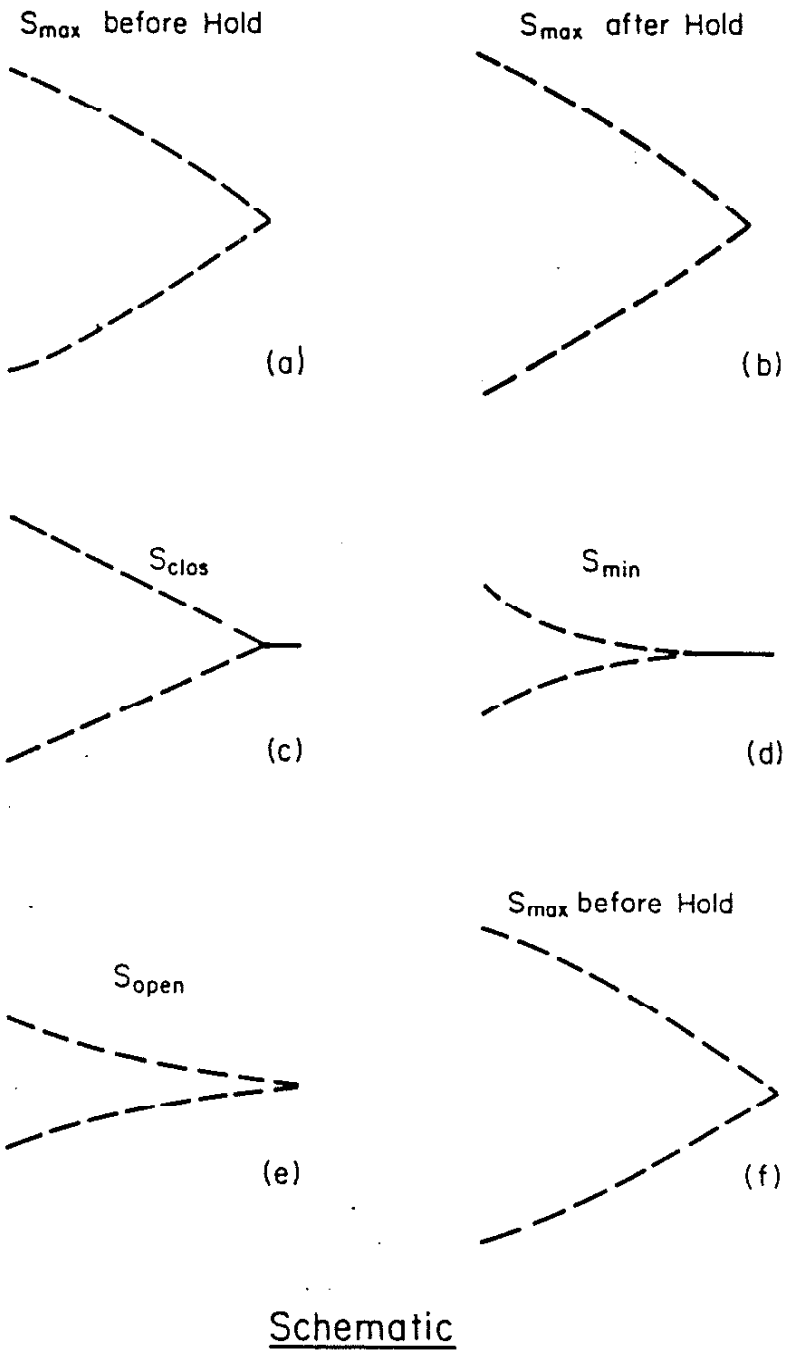

Figure 1a Schematic of crack displacement profiles during time-dependent cyclic loading with tensile hold periods

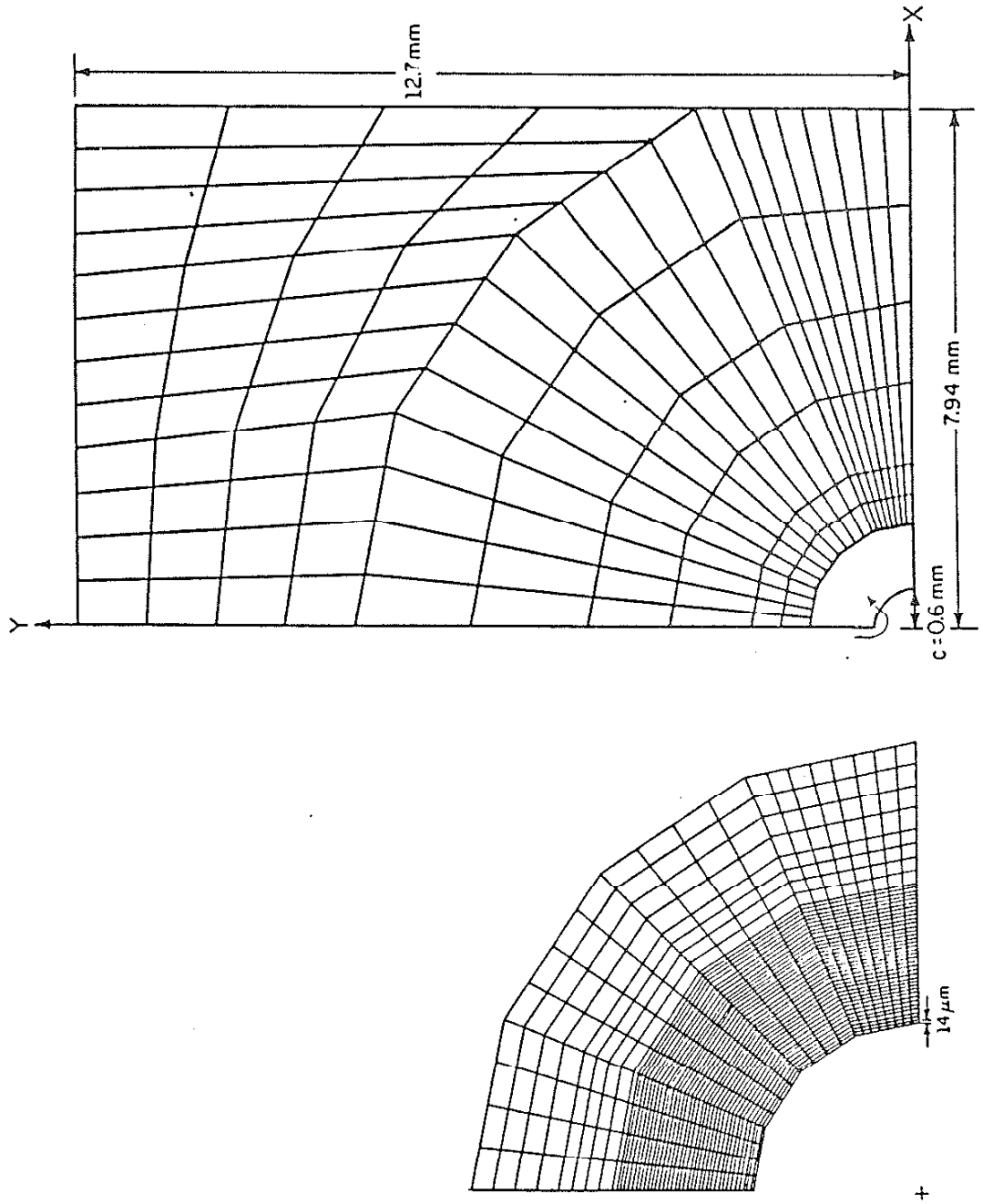

Figure 1b Finite element mesh used in this study (both the geometry and the fine mesh near the crack tip are indicated in the Figure)

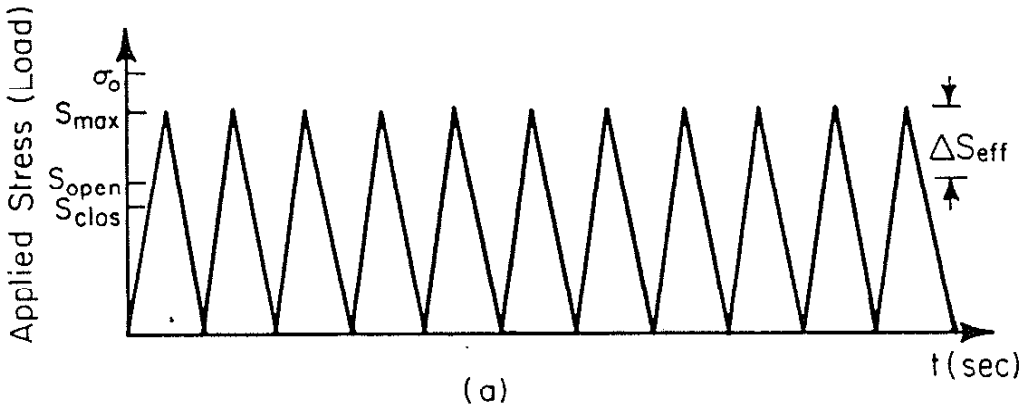

Figure 2a Continuous cycling considered in this study

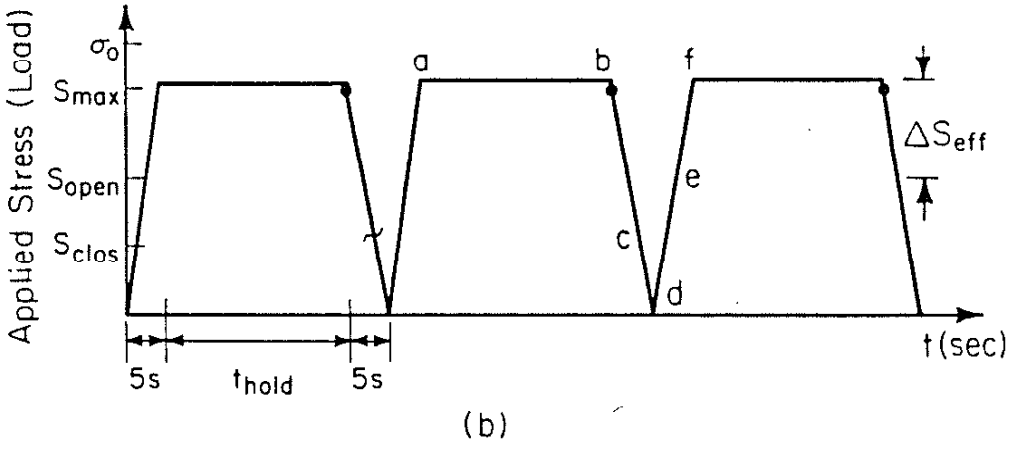

Figure 2b High temperature cycling with hold periods considered in this study (the crack opening and closure levels are indicated)

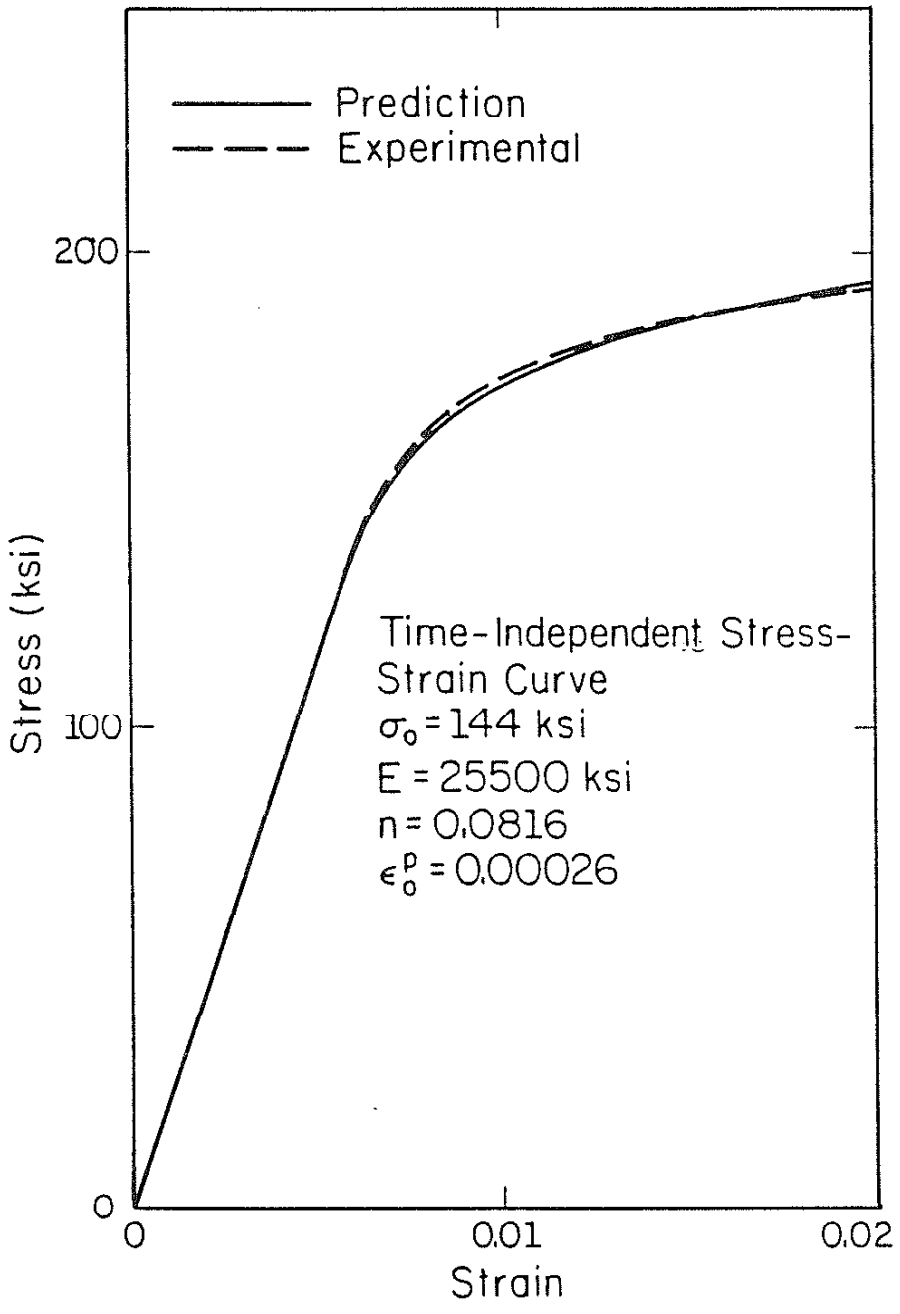

Figure 3 Stress-strain behavior of Rene 95 at 1200 ^{o}F (experiments and prediction) (σ_o=144 ksi, n=0.0816, ε_o^p=0.00026, E=25,500ksi)

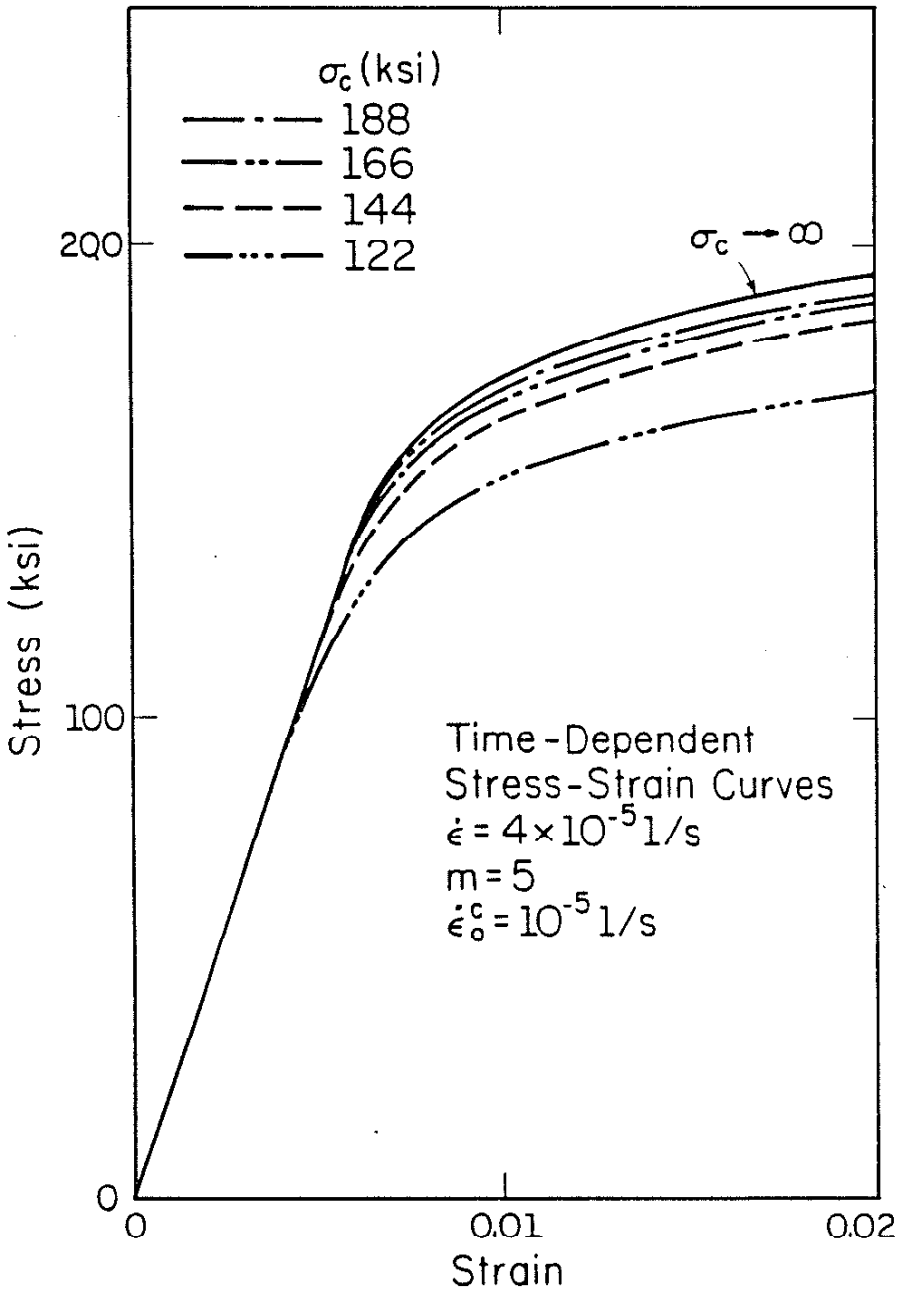

Figure 4a The influence of different σ_c levels in creep law on the stress-strain behavior up to ε=0.02 (strain rate = 4x10-5 1/s)

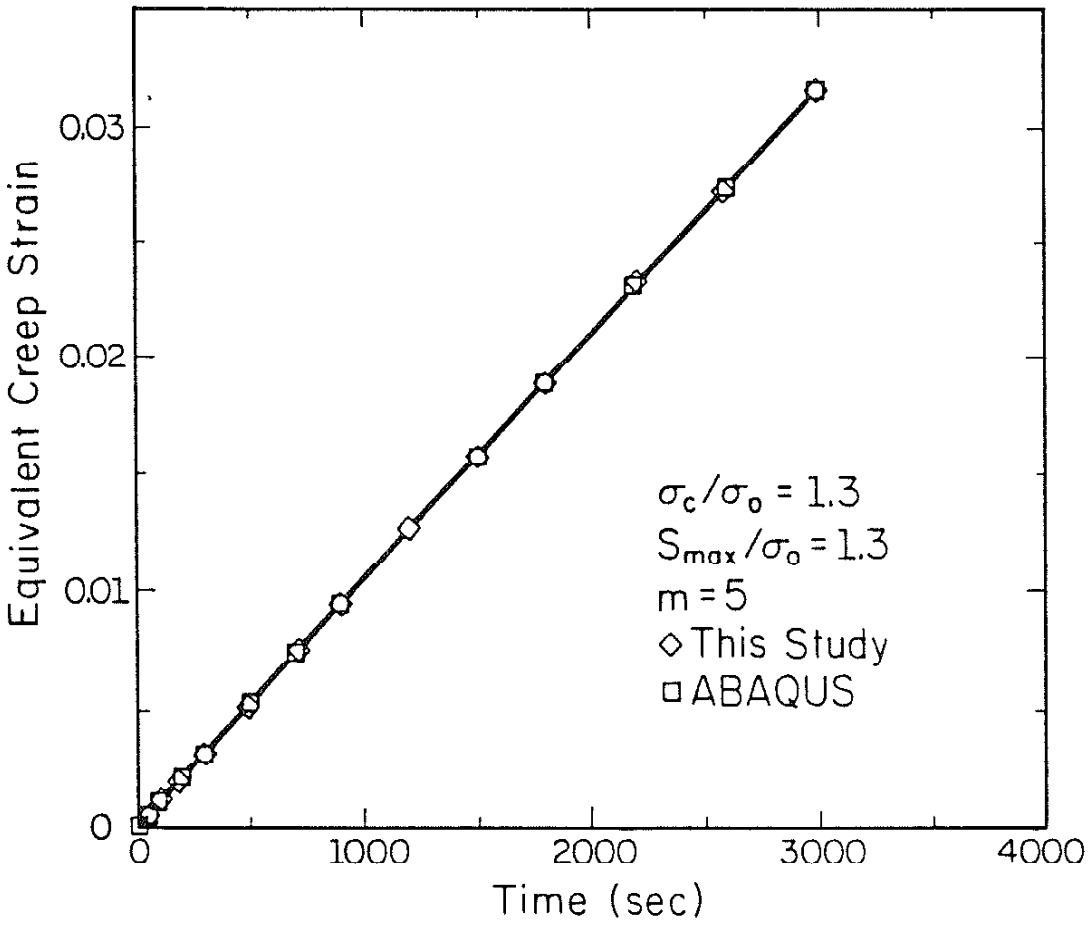

Figure 4b Comparison of equivalent creep strain changes with time using ABAQUS code and the finite element code developed in this study (plane stress, single element)

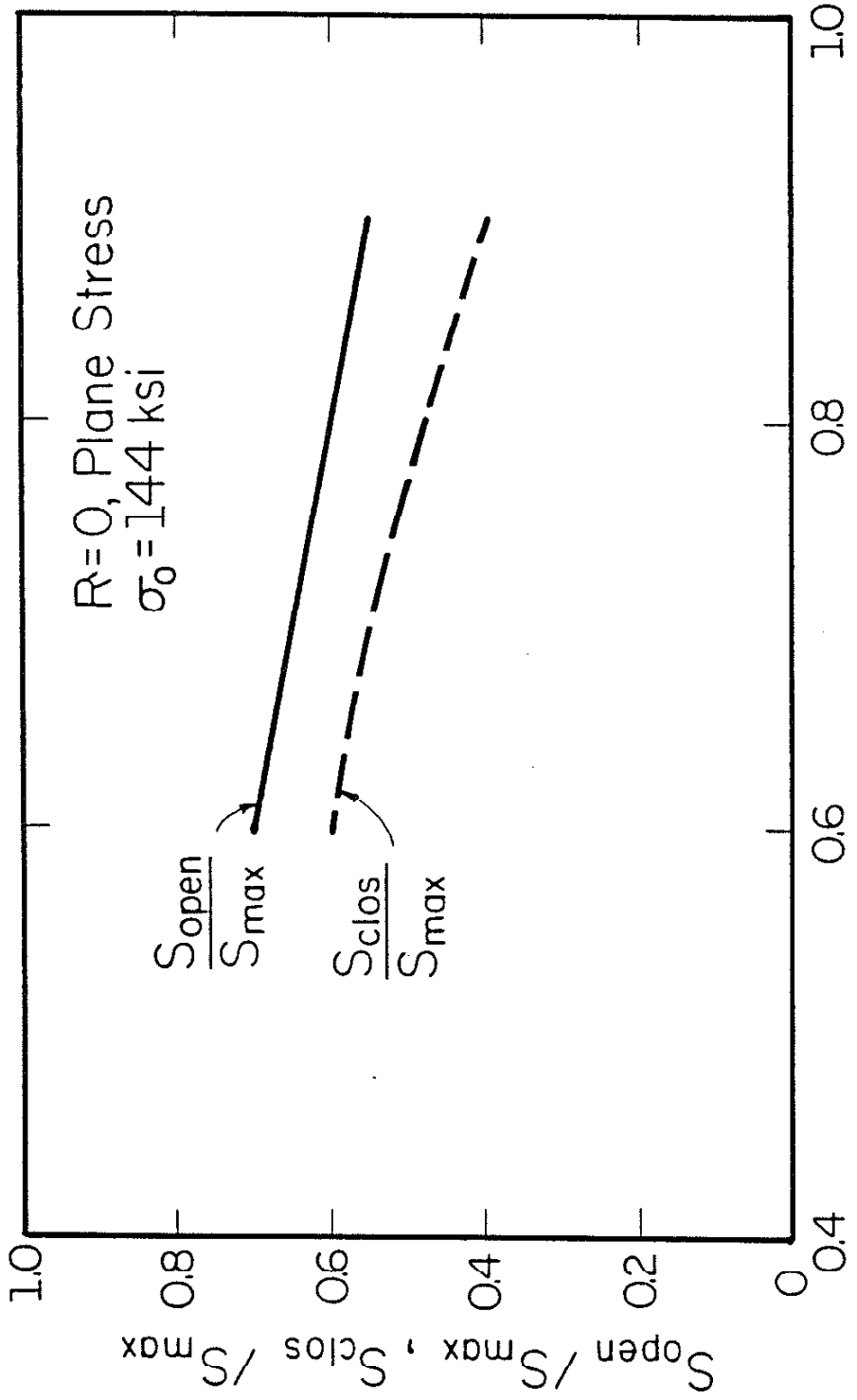

Figure 5 Crack opening and closure stress levels as a function of maximum stress for R = 0 continous cycling case.

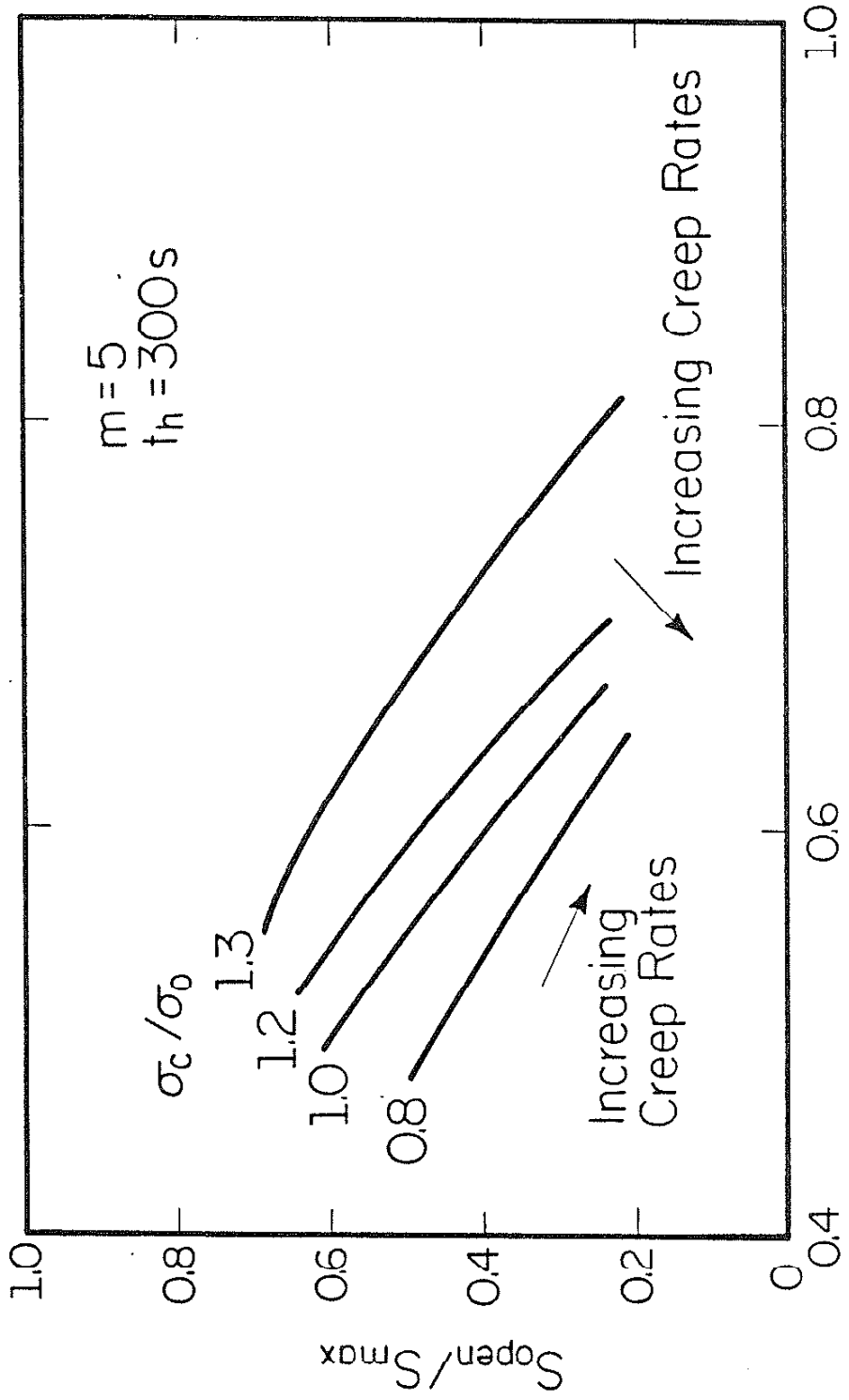

Figure 6 The influence of creep law on the crack opening level (t_h = 300 seconds, m = 5)

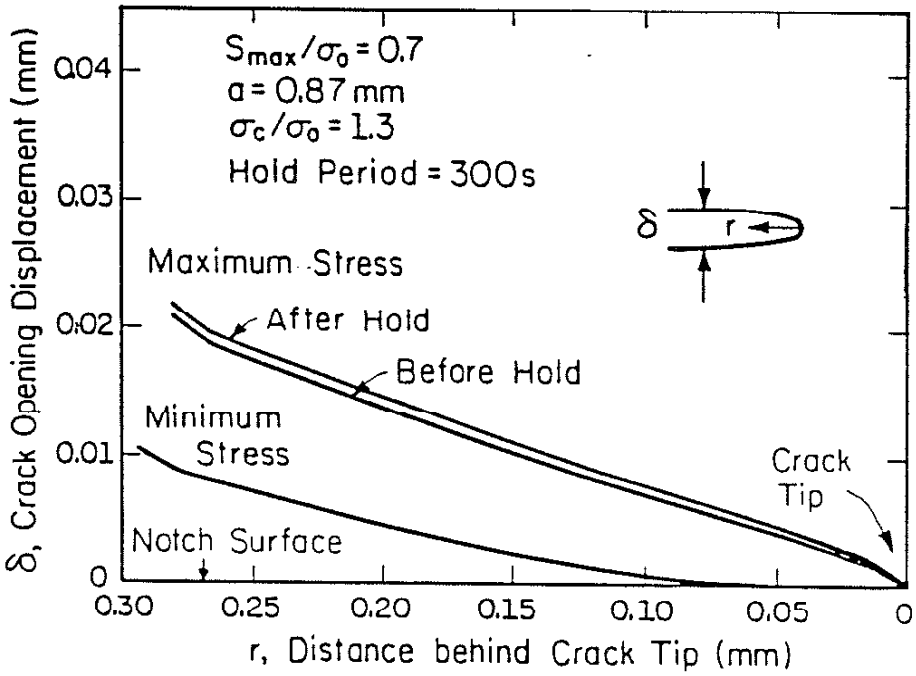

(a)

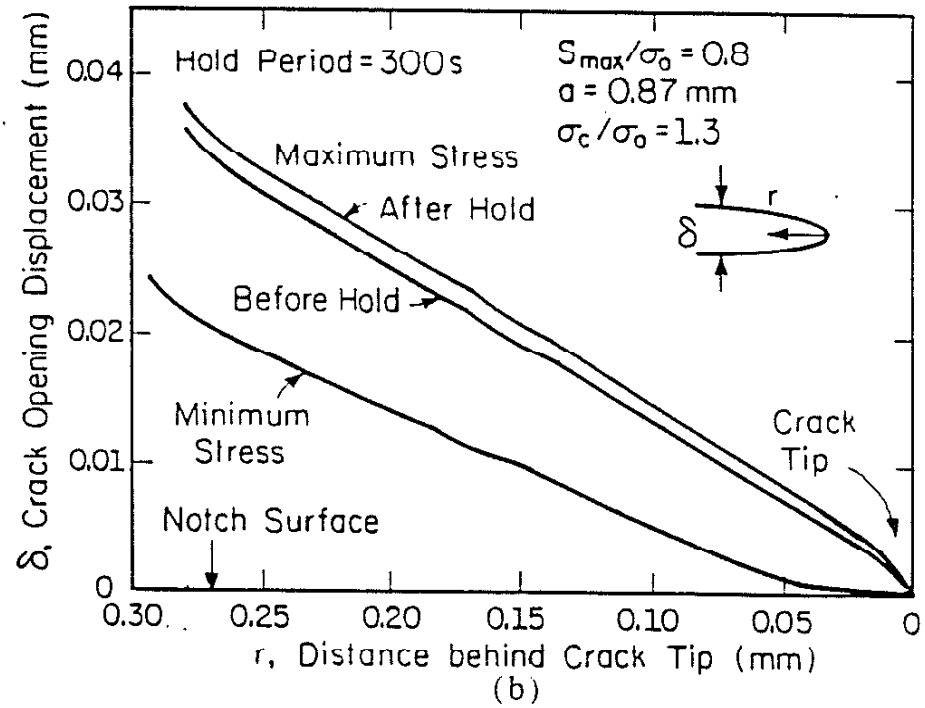

(b)

Figure 7a,b Crack opening displacements at maximum load prior to and after the hold period and at minimum load (S_{max}/σ_0 = 0.7, 0.8, a = 0.87 mm, $\sigma_c = 1.3\sigma_0$, m = 5)

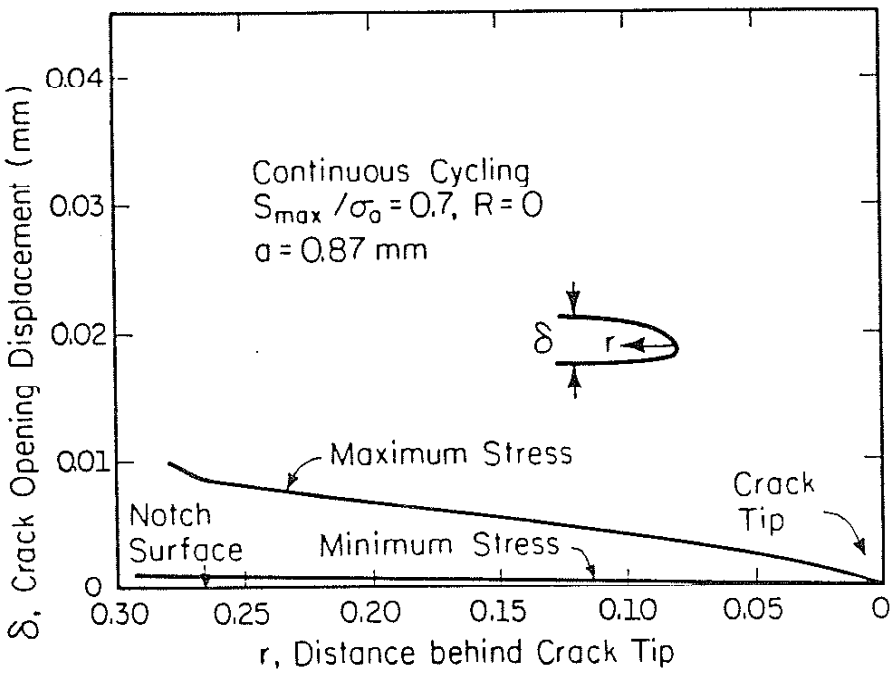

(c)

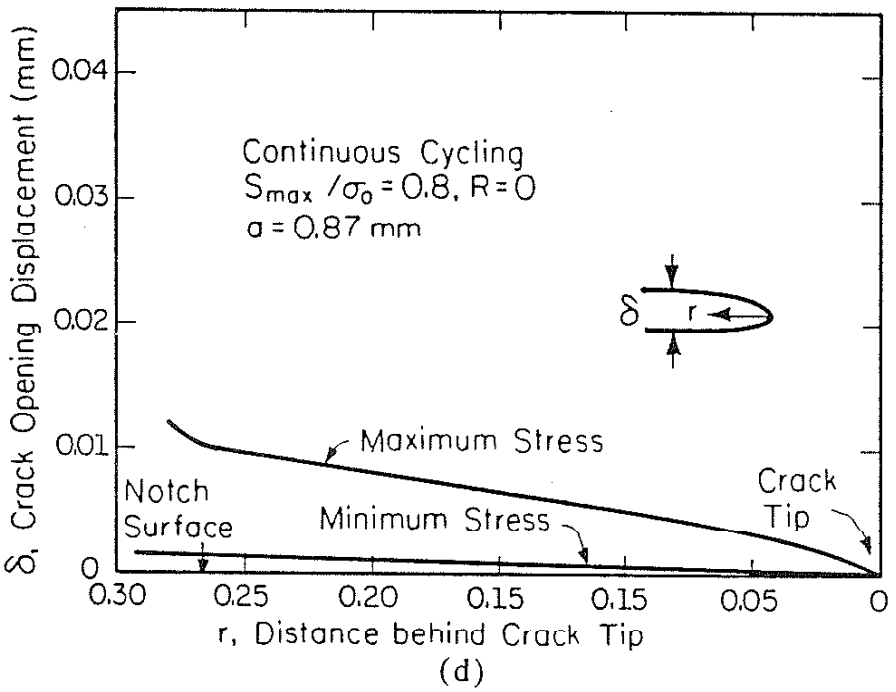

(d)

Figure 7c,d Crack opening displacements at maximum and minimum load for zero hold time case (S_{max}/σ_o = 0.7, 0.8, a = 0.87 mm)

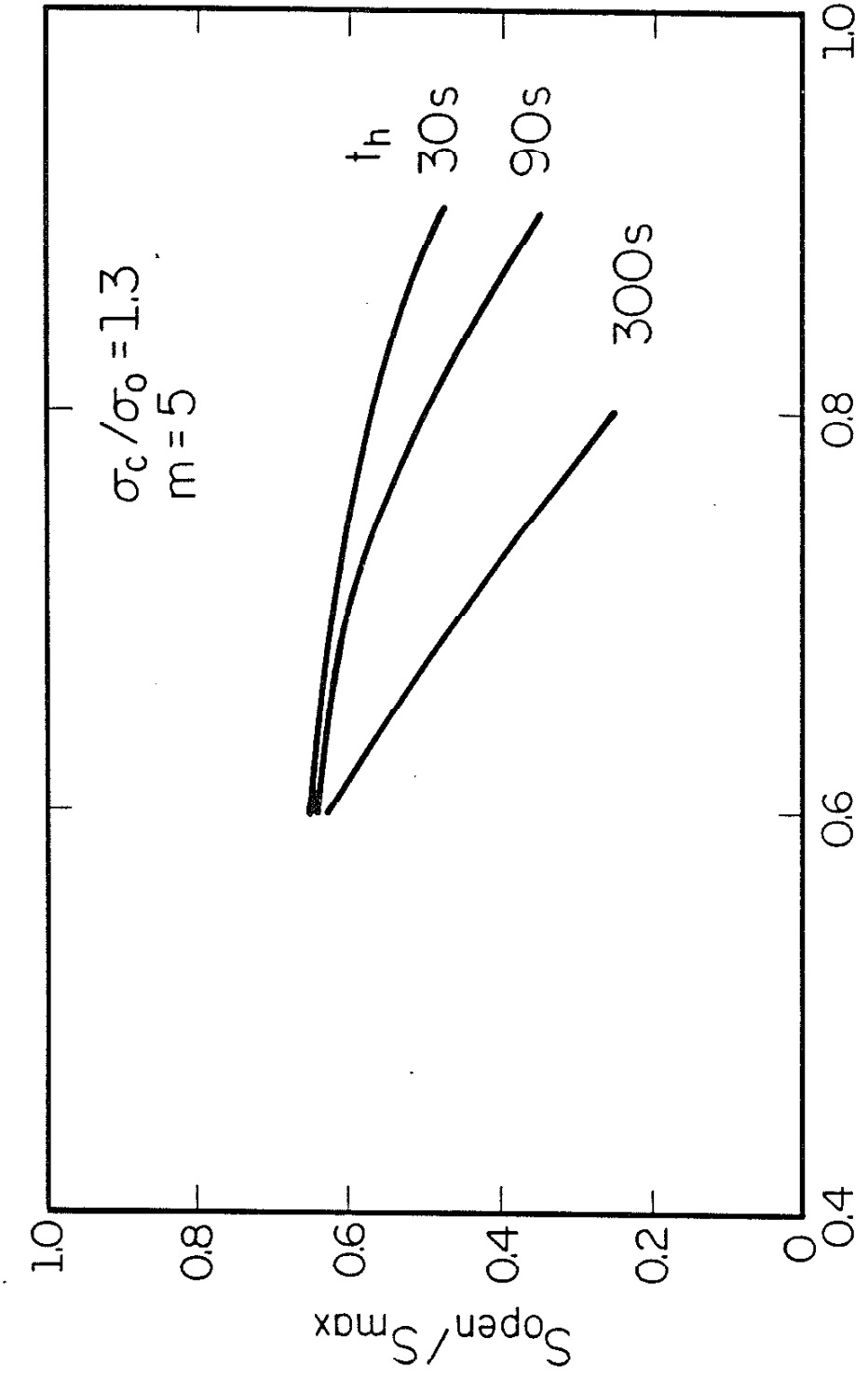

Figure 8 The stable S_{open}/S_{max} level obtained at different hold periods ($\sigma_c = 1.3\sigma_o$, a = 0.87 mm, t_h = 30s, 90s, 300s)

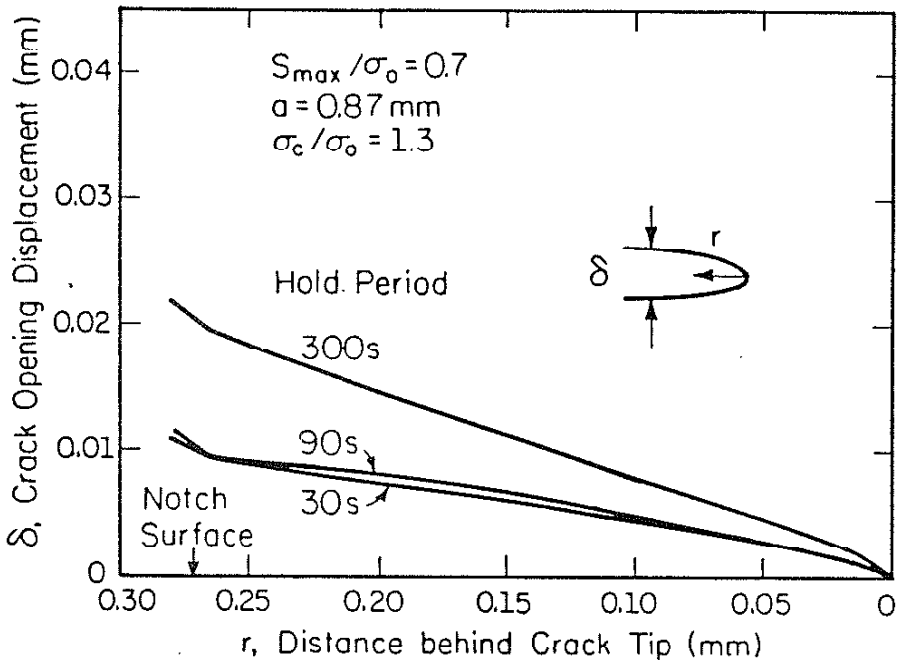

(a)

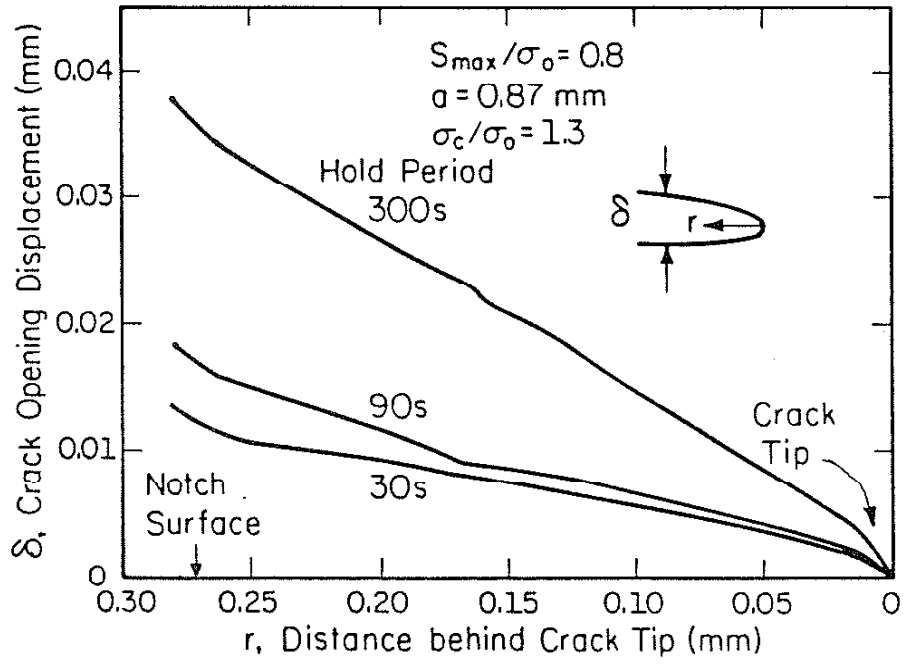

(b)

Figure 9a,b Crack opening displacements at maximum load at conclusion of the hold period for the case of different hold periods (S_{max}/σ_o = 0.7, 0.8, a = 0.87mm, $\sigma_c = 1.3\sigma_o$)

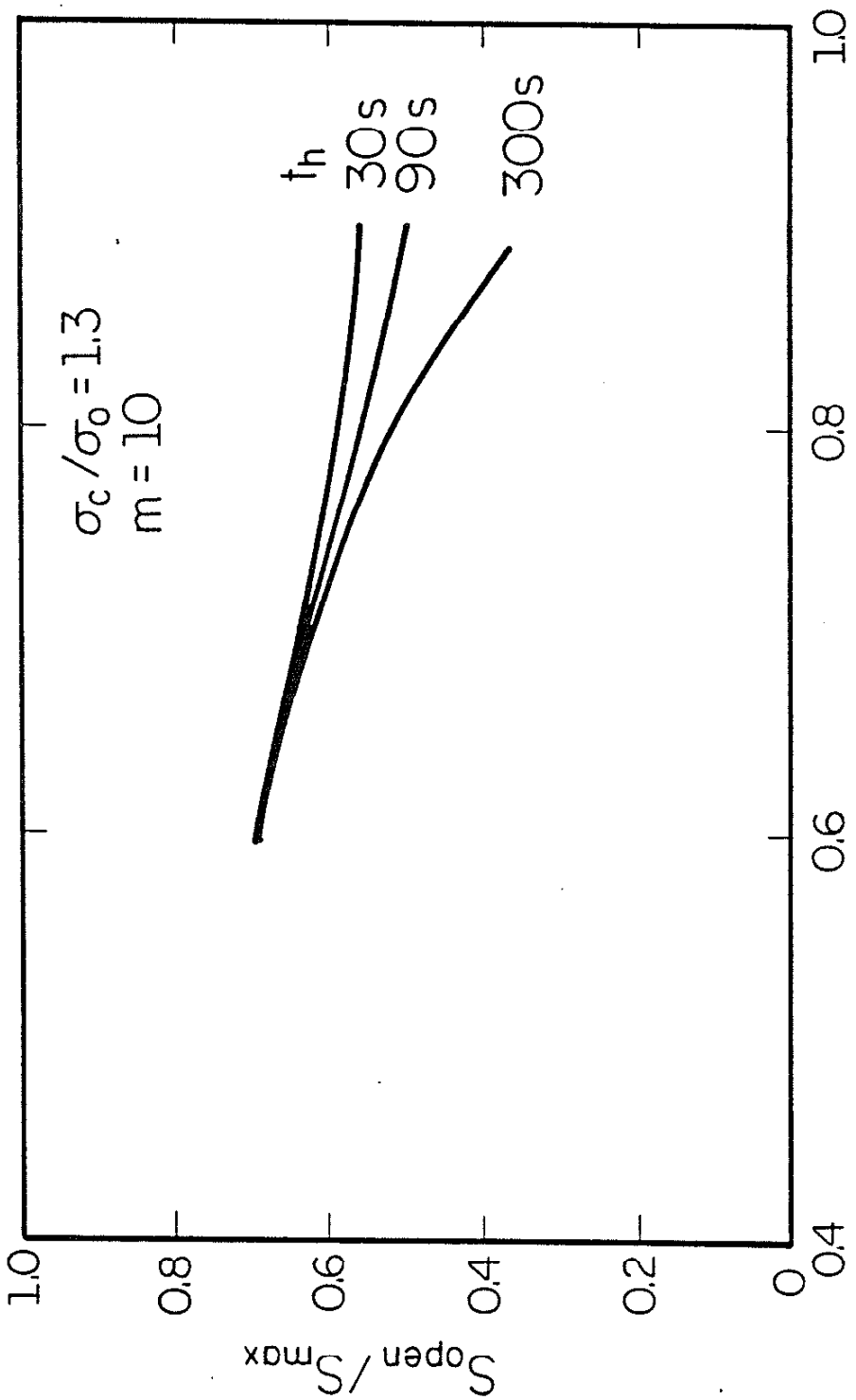

Figure 10 The effect of increasing creep exponent, m, on the crack opening and closure results

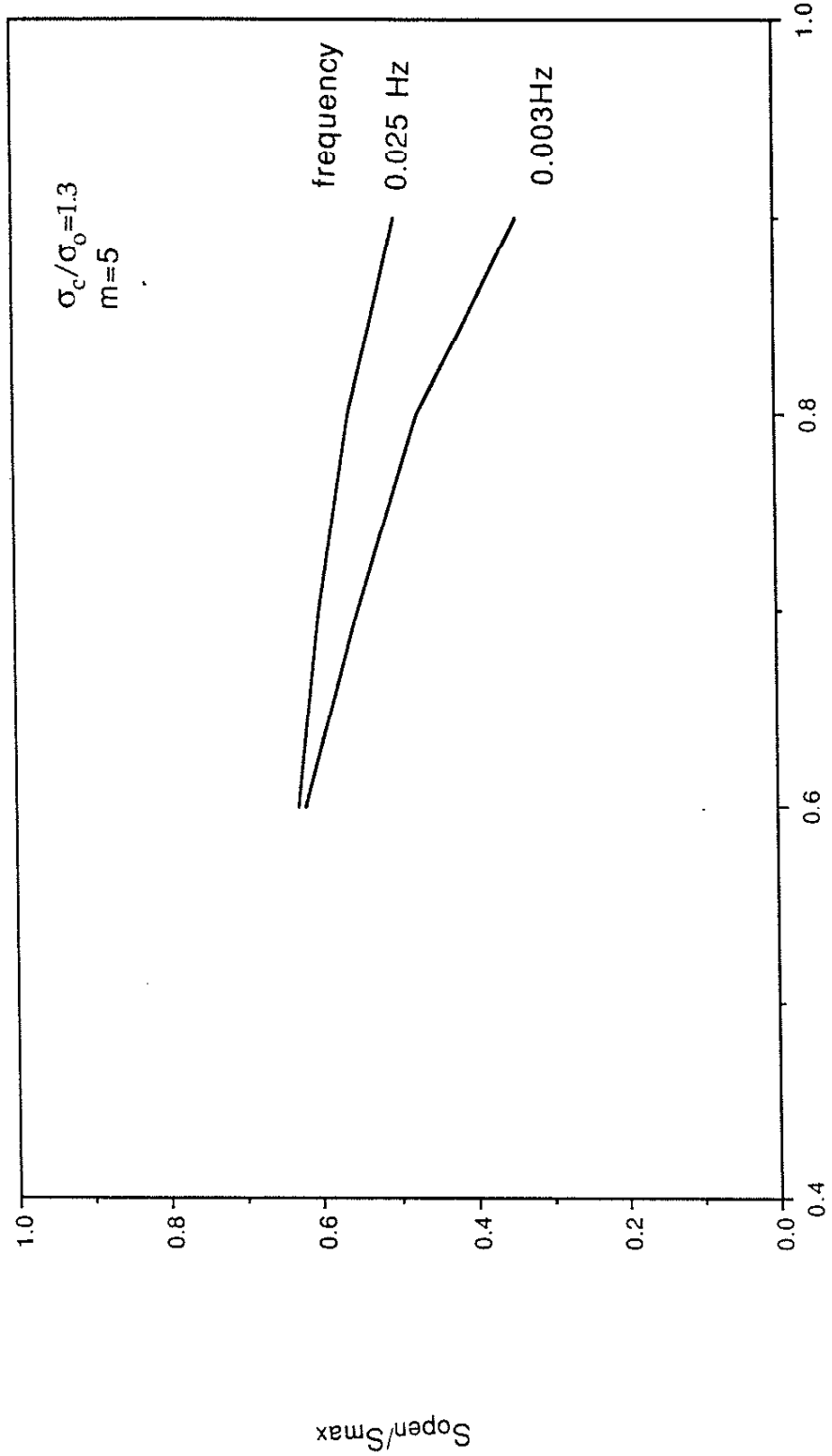

Figure 11 The effect of different loading frequencies on the crack opening results

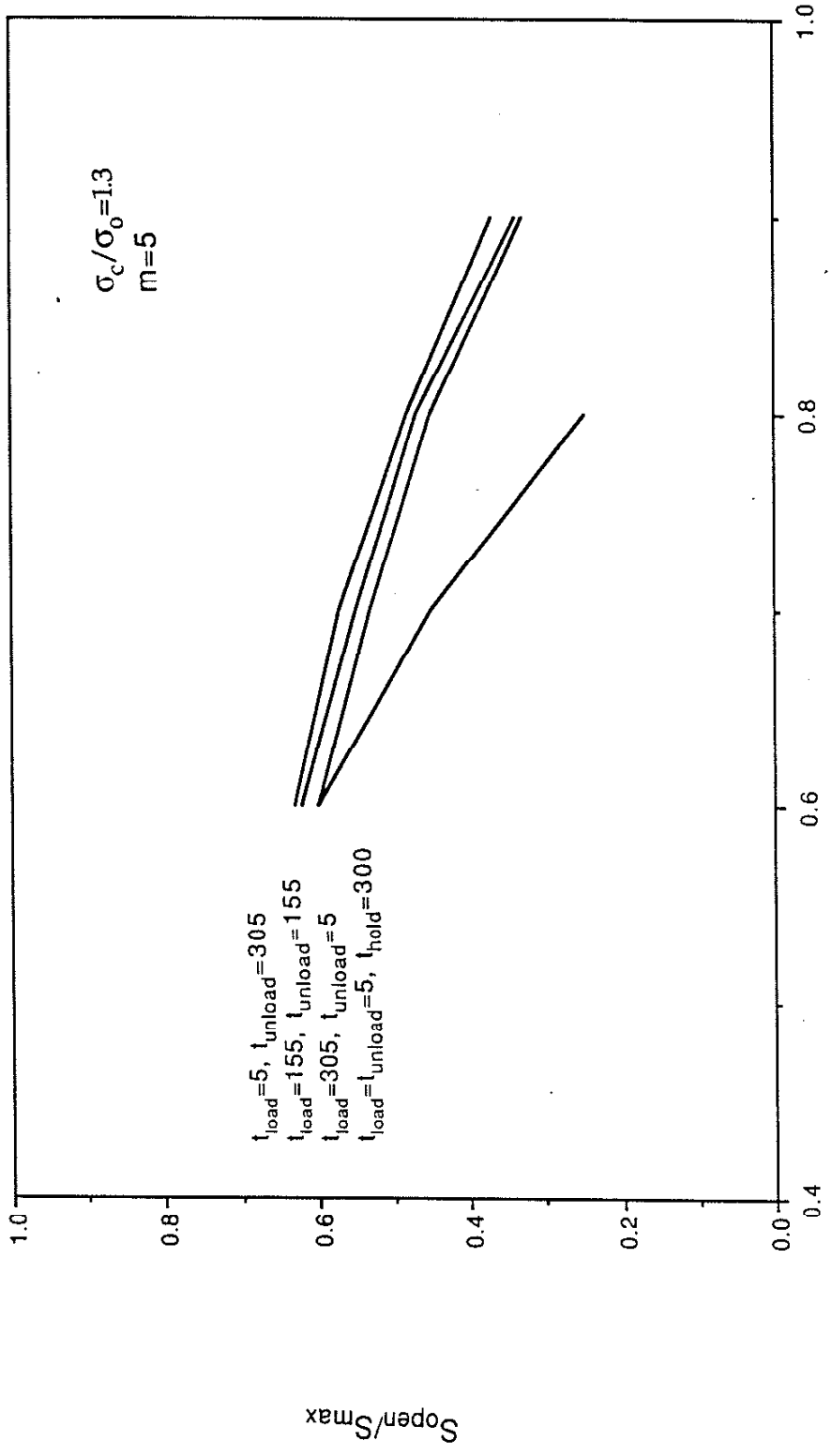

Figure 12 The effect of different cyclic waveform on the crack opening results

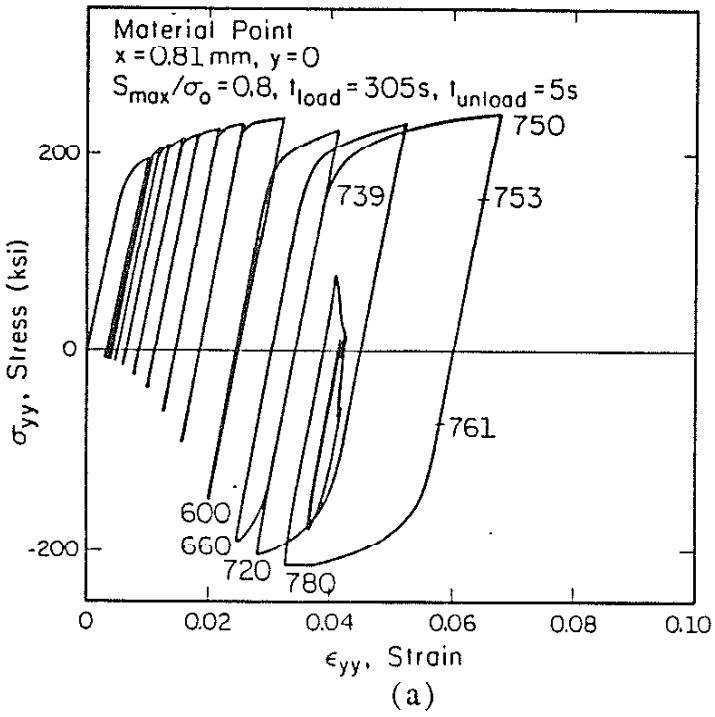

Figure 13a,b Cyclic stress-strain history along the crack line indicating the effect of waveform on stress changes. (S_{max}/σ_o = 0.8, x = 0.81mm)

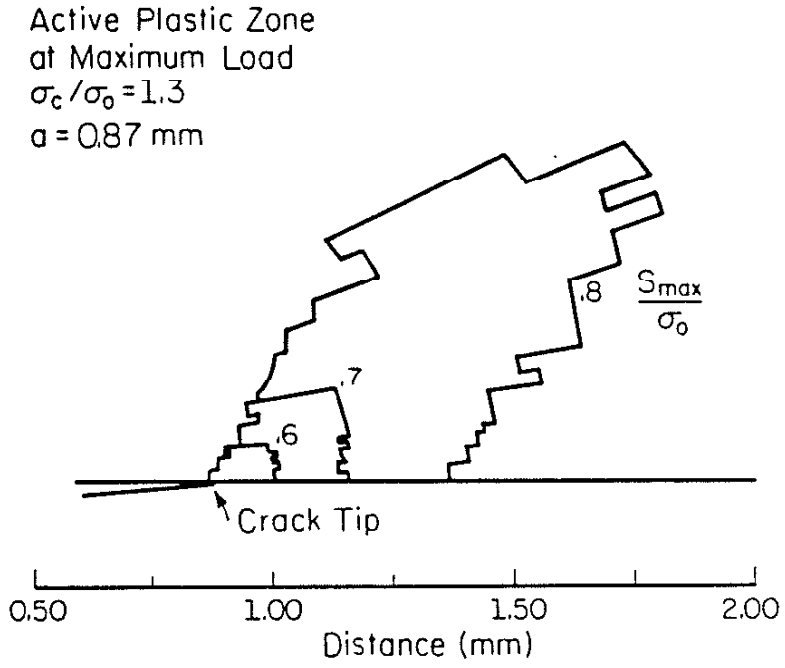

(a)

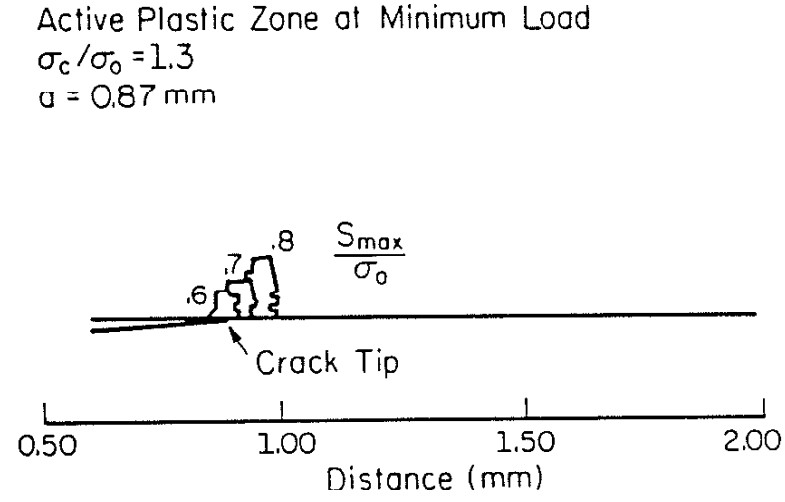

(b)

Figure 14a,b Plastic zone size at maximum load and at minimum load for S_{max}/σ_0 = 0.6, 0.7, 0.8 cases (a = 0.87mm, $\sigma_c = 1.3\sigma_0$, m = 5)

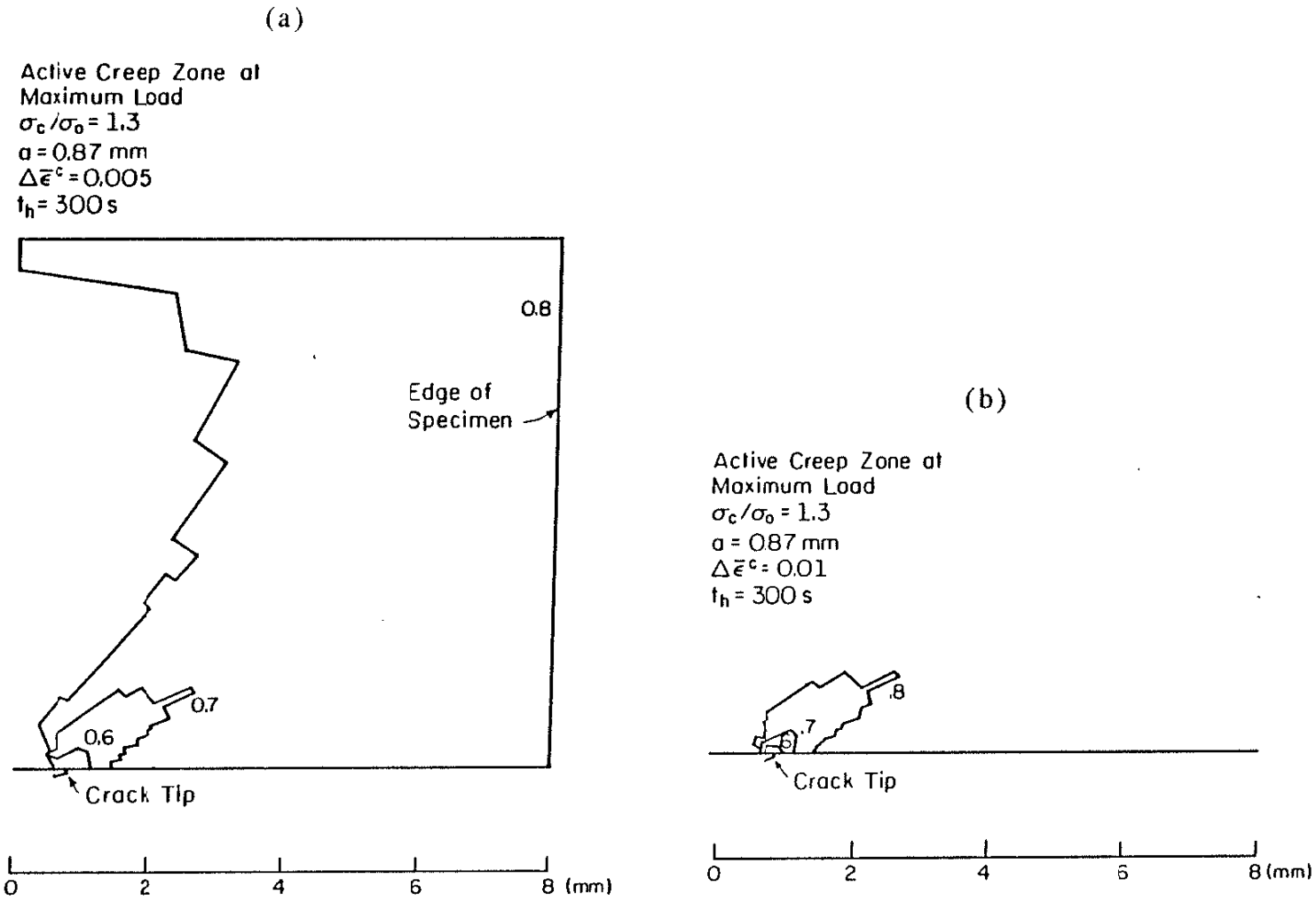

Figure 15a,b Creep zone sizes at maximum stress (after hold period) for S_{max}/σ_o = 0.6, 0.7 0.8 cases (a = 0.87 mm, $\sigma_c = 1.3\sigma_o$, m = 5, $\bar{\epsilon}^c$ = 0.005, 0.01 contours)

Active Creep Zone at
Maximum Load
σ_c/σ_o=1.3, m=5
S_{max}/σ_o=0.8, t_h=300s
$\Delta\bar{\varepsilon}^c$=0.005

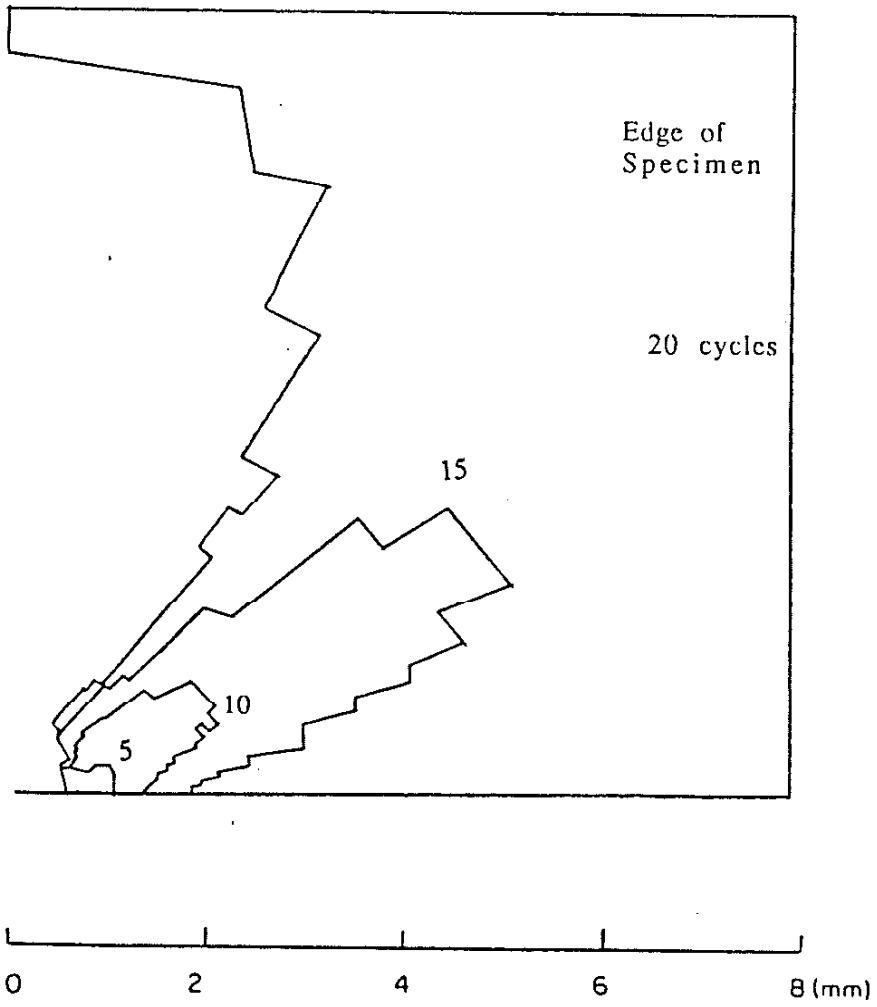

Figure 16 The creep zone size at maximum load (after hold period) increases with the cycling (S_{max}/σ_o = 0.8)

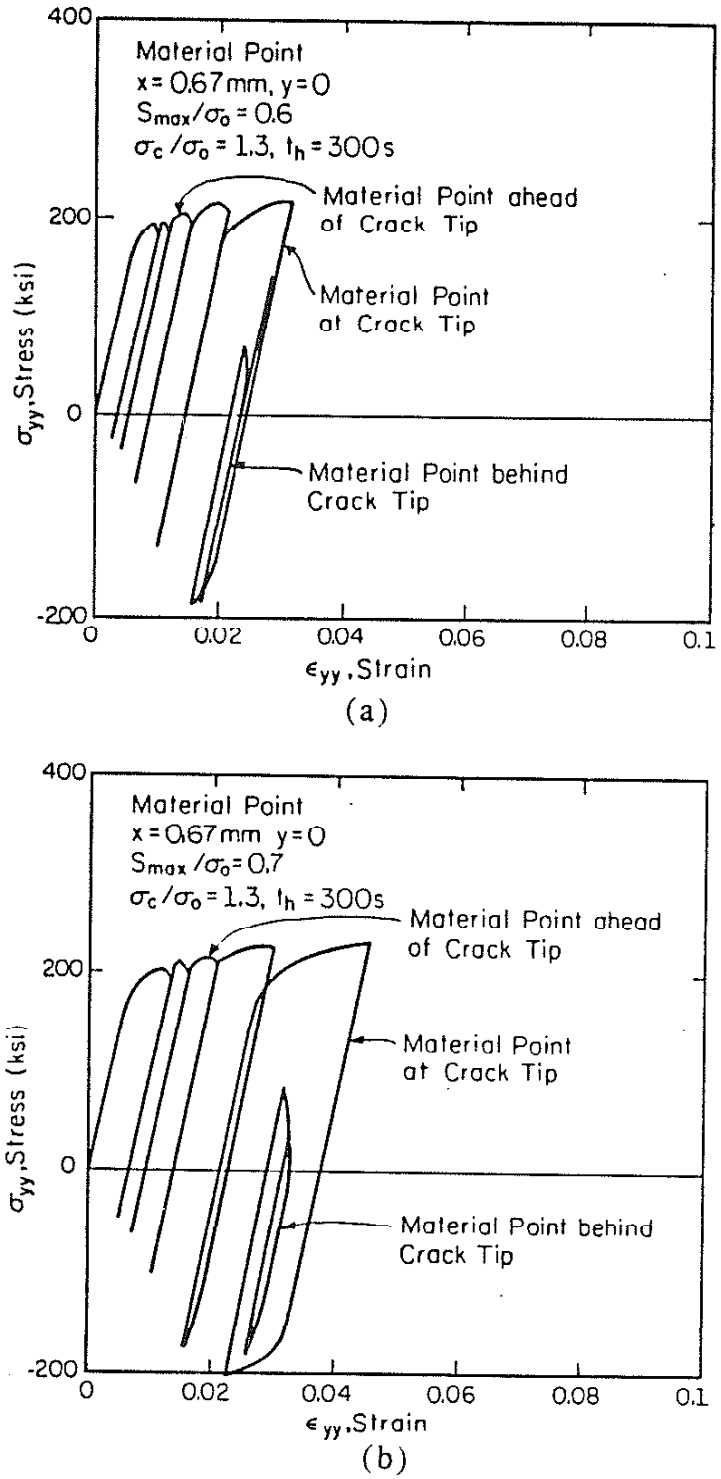

Figure 17a,b Cyclic stress strain history along the crack line indicating the effect of hold periods on stress changes and on mean strain increases with cycles (S_{max}/σ_o = 0.6 and 0.7, x = 0.67mm)

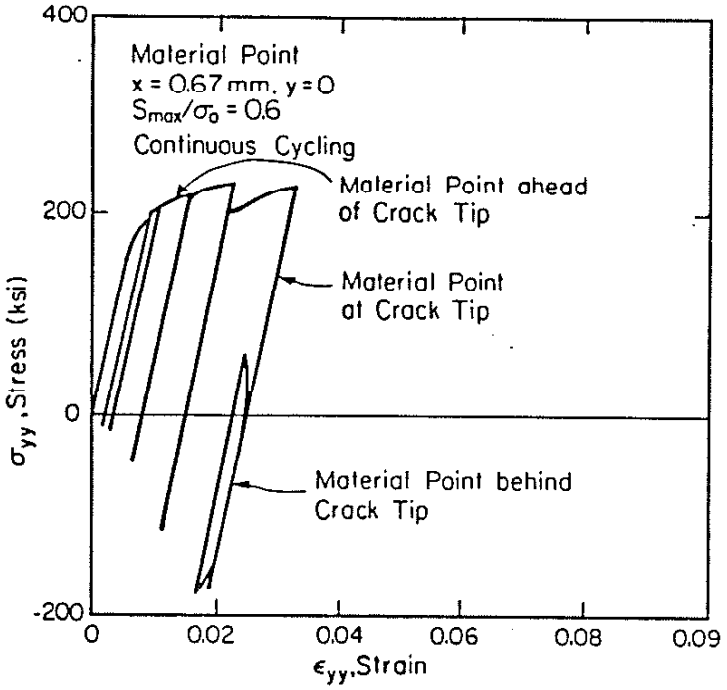

(c)

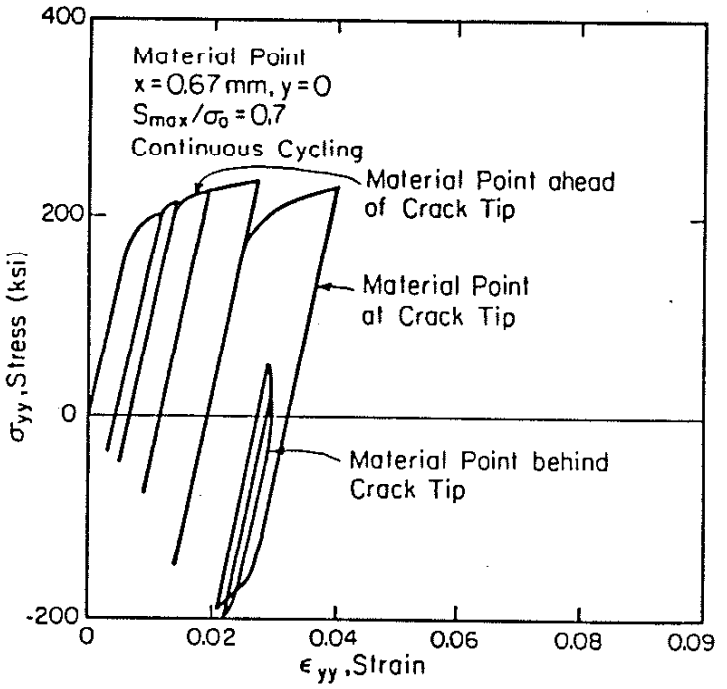

(d)

Figure 17c,d Cycling stress-strain history along the crack line in the absence of hold periods (S_{max}/σ_0 = 0.6 and 0.7, x = 0.67mm)

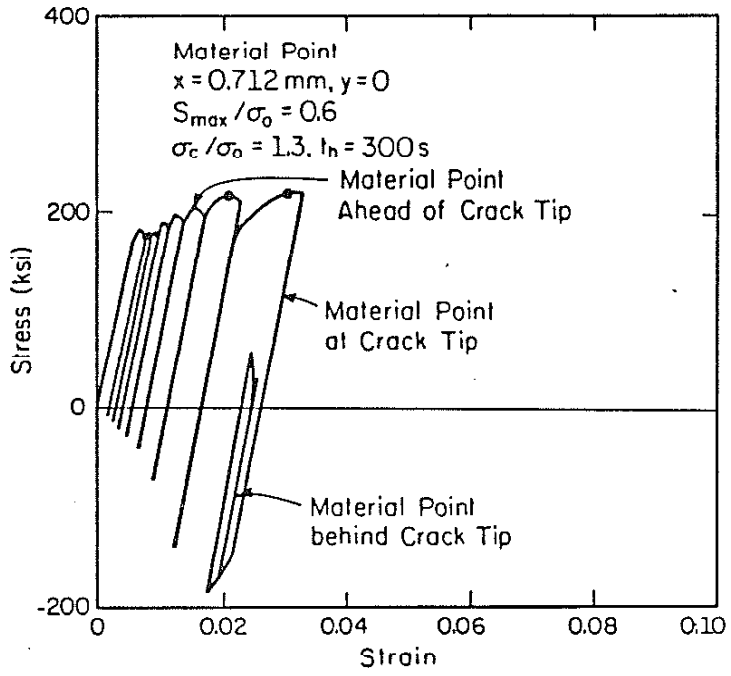

(e)

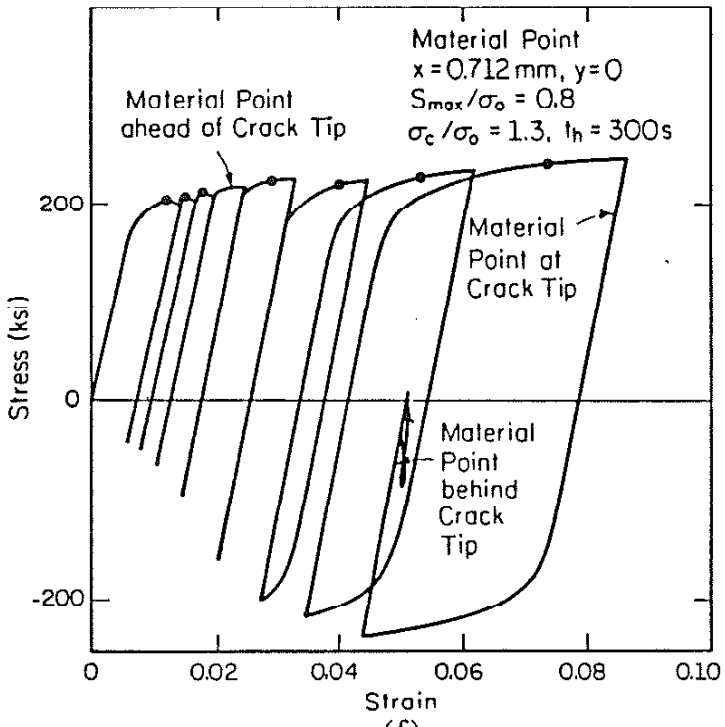

(f)

Figure 17e,f Cyclic stress-strain history along the crack line indicating the effect of hold periods on stress changes and on mean strain increases with cycles (S_{max}/σ_0 = 0.6 and 0.8, x = 0.712mm)

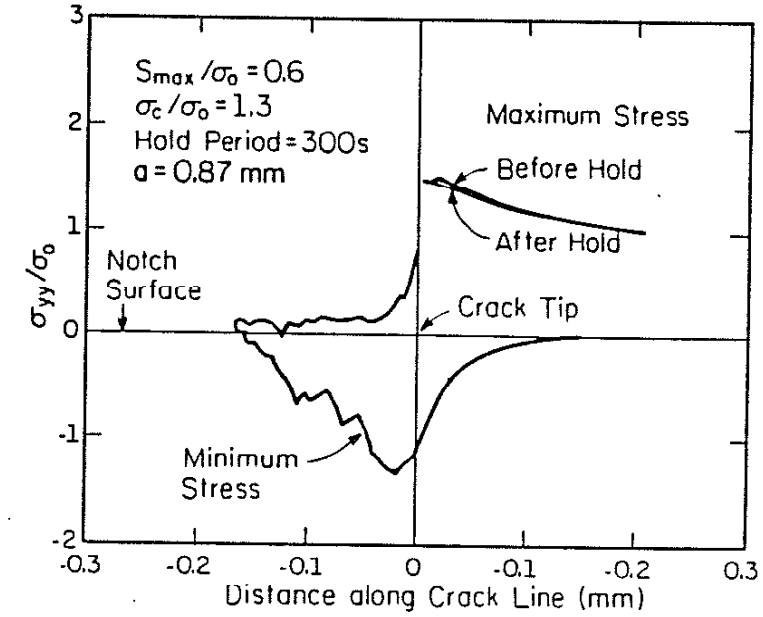

(a)

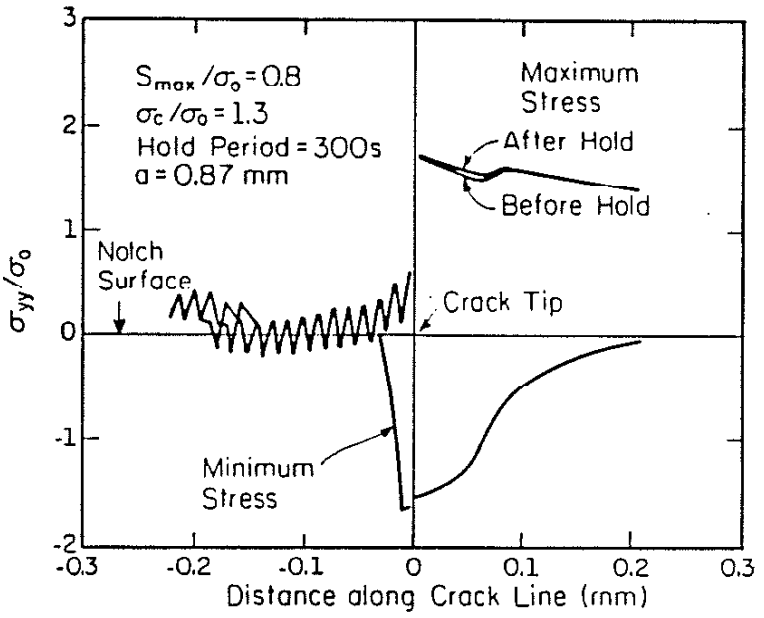

(b)

Figure 18a,b Stress distribution along the crack line at maximum (before and after tensile hold) and minimum applied stress levels (S_{max}/σ_o = 0.6, 0.8, a = 0.87mm, $\sigma_c = 1.3\sigma_o$, m = 5)

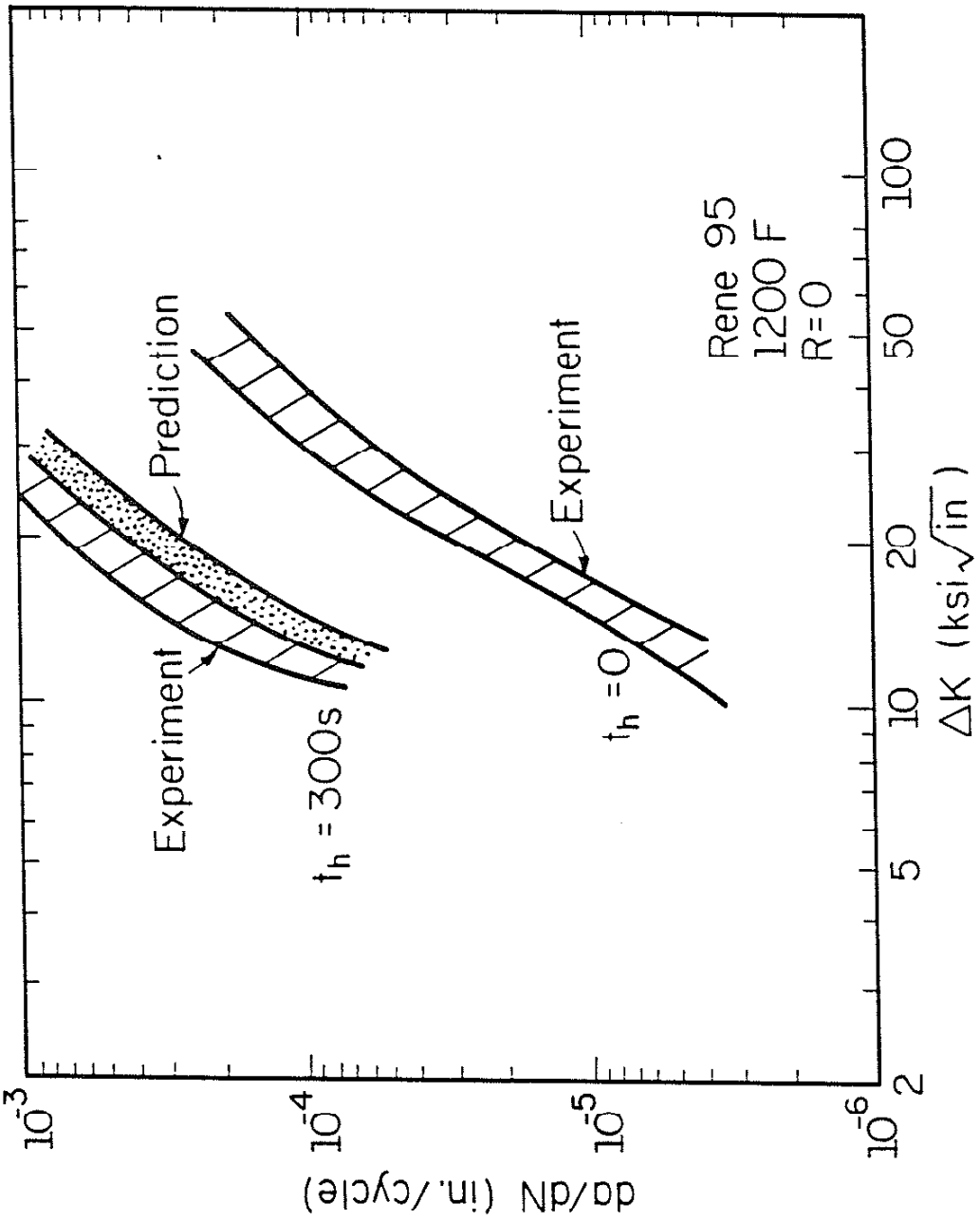

Figure 19 Prediction of crack growth rates on Rene 95 upon incorporating the effect of closure under hold time cases

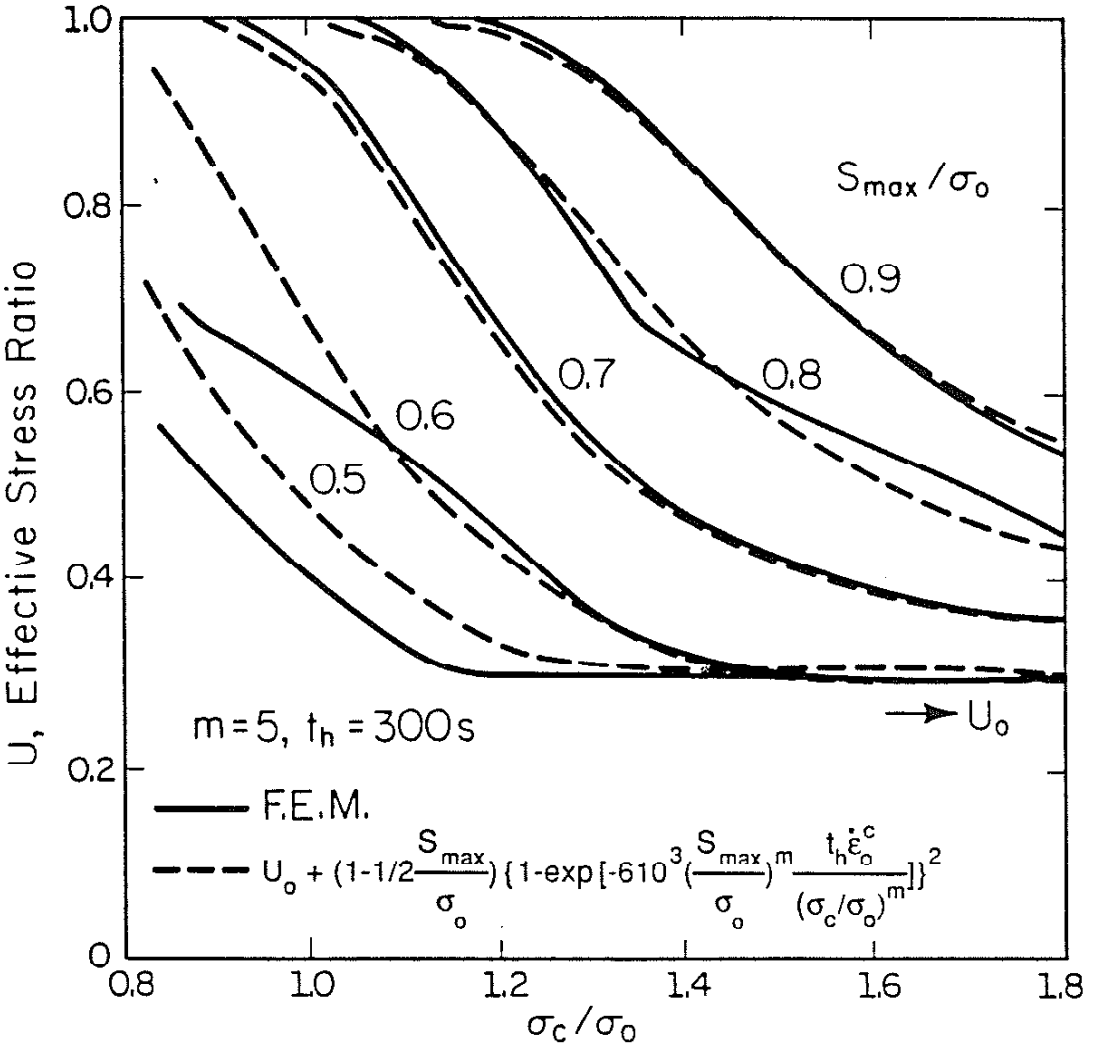

Figure 20 Comparison of F.E.M. results with predicted equation for effective stress ratio versus σ_c/σ_o

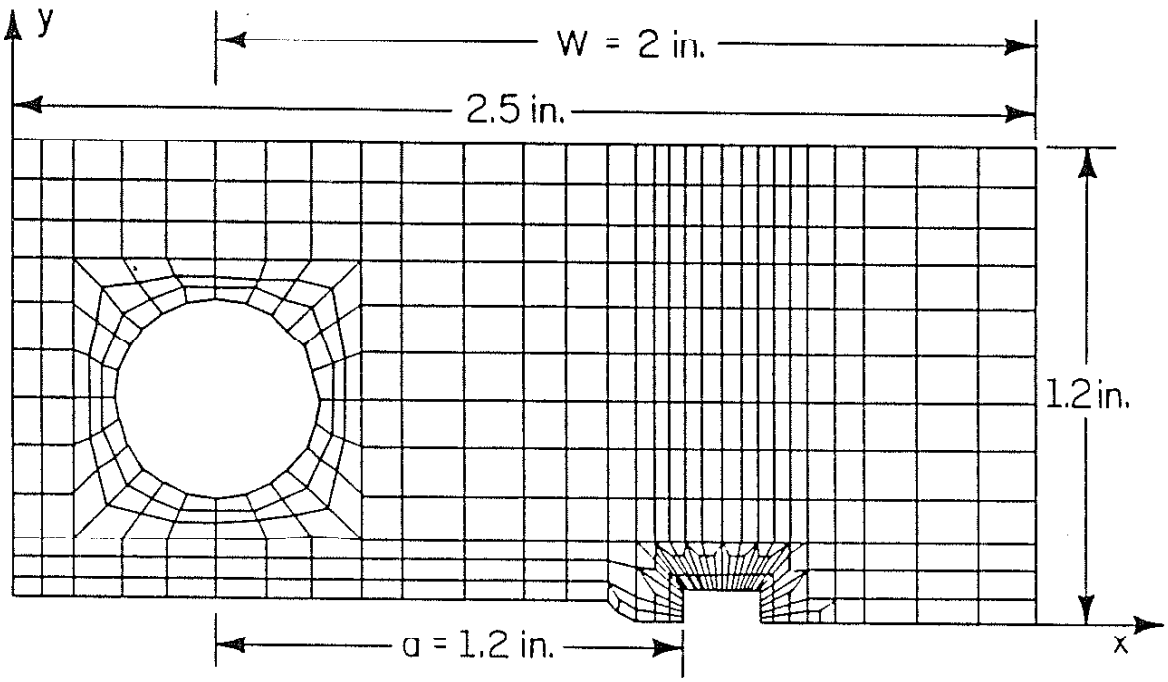

(a)

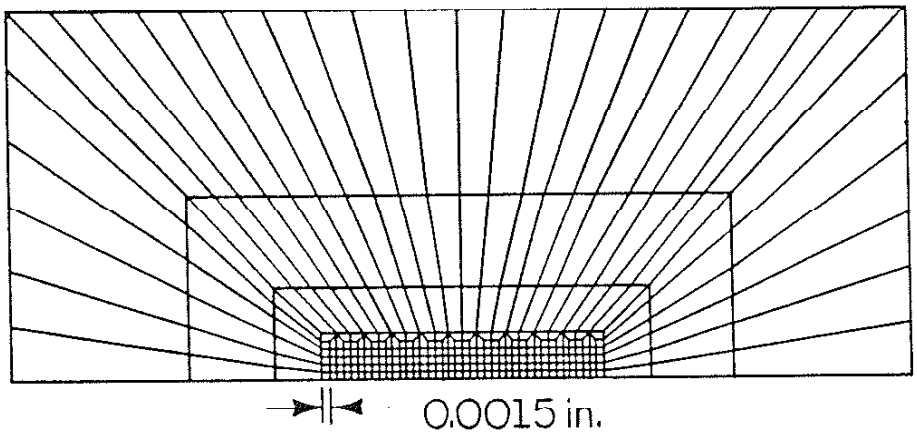

(b)

Figure 21a,b Finite element mesh used for CT specimen

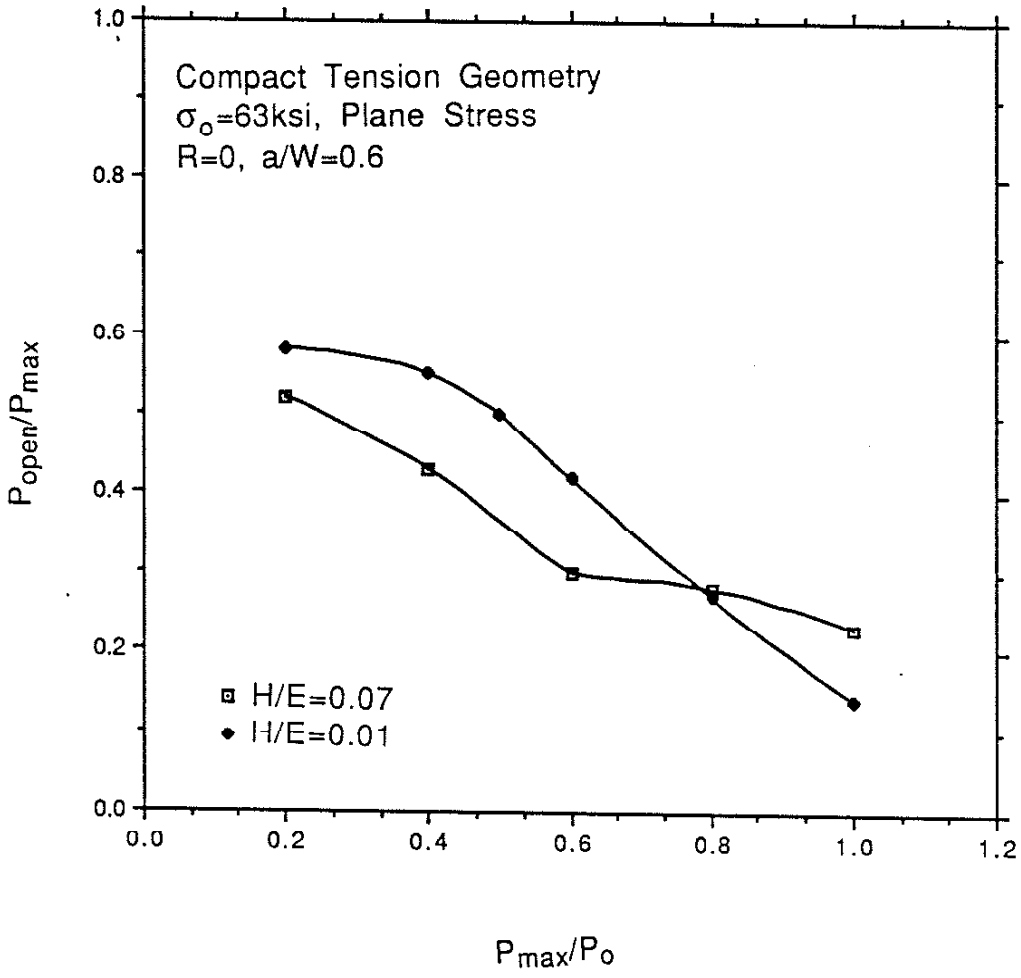

Figure 22 Results of crack opening load for H/E = 0.01 and H/E – 0.07 under plane stress condition

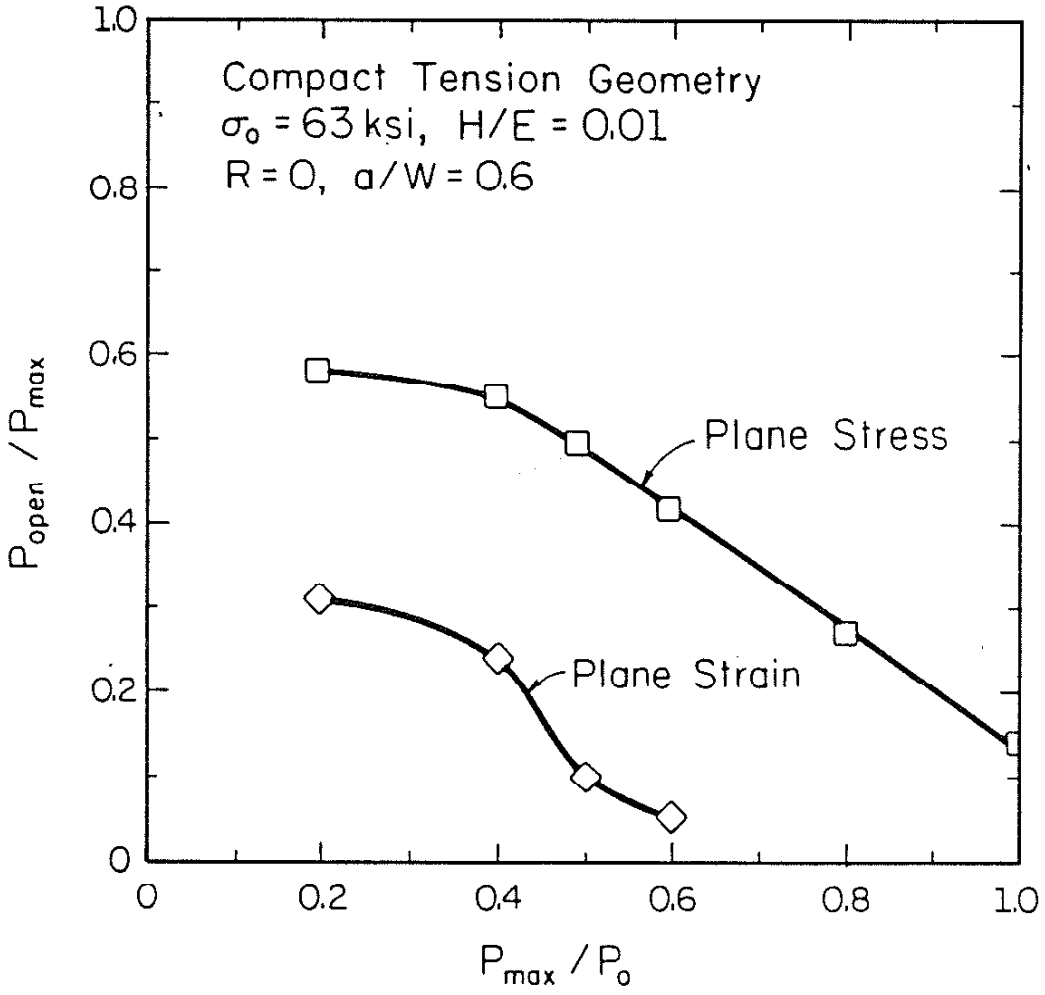

Figure 23 Results of crack opening load for H/E = 0.01 under plane stress and plane strain conditions

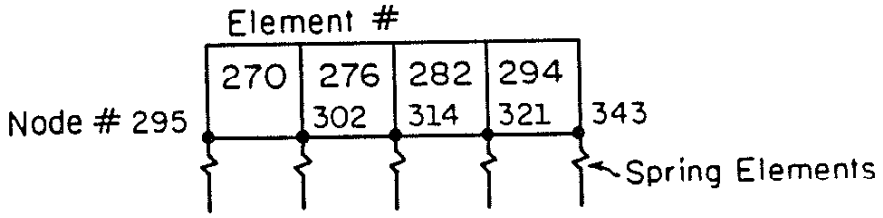

Figure 24 The element along the crack path. Element #282 lower left integration point is defined as the material point

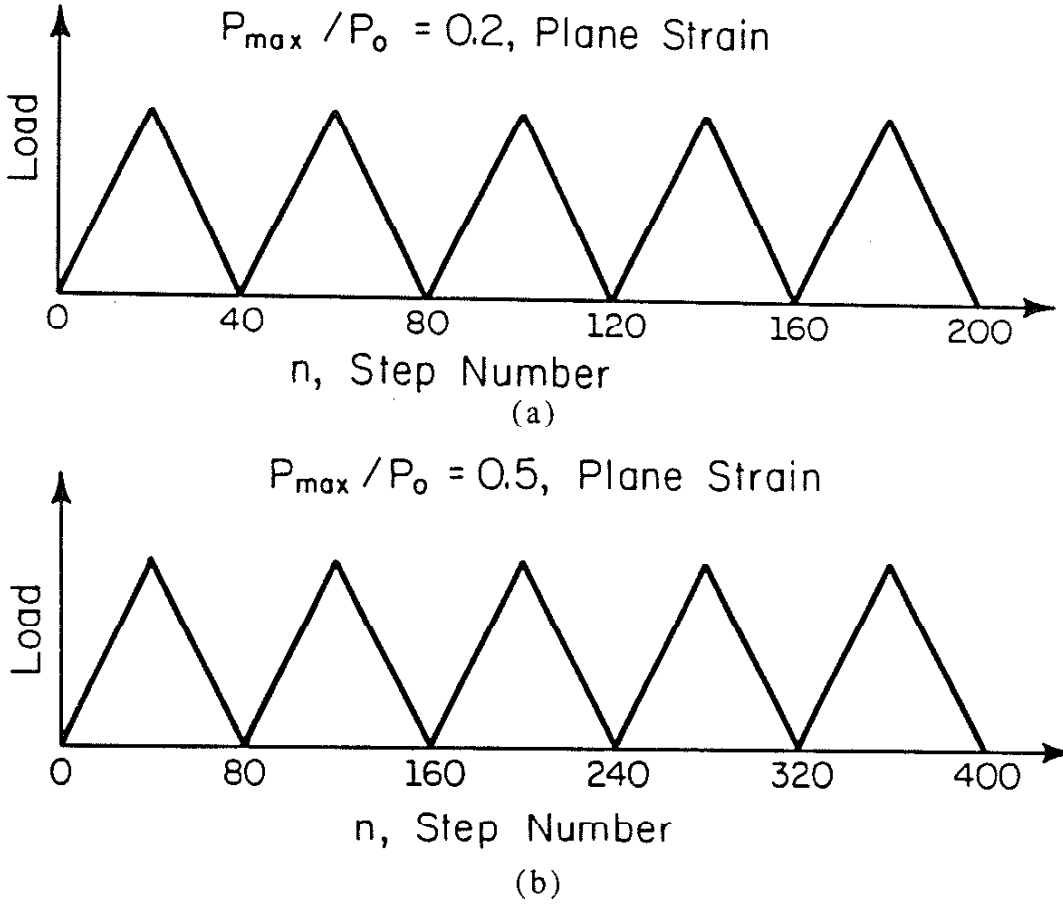

Figure 25a,b The load variation with step number for the cases of P_{max}/P_o = 0.2 and 0.5

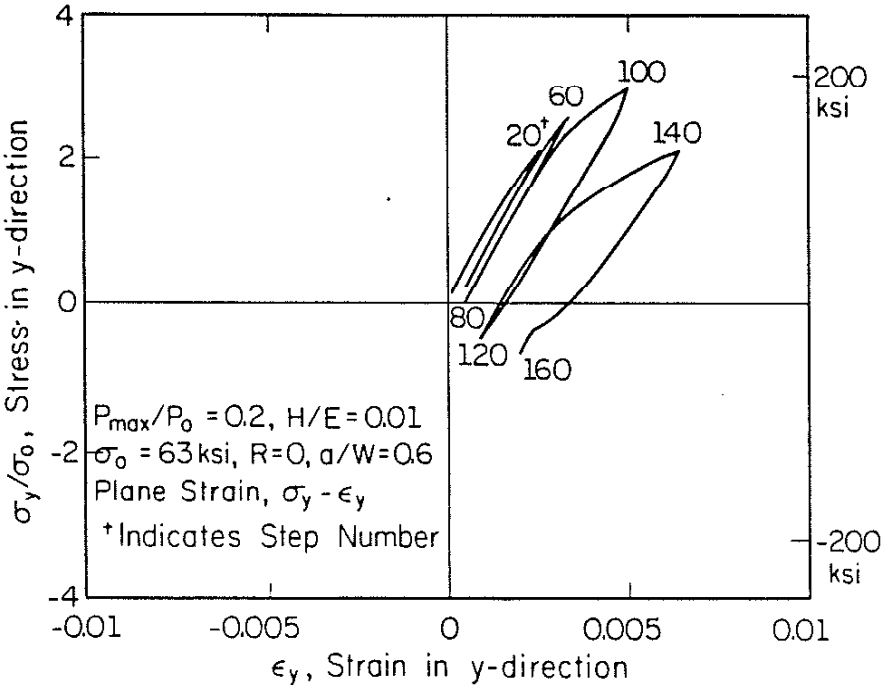

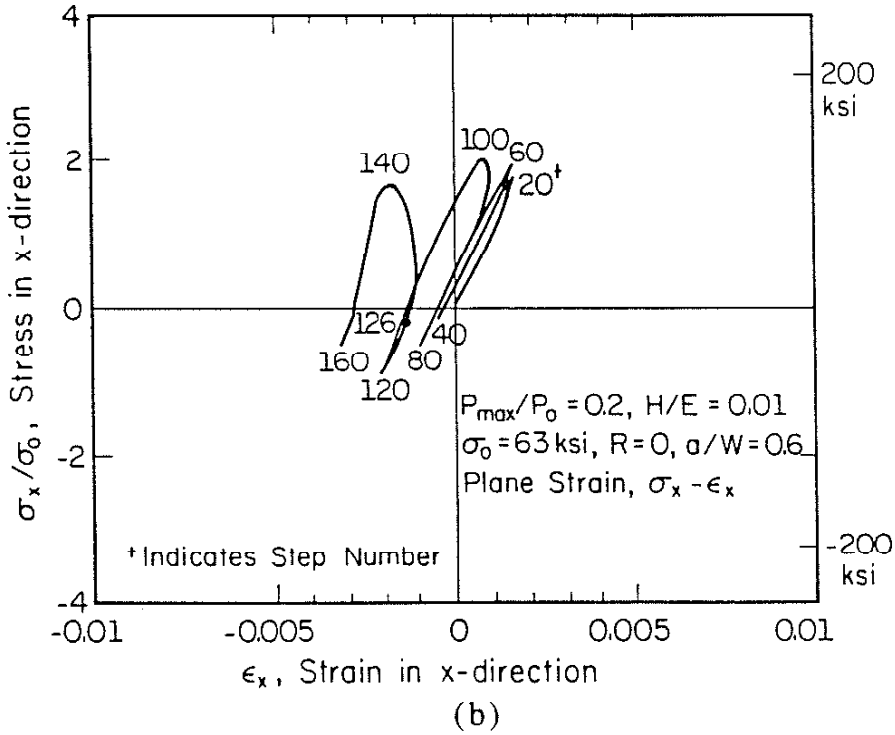

Figure 26a,b Stress-strain behavior at y and x directions at material point from Step #1 through #160. At Step #100 the crack tip has reached Element #282 (P_{max}/P_0 = 0.2, plane strain)

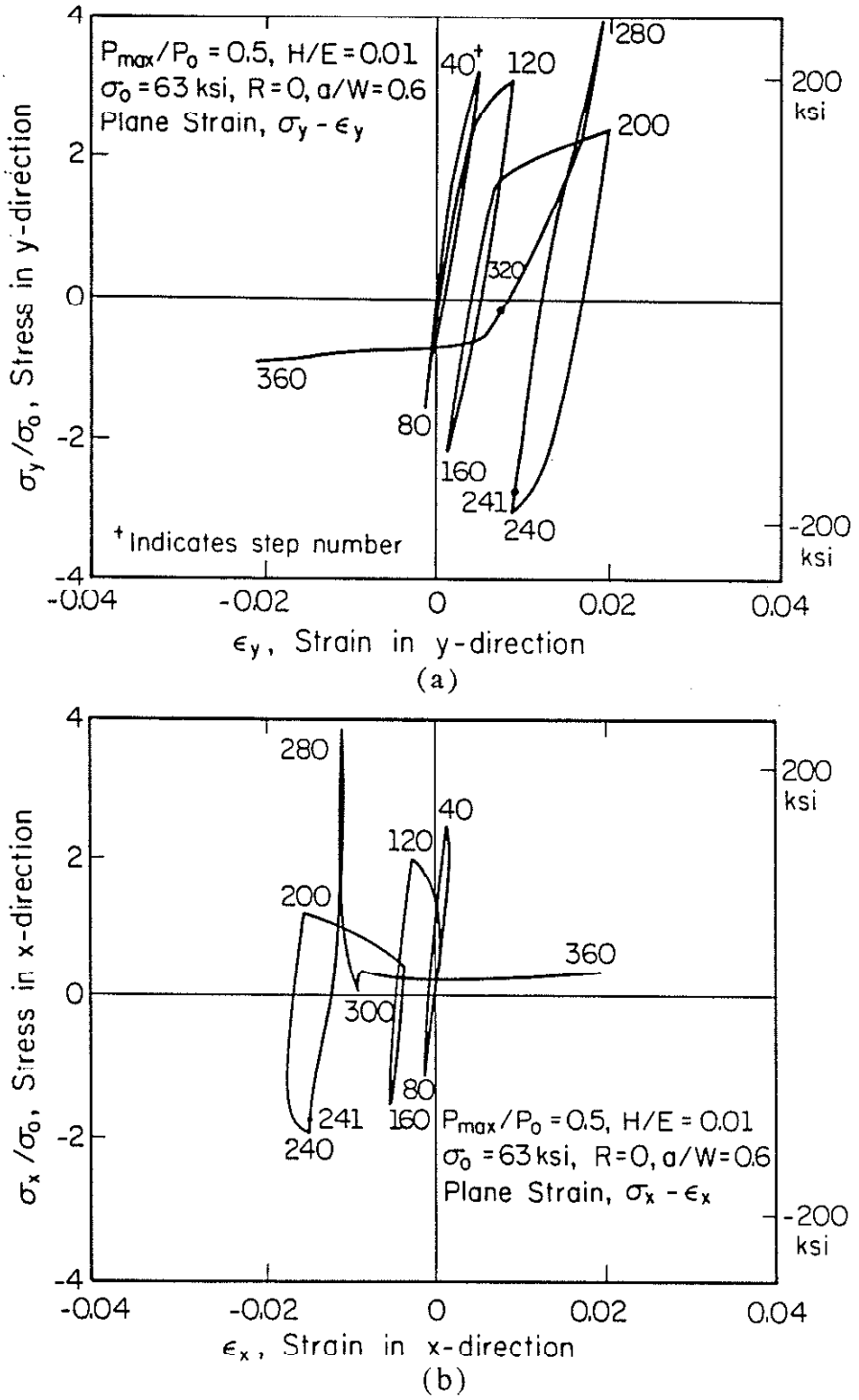

Figure 27a,b Stress-strain behavior at y and x directions at material point from Step #1 through #360. At Step #200 the crack tip has reached Element #282 (P_{max}/P_o = 0.5, plane strain)

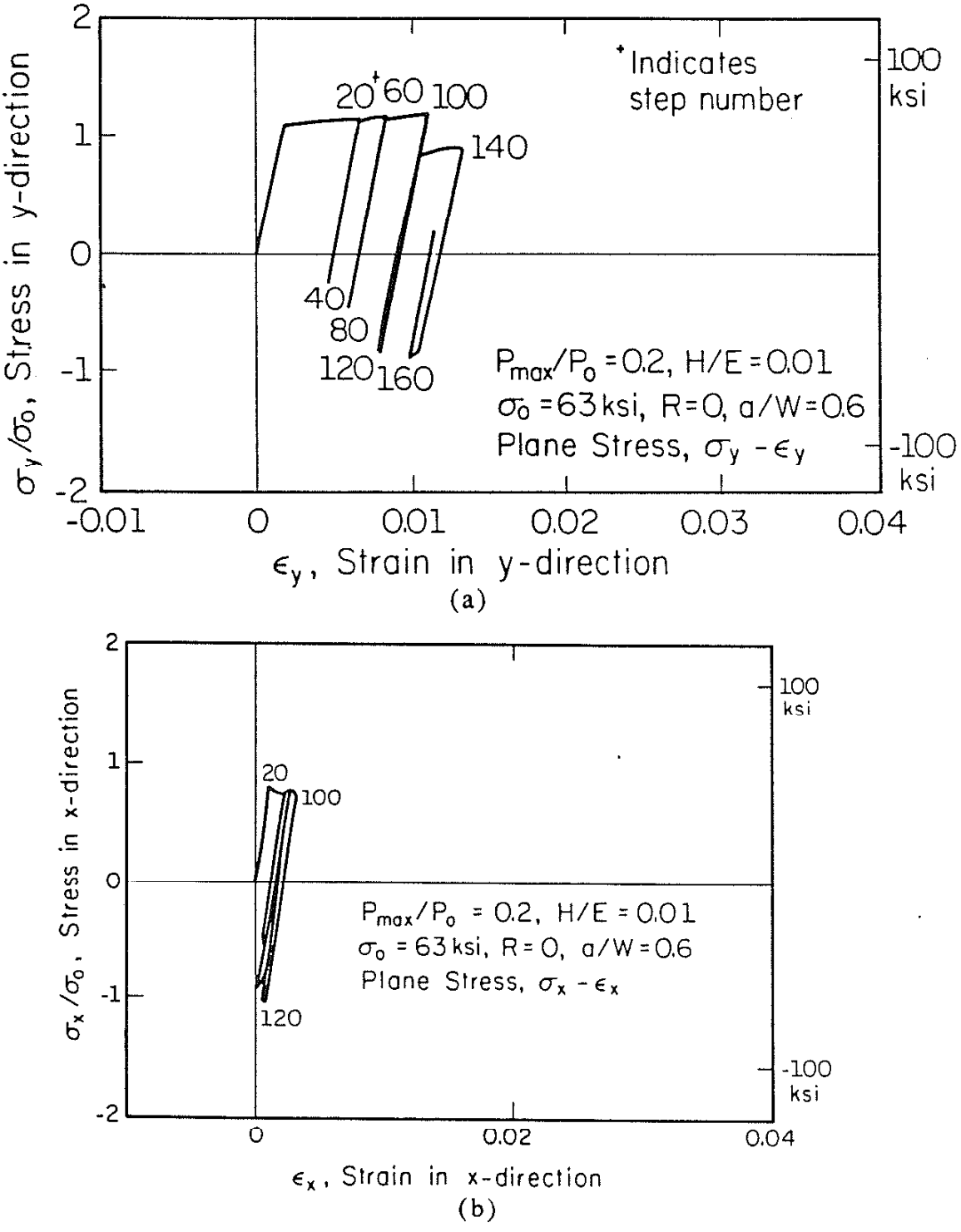

Figure 28a,b Stress-strain behavior at y and x directions at material point from Step #1 through #160. At Step #100 the crack tip has reached Element #282 (P_{max}/P_o = 0.2, plane stress)

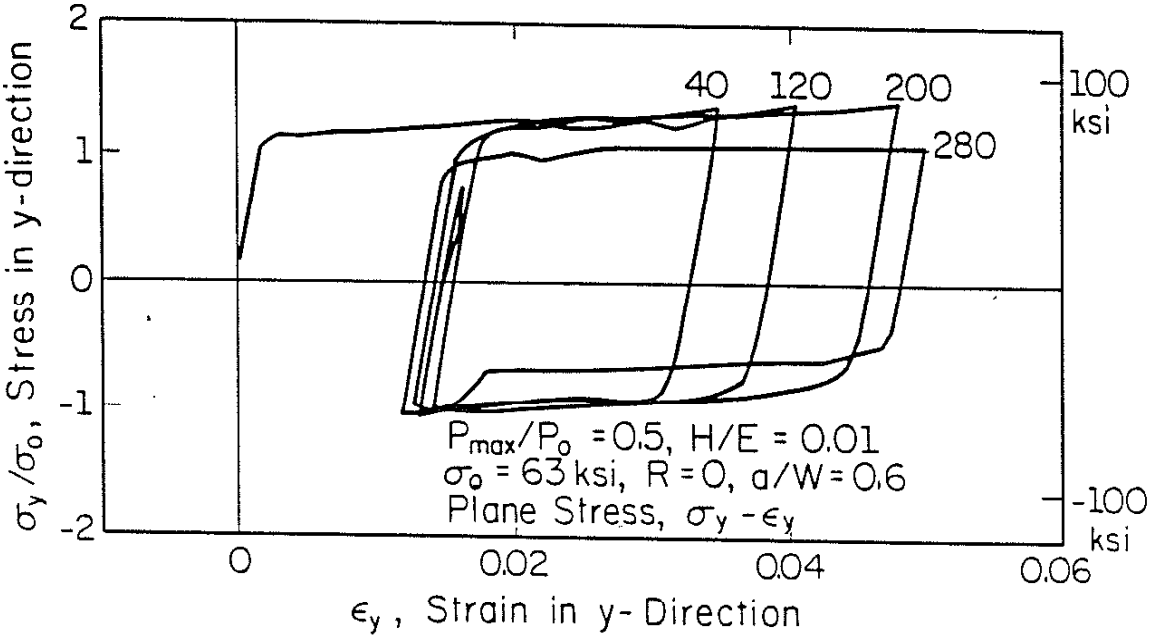

(a)

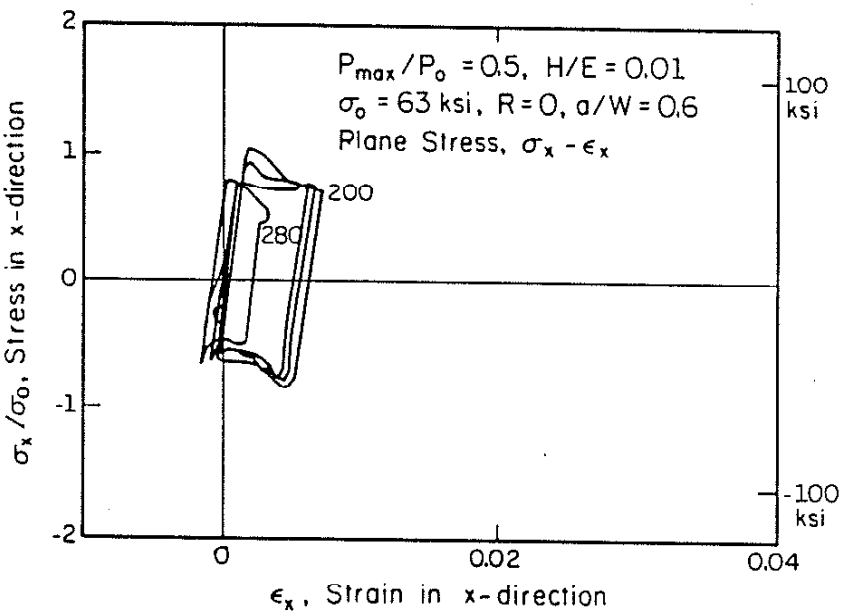

(b)

Figure 29a,b Stress-strain behavior at y and x directions at material point from Step #1 through #360. At Step #200 the crack tip has reached Element #282 (P_{max}/P_o = 0.5 plane stress)

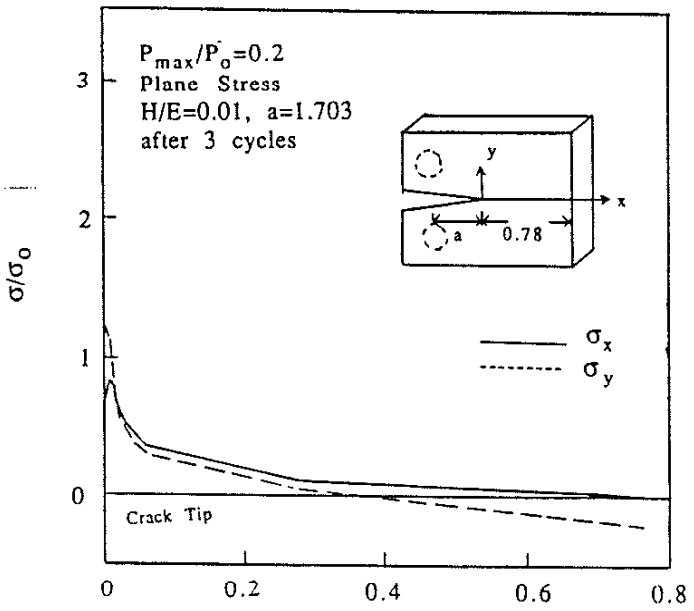

(a)

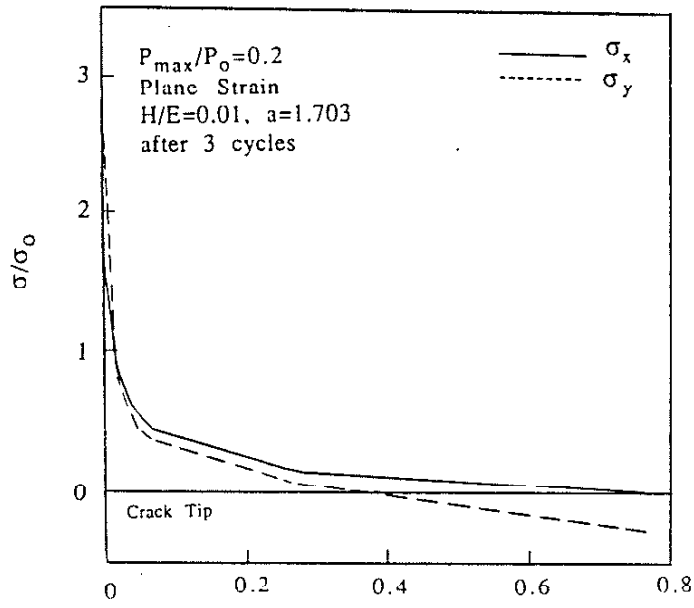

(b)

Figure 30a,b Normalized stress distribution ahead of crack at maximum load for plane stress and plane strain ($P_{max}/P_o = 0.5$)

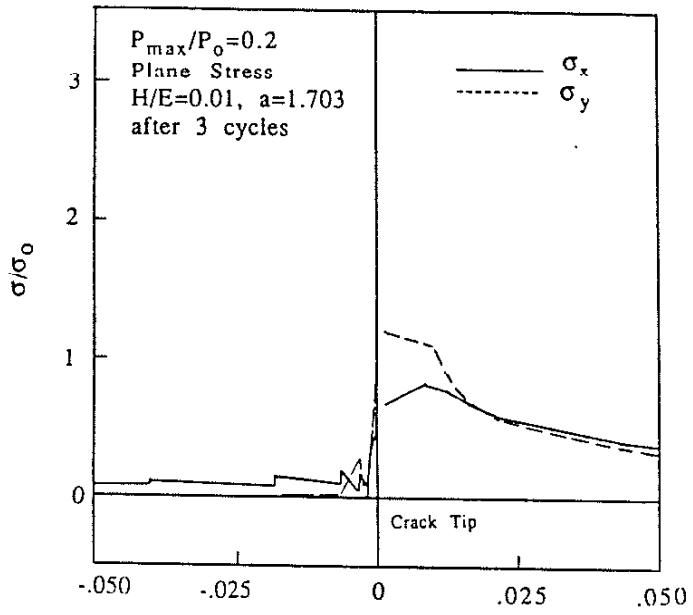

(c)

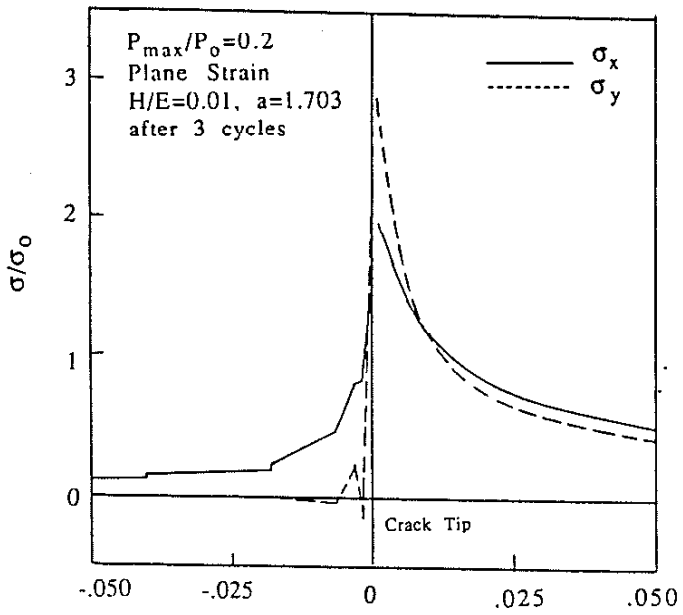

(d)

Figure 30c,d Normalized stress distribution near crack tip at maximum load for plane stress and plane strain (P_{max}/P_o = 0.5)

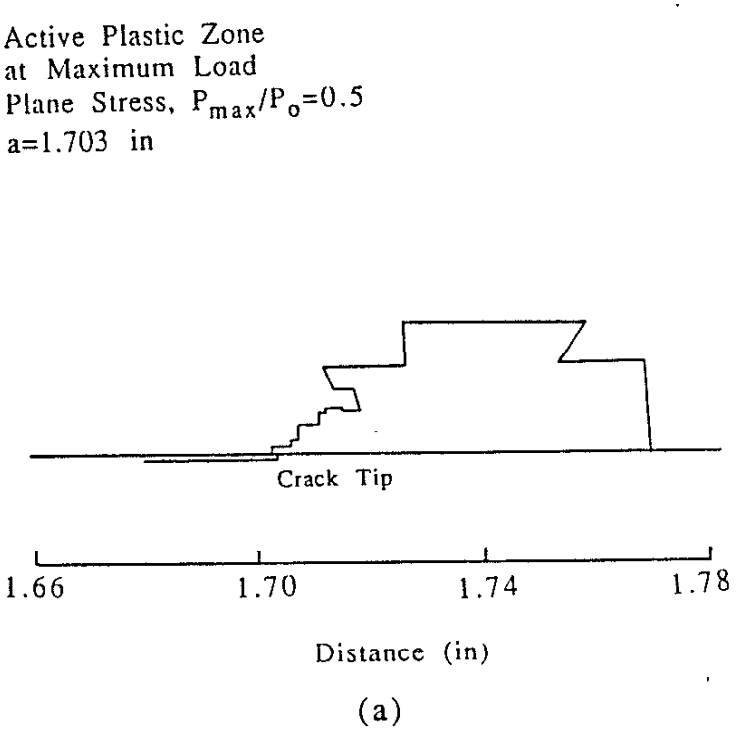

(a)

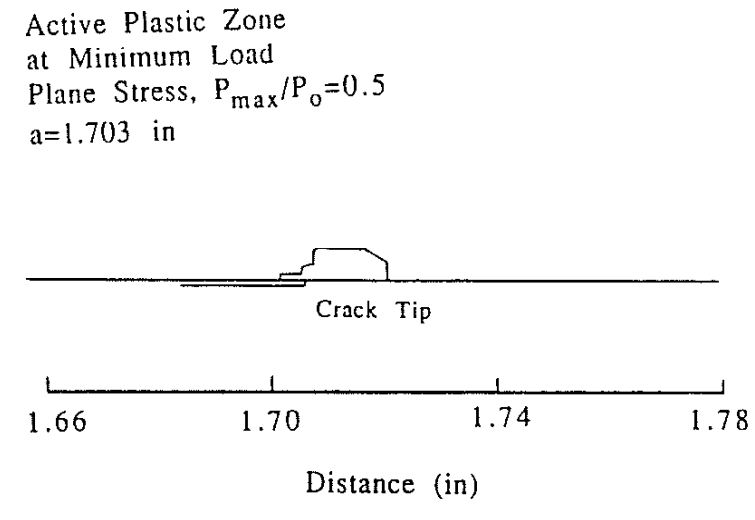

(b)

Figure 31a,b The forward and reversed plastic zone for P_{max}/P_o = 0.5, plane stress case.

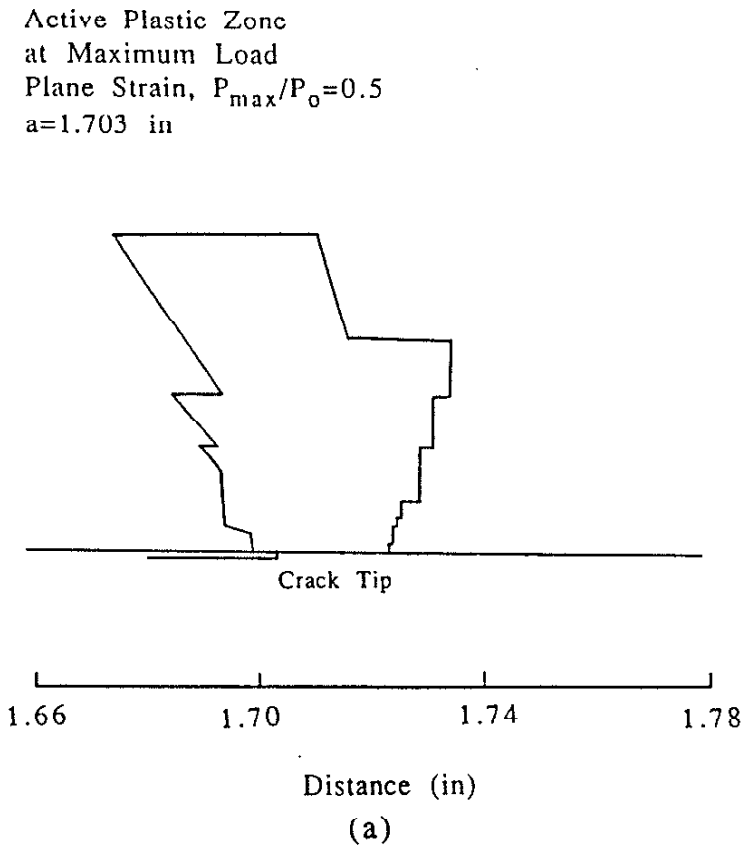

Figure 32a,b The forward and reversed plastic zone for P_{max}/P_o = 0.5, plane strain case.

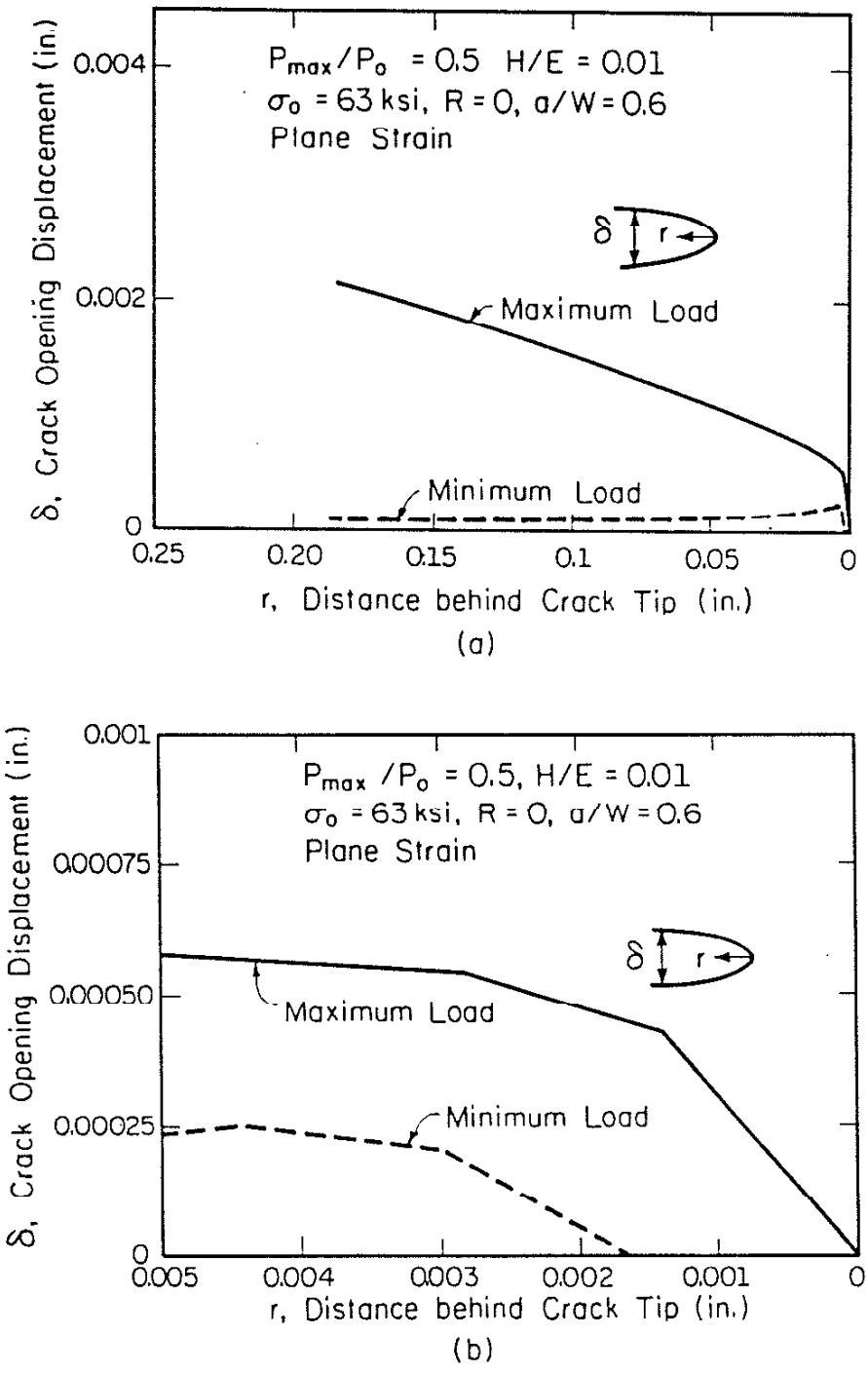

Figure 33a,b Crack opening displacement at maximum and minimum load for $P_{max}/P_o = 0.5$ plane strain case.

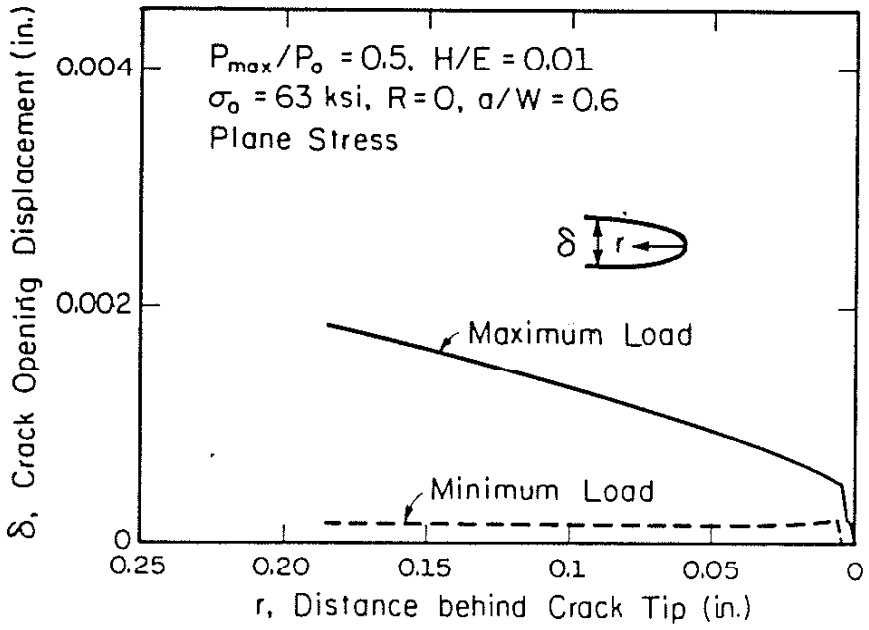

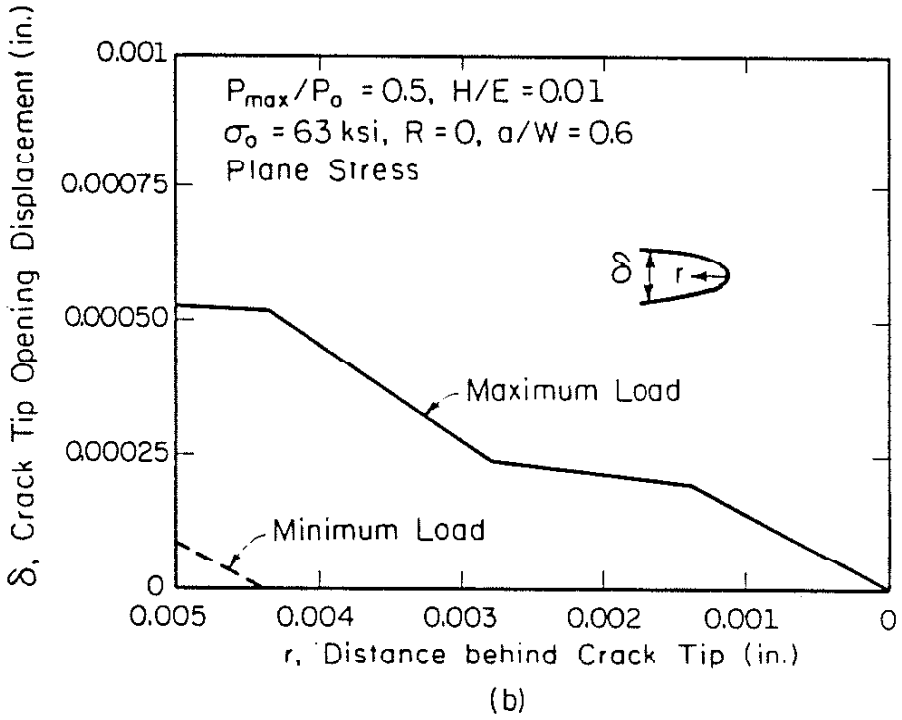

Figure 34a,b Crack opening displacement at maximum and minimum load for P_{max}/P_o = 0.5 plane stress case.

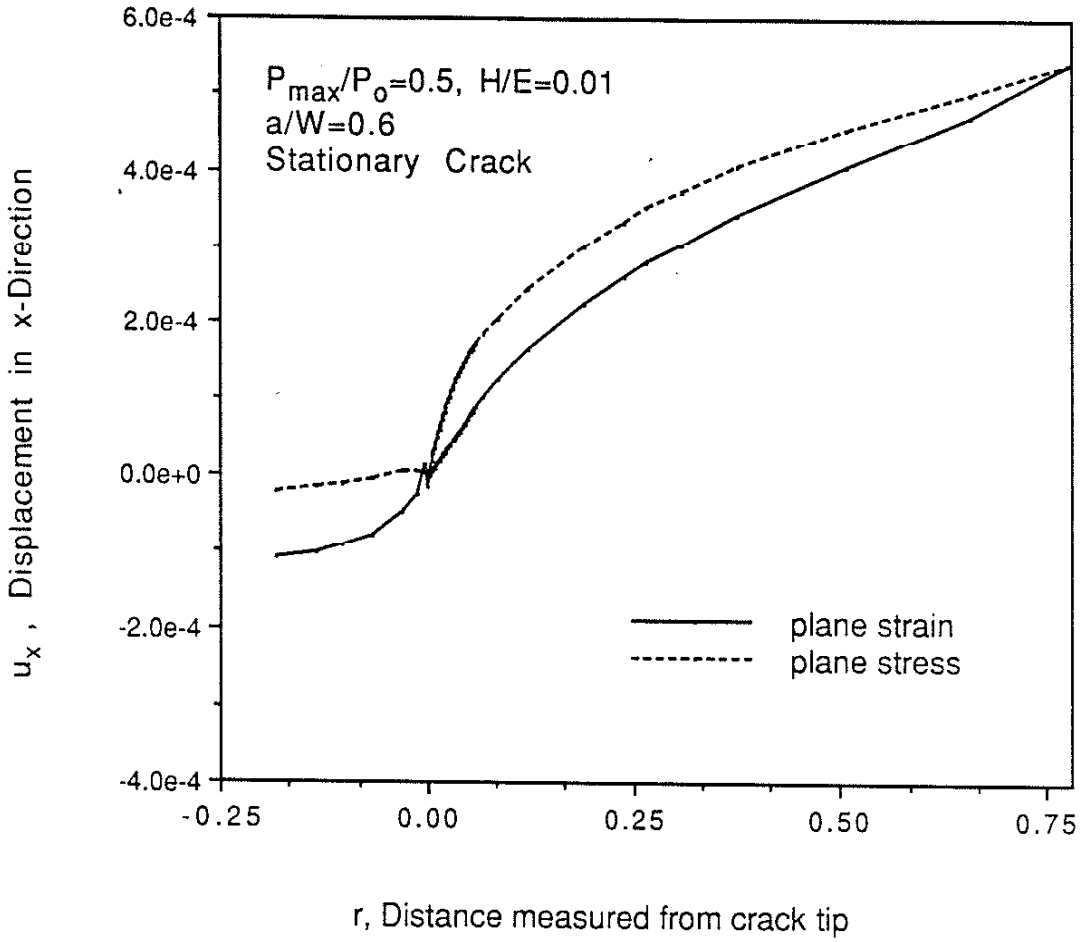

Figure 35 Displacement in x-direction along symmetric line at maximum load for initial crack (P_{max}/P_o = 0.5).

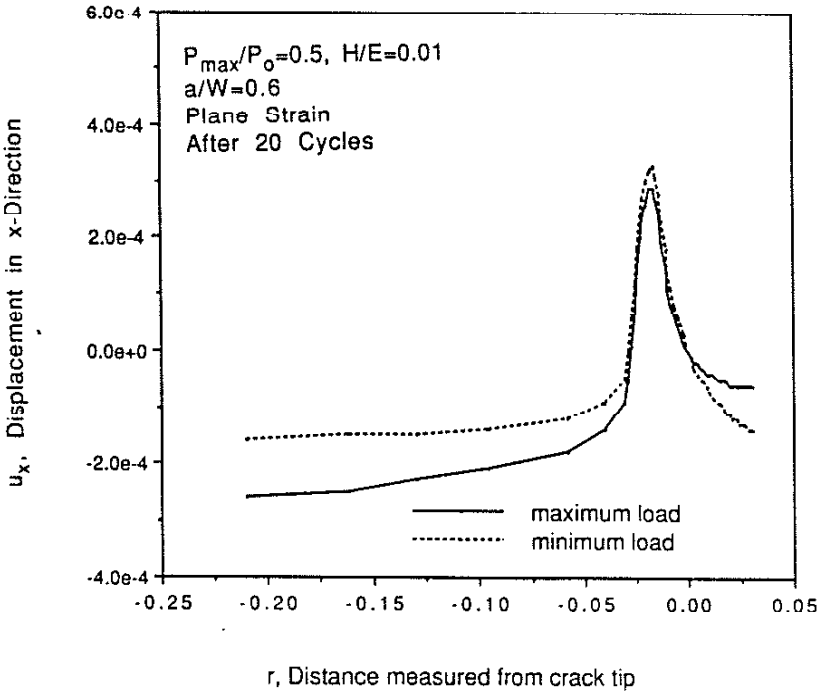

(a)

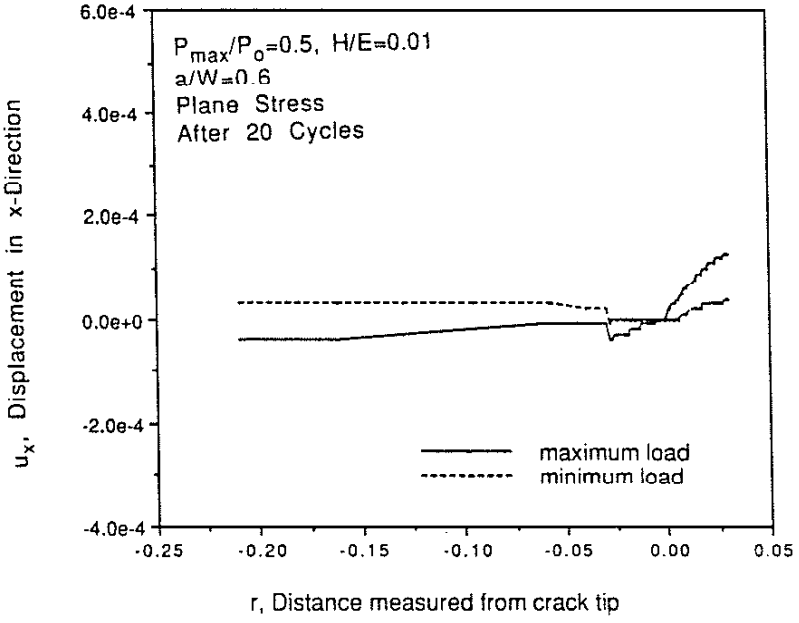

(b)

Figure 36a,b Displacement in x-direction near crack tip for plane strain and plane stress under maximum and minimum load ($P_{max}/P_o = 0.5$).

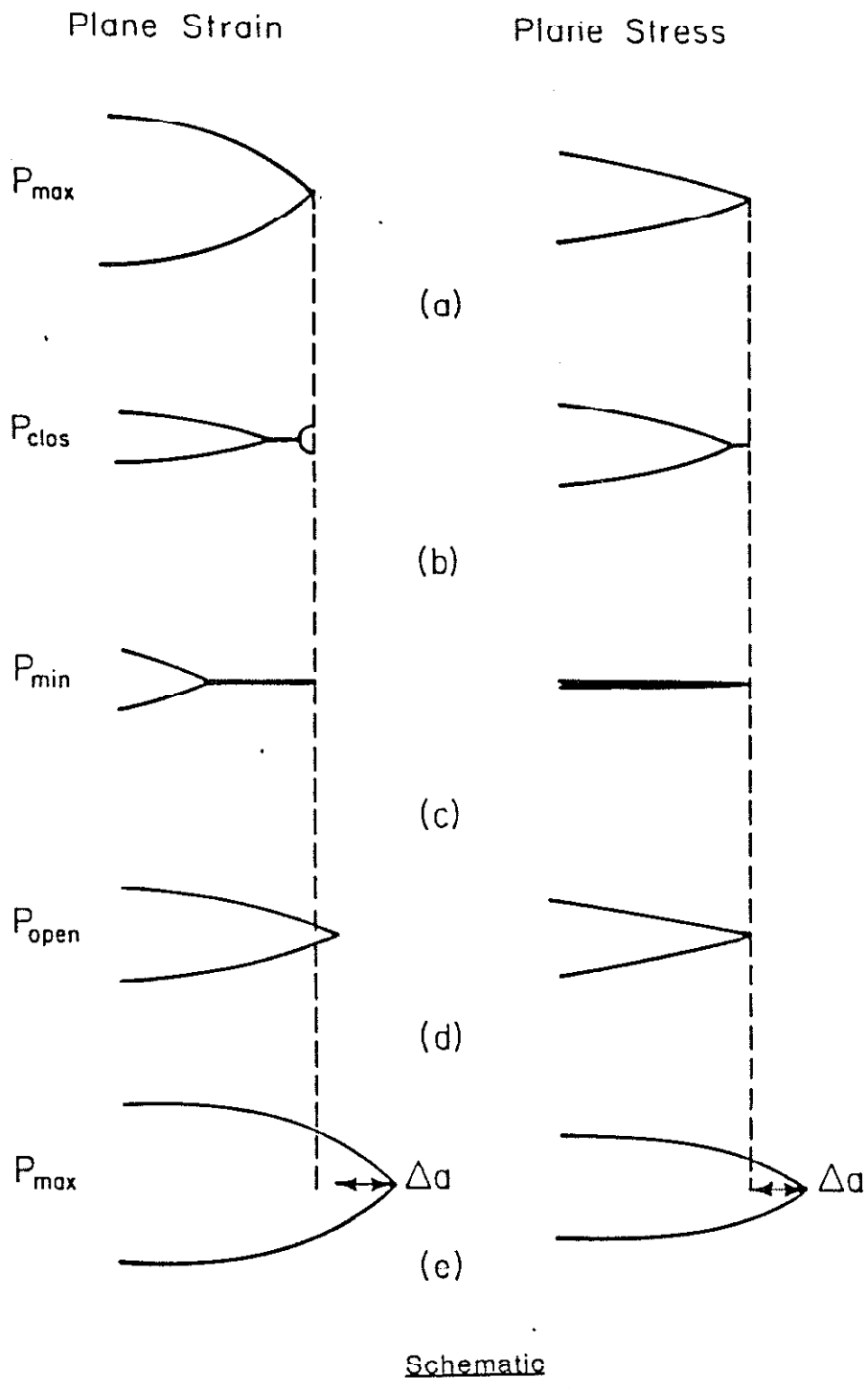

Figure 37 Schematic profile of crack surfaces during a loading cycle under plane strain and plane stress condition.

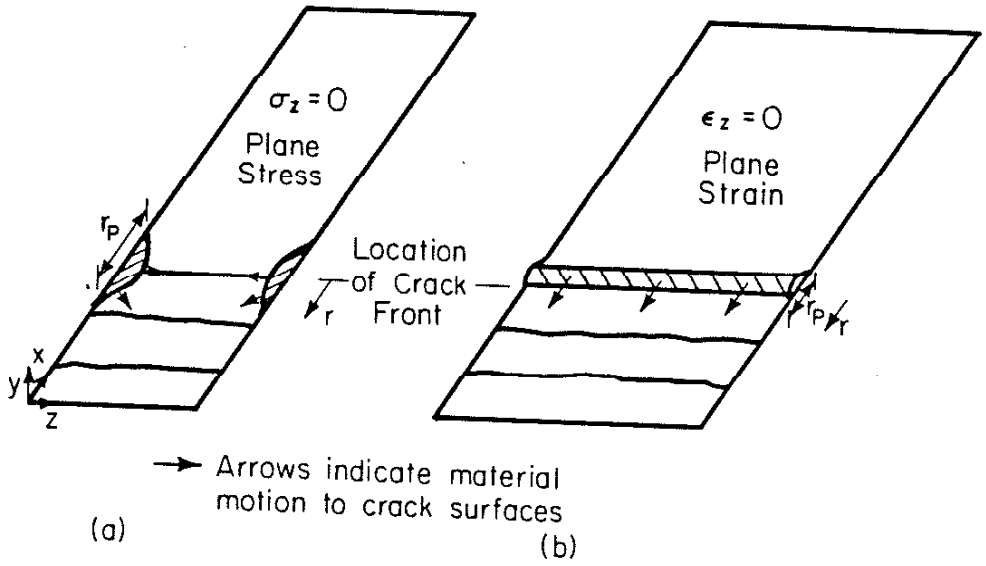

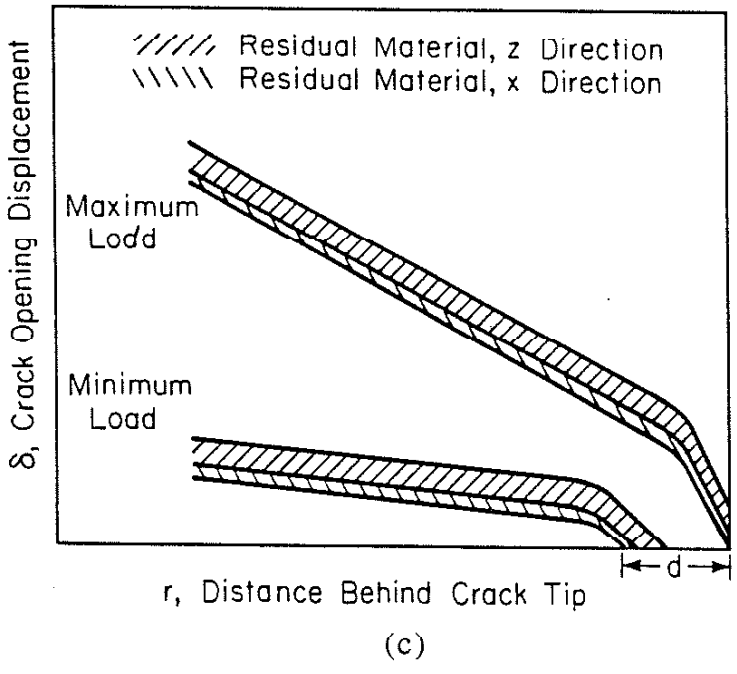

Figure 38 Schematic crack planes indicating mechanism of material transfer in plane strain and plane stress.

REFERENCES

1. Elber, W., "Fatigue Crack Propagation," Ph.D. Thesis, University of New South Wales, Australia, 1968.

2. Elber, W., "Fatigue Crack Closure under Cyclic Tension," Engineering Fracture Mechanics, Vol.2, 1970, pp. 37-45.

3 Elber, W., "The Significance of Fatigue Crack Closure," Damage Tolerance in Aircraft Structures, ASTM STP 486, 1971, pp. 230-242.

4 Socie, D. F., "Predict of Fatigue Crack Growth in Notched Members under Variable Amplitude Loading Histories," Engineering Fracture Mechanics, Vol. 9, 1977, pp. 849-865.

5. Lalor, P., H. Sehitoglu, and R. C. McClung, "Mechanics Aspects of Small Crack Growth from Notches--- The Role of Crack Closure," The Behavior of Short Fatigue Cracks, EFG Pub. 1, Mechanical Engineering Publications, London, 1986, pp. 369-386.

6. McClung, R. C. and H. Sehitoglu, "Closure Behavior of Small Cracks under High Strain Fatigue Histories," Mechanics of Fatigue Crack Closure, ASTM STP 982, American Society for Testing and Materials, Philadelphia, 1988, pp. 279-299.

7. Newman, J. C. Jr., M. H. Swain, and E. P. Phillips, "An Assessment of the Small-Crack Effect for 2024-T3 Aluminum Alloy," Small Fatigue Cracks, Proceedings of the Second Engineering Foundation International Conference/Workshop, Santa Barbara, California, January 5-10, 1986, pp. 427-452.

8. Newman, J. C. Jr., E. P. Phillips, and M. H. Swain, "Predicting the Growth of Small and Large Cracks Using a Crack-Closure Model," Mechanical Behavior of Materials--V, Proceedings of the Fifth International Conference, Beijing, China, pp. 51-60.

9. Sorensen, E. P., "A Numerical Investigation of Plane Strain Stable Crack Growth Under Small-Scale Yieleing Conditions," Elastic-Plastic Fracture, ASTM STP 668, Americal Society for Testing and Materials, 1979, pp. 151-174.

10. Kobayashi. H., and H. Nakamura, "Investigation of Fatigue Crack Closure (Analysis of Plasticity Induced Crack Closure)," Current

Research on Fatigue Cracks, MRS Vol.1, Society of Materials Science, Japan, 1985, pp.229-245.

11. Newman, J. C. Jr.,"A Finite-Element Analysis of Fatigue Crack Closure," Mechanics of Crack Growth, ASTM STP 590, American Society for Testing and Materials, 1976, pp. 281-301.

12. Anquez, L. and G. Baudin, "Correlation Between Numerically Predicted Crack Opening Loading and Measured Load History Dependent Crack Growth Threshold," Mechanics of Fatigue Crack Closure, ASTM STP 982, American Society for Testing and Materials, 1988, pp. 380-397.

13. Lalor, P. L. and H. Sehitoglu, "Fatigue Crack Closure Outside a Small-Scale Yielding Regime," Mechanics of Fatigue Crack Closure, ASTM STP 982, American Society for Testing and Materials, Philadelphia, 1988, pp. 342-360.

14. McClung, C. R.,"Fatigue Crack Closure and Crack Growth Outside the Small Scale Yielding Regime," Ph.D. Thesis, University of Illinois at Urbana-Champaign, 1987.

15. James. L. A., "The Effect of Frequency upon the Fatigue Crack Growth of Type 304 Stainless Steel at 1000 F," ASTM STP 513, American Society for Testing and Materials, 1972, pp. 218-229.

16. Saxena, A., "A Model for Predicting the Effect of Frequency on Fatigue Crack Growth Behavior at Elevated Temperature," Fatigue of Engineering Materials and Structures, Vol. 3, 1981, pp. 247-255.

17. Saxena, A., R. S. Williams, and T. T. Shih, "A Model for Representing and Predicting the Influence of Hold Time on Fatigue Crack Growth Behavior at Elevated Temperature," Fracture Mechanics:Thirteenth Conference, ASTM STP743, American Society for Testing and Materials, 1981, pp.86-99.

18. Manson, S. S., G. R. Halford, and M. Hirschberg, "Creep Fatigue Analysis by Strain Range Partitioning Method," NASA TMX-67838, 1971.

19. Saxena, A., J. and L. Bassani, "Time-dependent Fatigue Crack Growth Behavior at Elevated Temperature," Fracture: Interactions of Microstructure, Mechanisms and Mechanics, AIME Meeting, 1984, pp. 357-383.

20. Wareing, J. "Creep-Fatigue Interaction in Austenitic Stainless Steels," Metal. Transactions, Vol. 8a, 1977, pp. 711-721.

21. Antolovich, S. D., S. Liu, and R. Baur, "A Mechanistically Based Model for High Temperature LCF of Ni Base Superalloys," Superalloys 1980, 1980, pp. 605-613.

22. Challenger, K. D., A. K. Miller, and R. L. Langdon, "Elevated Temperature Fatigue with Hold Time in a Low Alloy Steel: A Predictive Correlation," J. Materials for Energy Systems, Vol. 3, 1981, pp.51-61.

23. Liu, H. W., and Y.Oshida, "Grain Boundary Oxidation and Fatigue Crack Growth at Elevated Temperatures," Theoretical and Applied Fracture Mechanics, Vol. 6, 1984, pp. 85-94.

24. Sehitoglu, H., "Crack Opening and Closure in Fatigue," Engineering Fracture Mechanics, Vol. 21, No. 2, 1985, pp. 329-339.

25. McClung, R. C., and H. Sehitoglu, "On the Finite Element Analysis of Crack Closure, Part I: Basic Modeling Issues, Part II: Numerical Results," submitted to Engineering Fracture Mechanics.

26. Biner, S. B., D. S. Wilkinson and D. Watt, "On the Stress and Strain Fields ahead of a Stationary Crack in Creeping Solids," Engineering Fracture Mechanics, Vol.21, No.2, pp. 315-328, 1985.

27. Prager. W., "The Theory of Plasticity: A Survey of Recent Achievements," James Clayton Lecture, Proc., Inst. Of Mech. Eng., Vol. 169, 1955, pp. 41-50.

28. Ziegler, H., "A Modification of Prager's Hardening Rule," Q. Appl. Math., Vol. XVII, 1959, pp.55-65.

29. Drucker, D., and L. Palgen, "On Stress-Strain Relation Suitable for Cyclic and Other Loading," ASME J. Appl. Mech., Vol. 48, 1981, pp. 479-485.

30. Sherwood, J. A., and D. C. Stouffer, "A Constitutive Model with Damage for High Temperature Superalloys," 3rd Symposium on Nonliear Constitutive Relations for High Temperature Applications, Univ. of Akron, 1986.

31. Inoue, T., S. Imatani and T. Sahashi, "On the Plasticity-Creep Interaction Behavior of SUS-304 Steel under Combined Stress State of Tension and Torsion," Proceedings of the Twentyeighth Japan Congrass on Materials Research, Kyoto, Japan, 1985.

32. Wu, K. H., "Creep-Fatigue Interaction of Notched 304 Stainless Steel Bars," Ph.D. Thesis, University of Illinois at Urbana-Champaign, 1984.

33. Fleck, N. A., and J. C. Newman, Jr., " Analysis of Crack Closure under Plain Strain Conditions," Mechanics of Fatigue Crack Closure, ASTM STP 982, American Society for Testing and Materials, Philadelphia, 1988, pp. 319-341.

34. Kumar, V., M. D. German, C. F. Shih, "An Engineering Approach for Elastic-Plastic Fracture Analysis," General Elecric Company, NP-1931, Research Project 1237-1, Topical Report, July, 1981.

35. Nagtegaal, J. C., D. M. Parks and J. R. Rice, "On Numerically Accurate Finite Element Solution in the Fully Plastic Range," Computer Methods in Applied Mechanics and Engineering, Vol. 4, 1974, pp.153-177.

36. Blom, A. F. and D. K. Holm, "An Experimental and Numerical Study of Crack Closure," Engineering Fracture Mechanics, Vol. 22, No.6, 1985, pp. 997-1011.